DETECTION OF FREEZING OF GAIT AND GAIT INITIATION FAILURE IN PEOPLE WITH PARKINSON'S DISEASE USING ELECTROENCEPHALOGRAM SIGNALS

By

Quynh Tran LY

Submitted to Faculty of Engineering and Information Technology

in partial fulfillment of the requirement for the degree of

Doctor of Philosophy

at the University of Technology Sydney

Sydney, December 2017

CERTIFICATE OF AUTHORSHIP/ORIGINALITY

I, Quynh Tran Ly, certify that the work in the thesis has not previously been submitted for a degree nor has it been submitted as part of requirements for a degree except as fully acknowledged within the text.

I also certify that the content of this thesis is my own work. Any help that I have received in my research work and the preparation of the thesis itself has been duly acknowledged. In addition, I certify that all information sources and literature used are indicated in the thesis.

Signature of Candidate

Production Note:
Signature removed prior to publication.

Quynh Tran Ly

Acknowledgement

First and foremost, I would like to thank Buddhism for the spiritual guidance, protection and so many blessings, which made me who I am today.

I would like to express my deepest gratitude to my Principal Supervisor, Professor Hung Tan Nguyen for providing intellectual guidance, constant support and sympathizing during my PhD journey. His invaluable knowledge in Electroencephalography and computational intelligence has enabled me to deeply understand the concept, keep me on the correct path and has contributed enormously to my research. I am very grateful to have had the chance to study and learn under his superb guidance and mentorship.

I would like to express my heartfelt thanks and memorize my research member and teacher Dr Ardi Handojoseno for providing valuable knowledge, support and friendship throughout my PhD journey. His insightful contribution and great assistance enabled me to go through and complete this research. I am very fortunate to have worked with and learned from him in his last three years. His intellect, kindness and compassion will always remain deeply in my heart.

I would like to express my extreme thanks my Co-supervisors, Dr Rifai Chai, Dr Nghia Nguyen for providing knowledge in computational intelligence, support in improving my research and encouragement during my PhD journey. I would like to truly extend my thanks to my key research colleague Dr Moran Gilat for helping in data collection, providing valuable science knowledge and great assistance in writing as well as editing all my published papers. I would like to thanks all my colleagues in Centre for Health Technology, my family and friends who supported and shared with me during my PhD journey.

Finally, and most importantly, my constant love and appreciation deeply goes out to my parents, my husband Tri Nguyen and my daughters Tran Nguyen, Hanh Nguyen. They are always an endless source of encouragement, strength and love in my life.

"This thesis is especially dedicated to my dearest parents Dich Cam Ly, Thi Tinh Tran, my husband Van Minh Tri Nguyen, my daughters Thien Nha Tran Nguyen and An Dieu Hanh Nguyen for their endless love, care and encouragement ..."

Contents

Contents

List of Figures

List of Tables

Abbreviations

3D: Three Dimensions

ANN: Artificial Neural Networks

BSS: Blind Source Separation

BNN: Bayesian Neural Networks

CF: Centroid Frequency

CWT: Continuous Wavelet Transform

DWT: Discrete Wavelet Transforms

ECG: Electrocardiography

EEG: Electroencephalography

EMG: Electromyography

EW: Effective Walking

FFT: Fast Fourier Transform

fMRI: function Magnetic Resonance Imaging

FOG: Freezing of Gait

FOGQ: Freezing of Gait Questionnaire

H&Y: Hoehn and Yahr stage

GIF: Gait Initiation Failure

GS: Good Start

GT: Good Turn

ICA: Independent Component Analysis

ICA-EBM: Independent Component Analysis Entropy Boundary Maximization

ICs: Independent Components

MMSE: Mini-Mental State Examination

PD: Parkinson's disease

PSD: Power Spectral Density

PSE: Power Spectral Entropy

pSMA: pre-Supplementary Motor Area

SVM: Support Vector Machine

ST: S-Transform

TF: Turning FOG

TUG: Timed Up and Go

UPDRS: Unified Parkinson's disease Rating Scale

WE: Wavelet Energy

WCS: Wavelet Centroid Scale

WEE: Wavelet Energy Entropy

Abstract

Parkinson's disease (PD) is the second most common age related neurodegenerative disorder, affecting approximately 1-2% of the elderly population. Freezing of Gait (FOG) is a very disabling feature of PD that causes frequent falls. During FOG, patients are suddenly unable to take a step despite the intention to walk or continue moving forward. The neural mechanisms of FOG are unclear and treatments have only limited effectiveness.

Based on contexts of behavioural measures in daily life, different types of FOG have been observed including: freezing when turning (TF); freezing when getting through narrow doorways; freezing when reaching a target; freezing when straight walking or freezing when initiating gait to start a movement (GIF). TF and GIF are recognized to be the most frequent triggers of FOG seen in PD patients.

To detect FOG, using parameters extracted from the Electroencephalogram (EEG) is one of the most promising methods. In the comparison of using "body-worn" sensors technique, EEG measures the activity of the brain where the root of FOG is occurring. Therefore, EEG will be quicker to detect FOG than "body-worn" sensors because of the time the neural signal has to travel all the way to the legs to be measured, thus offering the most optimal time window for intervention to overcome FOG.

The research in this thesis introduces advanced algorithms for FOG detection using EEG signals. These algorithms have been developed and applied successfully to detect FOG and its two common subtypes (GIF, TF) based on various features extractions and classifiers, providing high accuracy for detection. It was found that the combination of Independent Component Analysis Entropy Boundary Minimization (ICA-EBM), S-Transform (ST) and Bayesian Neural Networks (BNN) proved to be a very robust and effective method for freezing detection.

In the first study, abnormal changes of EEG signal to detect FOG were investigated. By using Fast Fourier Transform as the feature extraction and Artificial Neural Networks

(ANN) as a classifier, the EEG data of FOG could be detected effectively from seven PD patients with sensitivity, specificity and accuracy of 72.20%, 70.58% and 71.46%, respectively. Furthermore, FOG episodes were found to be associated with significant increases in the high beta band (21-38Hz) across the central, frontal, occipital and parietal EEG sites.

In the second study, the dynamic brain changes underlying a GIF episode and its detection were investigated in four PD patients. This research studied the brain activity underlying GIF by analyzing Wavelet Transform (WT) of EEG signals. Using ICA-EBM for EEG source separation, WT for feature extraction and Support Vector Machine (SVM) for classification, the correct identification of GIF episodes was improved with sensitivity, specificity, and accuracy of 83.94%, 89.39% and 86.67%, respectively.

The final classification results produced by this dissertation indicated that by applying source separation ICA-EBM for pre-processing EEG data, time-frequency ST techniques for feature extraction and BNN for classification, a freezing event can be successfully detected using EEG signals. The results for the TF detection were achieved with sensitivity, specificity, and accuracy of 83.00%, 87.60% and 85.40%, respectively. The results for the GIF detection were relatively similar with sensitivity, specificity, and accuracy of 88.96%, 90.26% and 89.50%, respectively.

With the final performance (ICA-EBM, ST, BNN) achieved by this thesis, future work will be carried out to pursue the eventual aim of the current research, which is developing an EEG-based system for detecting FOG that can be applied in real-time.

Chapter 1

Introduction

1.1 MOTIVATION

Parkinson's disease is the second most common age related neurodegenerative disorder, affecting approximately 1-2% of the elderly population (De Lau & Breteler 2006). According to a report by Parkinson Australia, over 64,000 Australians had a diagnosis of PD in 2011 (Essential & CPE 2012), a prevalance that has signifcantly risen to over 108,000 patients in 2017 (Parkinson's & Australia 2017). The number of people with PD has been predicted to double over the next 20 years due to the global ageing population

(Factor & Weiner 2007) and PD has been considered as one of the greatest threats to public health, generating an enormous cost burden to the society (Huse et al. 2005; Saarni et al. 2006).

PD is characterized by the degeneration of dopamine producing neurons in the substantia nigra that innervate the basal ganglia (Agid et al. 1989). One role of dopamine is to enable smooth motor control; therefore, the loss of this neurotransmitter might make the muscles overly tense, cause tremor, joint rigidity and slow movement in PD (Hughes et al. 1992; Levy et al. 2002). Patients with PD suffer from both motor symptoms including bradykinesia or akinesia, tremor at rest, rigidity and postural instability (Braak et al. 2004; Jankovic 2008) as well as non-motor symptoms including sensory abnormalities, cognitive impairments, autonomic dysfunction and mood disorder that often develop after several years of the disease (Caballol, Martí & Tolosa 2007; Chaudhuri, Healy & Schapira 2006). As their disease progresses, the vast majority of patients also develop the freezing phenomenon (Giladi, Kao & Fahn 1997), which manifests as both freezing of gait (FOG) and gait initiation failure (a sub-type of FOG, otherwise called start hesitation) (Schaafsma et al. 2003).

Clinically, FOG is often described by the patients as a feeling like their feet are “glued to the floor” (Nutt et al. 2011). During FOG, the patients are suddenly unable to take a step despite the intention to walk or continue moving forward (Nutt et al. 2011). The assessment of FOG is difficult because patients may not experience freezing in the clinical setting or sometimes do not have a proper understanding of what actual freezing looks likes (Snijders et al. 2012). Although FOG does not occur constantly, there are certain triggers that often cause a freeze, these include: initiating the first step (gait initiation failure – GIF), turning (Turning FOG), navigating environmental features, such as narrow doorways (narrow FOG), reaching a target (target FOG) and occasionally during straight walking (runway FOG) (Nutt et al. 2011; Schaafsma et al. 2003). Furthermore, cognitive dual tasking (i.e. performing a thinking task while walking) can also trigger a freeze (Spildooren et al. 2010). FOG is associated with a high risk for falls

and leads to significant morbidity in PD (Backer 2006). FOG has thus been identified as the most distressing symptom contributing to a poor quality of life for patients with PD (Walton et al. 2015).

Unfortunately, FOG is a very complex symptom of the brain and the causes of FOG remain poorly understood (Nieuwboer & Giladi 2013). One of the biggest problems is that neuroimaging techniques, such as fMRI, do not allow patients to walk inside the scanner (Shine, Naismith & Lewis 2011). Therefore, these techniques are limited in their ability to investigate FOG.

To date, a number of functional MRI studies have been conducted to explore several aspects of the freezing phenomenon (Gilat et al. 2015; Peterson et al. 2014; Shine, Moustafa, et al. 2013; Snijders et al. 2011). These neuroimaging results highlighted the key aspect that FOG behavior is associated with maladaptive changes in both cortical and subcortical processes in the brain, that ultimately cause the patients to become unable to move their feet during FOG (Lewis & Shine 2016). However, though insights have been gained using fMRI, this technique is not able to investigate the neural mechanisms underlying actual freezing episodes that occur while walking.

Treating FOG is very challenging (Nonnekes et al. 2015). For instance, current dopaminergic replacement therapy reduces the appearance of FOG, but only in the short term for most PD patients (Nonnekes et al. 2015). Moreover, deep brain stimulation (DBS), which is reliably effective for cardinal motor symptoms of PD, does not adequately alleviate freezing (Nonnekes et al. 2015). It is possible that much of the failure of DBS to alleviate freezing may relate to the paroxysmal and functional nature of the phenomenon (Shine, Halliday, et al. 2014). Furthermore, somatosensory cues including, visual and auditory cues have been shown to reduce FOG (Nieuwboer 2008a). It is believed that cueing acts by requiring patients to step using goal-directed movements that do not require processing in the impaired basal ganglia (Lewis & Barker 2009). However, the effects of cueing are dramatically lost over time, possibly as patients habituate to the

novelty of the cue (Lewis & Barker 2009). There is therefore a need to develop appropriate "on demand" treatment strategies (Velik 2012) that may help to tailor treatments.

This thesis, therefore, used electroencephalography (EEG) to investigate FOG for three main reasons. First, EEG is non-invasive and has no side effects and could be offered to all patients, including those with advanced stages of PD. Second, EEG allows for the investigation of the cortical neural mechanisms underlying FOG during actual gait (Velu et al. 2014). Third, the high temporal resolution of EEG might make it deal to 'detect' when a FOG event occurs (Handojoseno et al. 2014; Handojoseno et al. 2012; Handojoseno, Shine, et al. 2015). Knowing when FOG occured would allow for the timely implementation of treatment strategies for FOG, such as cueing or DBS, in order to overcome or even prevent the occurrence of FOG.

1.2 PROBLEM STATEMENT

In recent years, because FOG has been considered as a neurological disorder, few attempts have been made to detect the episode of FOG based on brain signal (EEG) (Jahn et al. 2008). In addition, there are a large number of studies using "body-worn" sensors such as accelerometers, goniometers and electromyography (EMG) as an indicator for FOG detection (Han et al. 2006; Nieuwboer et al. 2001). Electrocardiography (ECG) was also analysed and reported as significant changes in the comparison between FOG and normal walking from the data of 11 PD patients (Mazilu et al. 2015). Moreover, a wearable device using acceleration sensors to measure patient's movements has also been developed (Bachlin et al. 2010; Moore, MacDougall & Ondo 2008).

The biggest advantage of EEG over "body-worn" sensors is that EEG measures the activity of the brain where FOG is caused. Therefore, EEG will be quicker to detect FOG than "body-worn" sensors because by the time "body-worn" sensors detect the freeze, the brain is already in a complete freezing state, making it more difficult to overcome a freeze (Lewis & Shine 2016). As a result, "body-worn" sensors are somewhat 'too late' in

detecting FOG. The neural signal has to travel all the way to the legs to be measured, whereas EEG directly measures the earliest onset of FOG from the brain itself, thus offering the most optimal time window for intervention to overcome FOG. Also, researches using "body-worn" sensors are limited in the detection FOG by different walking styles seen in PD patients. In fact, the accelerometer cannot differentiate the complete motor block associated with FOG from the period of voluntarily stopping in a patient with PD during walking and turning movement (Mazilu et al. 2012; Moore, MacDougall & Ondo 2008; Niazmand et al. 2011).

Our primary aim is to better understand the freezing phenomenon and to develop a device that can aid medical treatment for FOG in PD patients. Using a brain signal appears to be a potentially effective solution, as it has been shown to provide information on the different gait tasks (i.e. turning and initiating gait). Moreover, it can measure scalp locations of the brain which is associated with the cause of FOG (Handojoseno et al. 2012; Handojoseno, Shine, et al. 2015). EEG appears as a promising device for the detection of FOG in PD patients due to its portability, affordability, and convenience of use. It is hoped that the cueing and DBS treatments can be modified to only activate when required in the onset of FOG, thus improving their effectiveness.

Our research team has recently shown that 'surface EEG' measurement can be utilized to detect specific brain signal changes that herald an episode of FOG when patients are walking and turning (Handojoseno, Gilat, et al. 2015; Handojoseno, Shine, et al. 2015). The term non-invasive 'surface EEG' electrodes was used to separate it from other types of EEG such as minimal invasive EEG or implanted EEG. However, to date, no study has investigated the EEG signals underlying GIF. In addition, it remains unclear what montage of EEG leads can provide the most sensitive and accurate detection of FOG episodes. Finally, much work is still needed to develop the most optimal EEG signal pre-processing (artefact handling, amplifier and filtering), EEG signal transmission data mode (wireless), EEG signal feature extraction (feature extraction and selection), and EEG signal classification (better sensors for detection). As such, this thesis will be using

EEG to investigate the neural mechanism underlying different sub-types of FOG and to determine the most optimal EEG montage for the development of a real-time FOG detection device during actual ambulation. Also, further testing of EEG processing will be performed to inform future treatment development in patients with PD.

1.3 THESIS OBJECTIVES

This thesis aims to develop a new methodology for understanding and detecting five sub-types of FOG (Turning FOG, Narrow FOG, Target FOG, Runway FOG and GIF) based on brain signals collected from PD patients during the performance of gait task. This thesis used Ag/AgCl scalp electrodes of a Biosemi ActiveTwo system to measure the EEG data from 32 electrodes positioned over main cortical regions. Using EEG, the cortical activity can be studied through the time-varying changes in certain spectral bands, allowing insights into the poorly understood neural mechanism of FOG.

The first objective of this thesis is to develop a computational intelligence method to understand and detect four sub-types of FOG, namely Turning FOG, narrow FOG, target FOG and runway FOG using EEG signals. Further, this research aims to determine the most optimal EEG montage for the identification of these subtypes of FOG using a 32-channel EEG system. Technically, we used input as Fast Fourier Transform (FFT) based featured extracted from every single channel to find the optimal EEG montage using Artificial Neural Networks (ANN) for FOG detection. This also allowed the most optimal montages to be used in the following research studies in this thesis to improve computation efficiency, robustness of the classification system and convenience for the use of ambulatory EEG by patients, as fewer sensors are required.

The second objective is to understand and detect another subtype of FOG named GIF, which occurs when patients are about to start walking (i.e., initiate the first step). An improved computational intelligence method will be addressed further to detect the episode of GIF. The method of GIF detection is based on classification algorithms such as Support Vector Machine (SVM) with the input of features based on the combination

of Independent component analysis by entropy boundary minimization (ICA-EBM) and Wavelet transform (WT). This research also aimed to explore whether the classification results could be detected with a small number of EEG channels such as two EEG channels to further improve patient convenience.

The third objective is to develop an advanced computational intelligence method for FOG detection to improve the accuracy of the system. This classification system was optimized by maximizing separation between signals using ICA-EBM for the advanced pre-processing technique. The features were extracted in S-Transform (ST) and Bayesian Neural Networks (BNN) optimized classification. Because Turning FOG and GIF are the most common triggers for freezing (Schaafsma et al. 2003), these subtypes were used to test this new method (ICA-EBM, ST, BNN).

1.4 THESIS CONTRIBUTIONS

The thesis builds on the project of understanding and detecting freezing of gait in Parkinson disease. The contributions of this thesis can be summarized as follows:

- Firstly, this research has investigated and discovered the abnormal changes of EEG signal underlying four sub-types of FOG and the ability to detect FOG based on optimal EEG montages. Using FFT as the feature extraction and a feed-forward neural networks as a classifier, the EEG data of FOG could be detected effectively in seven PD patients with FOG. Using an EEG system with fifteen channels provides accuracy results of around 70%. Further, this thesis was able to show that such accuracy could be obtained using only two input channels. Regarding the brain alterations, FOG episodes were found to be associated with significant increases in the high beta band (21-38Hz) across the central, frontal, occipital and parietal EEG sites. The study that shows the feasibility of using EEG approach in FOG detection is reported in (Ly et al. 2016).

- Secondly, this research utilized an EEG technique to investigate the dynamic brain changes underlying GIF episode and aims to detect the occurrence of GIF in four PD patients. This research studied the brain activity underlying GIF by analyzing WT of EEG signals. By implementing WT as input features with SVM as a classifier, the proposed system was able to detect GIF events with a classification performance of accuracy at 80.6%. Using ICA-EBM for EEG source separation, WT for feature extraction and SVM for classification, the correct identification of GIF episodes was improved with an accuracy of around 86.67%. The study that showed the feasibility of using this new approach in GIF detection is reported in (Ly et al. 2017b).
- Thirdly, this research presented a novel methodology for FOG detection where ICA-EBM for source separation, Stock-well Transform (ST) techniques for feature extraction and BNN for classification were used. The results of this analysis demonstrated the correct identification of two of the most provoking triggers of FOG (Turning FOG and GIF) with an accuracy of around 89%. These results suggest that our proposed methodology is a promising non-invasive approach to improve FOG detection in PD. The study that showed the feasibility of using this new approach in Turning FOG and GIF detection is reported in (Ly et al. 2017a).

1.5 THESIS OUTLINE

This thesis consists of six chapters, an appendix and references. The chapters of this thesis are organized as below:

Chapter 2 reviews literature associated with the FOG and its sub-types based on the Time Up and Go (TUG) tasks that are often used to study FOG (Snijders et al. 2012). This chapter covers the key fundamentals to the understanding of PD, including history, the

pathophysiology, especially related to gait movement and FOG, diagnosis and treatment. It then provides the category of five sub-types of FOG and the need to divide them into two main groups for further analysis (namely FOG that occurs during gait and FOG that occurs when initiating gait). After that, the scope is also narrowed to focus on the detecting strategies of these two groups of FOG, providing a brief outline of the proposed FOG detection strategy regarding the development of a classification system for detecting different sub-types of FOG during ambulation using EEG signal.

Chapter 3 illustrates the initial works on the detection of the first group, which includes the four subtypes of FOG that occur during gait, based on FFT for feature extraction. This study investigated periods of FOG (Turning FOG, Narrow FOG, Target FOG and Runway FOG) compared to periods of normal conditions (Good Turn, Good Narrow, Good Target, and Good Runway). Different EEG parameters in the form of Power Spectral Density, Centroid Frequency and Power Spectral Entropy (PSE) were extracted and analysed to find important features that were significantly changed during FOG compared to normal conditions. It is followed by the classification of the data for the detection of freezing using the artificial neural network. In addition, this chapter determined the most optimal montage of sensors to detect FOG amongst a 32-channel EEG system.

Chapter 4 presents the strategy of detecting GIF (the second group of FOG) where the freezing happens at the start of gait. This study compares GIF episodes with Good Start (GS) of gait initiation without GIF during several standardized TUG assessments. This research studied the brain activity underlying GIF by analyzing wavelet analysis (Wavelet Energy, Wavelet Centroid Scale, and Wavelet Energy Entropy) of EEG signals. The method of GIF detection is based on a combination of ICA-EBM for source separation, WT for feature extraction and SVM for classifier (ICA-EBM, WT, SVM).

Chapter 5 shows the strategy of developing a faster and better classification system for detecting two common sub-types of FOG including Turning FOG and GIF. Optimization

of the features was investigated using a combination of ICA-EBM for source separation and S-Transform (ST) as a feature. Optimization of the classifier was investigated by using Bayesian regularization in this chapter. The results of this study suggest that our proposed methodology (ICA-EBM, ST, BNN) is a promising non-invasive approach for improving classification accuracy during ambulation in PD patients.

Chapter 6 presents the overall discussion and conclusions and future direction for this research. The discussion covers the important finding of the brain pattern and different detection methods utilized in the study for all subtypes of FOG using EEG signal. The chapter ends with suggestions for possible directions for future work for real-time detection of FOG.

1.6 THESIS PUBLICATIONS

Conference papers:

- [1] **Ly, Q.T.**, Handojoseno, A.M.A., Gilat, M., Chai, R., Ehgoetz Martens, K.A., Georgiades, M.J., Naik, G.R., Tran, Y., Lewis, S.J.G. & Nguyen, H.T. 2017, 'Detection of Turning Freeze in Parkinson's Disease based on S-Transform Decomposition of EEG Signals', *Proceedings of the 39th Annual International Conference of the IEEE Engineering in Medicine and Biology Society 2017*, 39th Annual International Conference of the IEEE Engineering in Medicine and Biology Society, IEEE, July 11-15, Jeju Island, Korea, pp. 3044-3047

- [2] **Ly, Q.T.**, Handojoseno, A.M.A., Gilat, M., Chai, R., Ehgoetz Marten, K.A., Georgiades, M.J., Naik, G.R., Tran, Y., Lewis, S.J.G. & Nguyen, H.T. 2017, 'Detection of Gait Initiation Failure in Parkinson's Disease based on Wavelet Transform and Support Vector Machine', *Proceedings of the 39th Annual International Conference of the IEEE Engineering in Medicine and Biology Society 2017*, 39th Annual International Conference of the IEEE Engineering in Medicine and Biology Society, IEEE, July 11-15, Jeju Island, Korea, pp. 3048-3051

- [3] **Ly, Q.T.**, Handojoseno, A.M.A., Gilat, M., Nguyen, T.N., Chai, R., Tran, Y., Lewis, S.J.G. & Nguyen, H.T. 2016, 'Detection of Gait Initiation Failure in Parkinson's Disease Patients using EEG Signals', *Proceedings of the 38th Annual International Conference of the IEEE Engineering in Medicine and Biology Society 2016*, 38th Annual International Conference of the IEEE Engineering in Medicine and Biology Society, IEEE, August 16-20, Orlando, USA, pp. 1599-1602

- [4] **Ly, Q.T.**, Handojoseno, A.M.A., Gilat, M., Nguyen, T.N., Chai, R., Tran, Y., Lewis, S.J.G. & Nguyen, H.T. 2016, 'Identifying Montages that Best Detect the Electroencephalogram Power Spectrum Alteration during Freezing of Gait in Parkinson's Disease Patients', *Proceedings of the 38th Annual International Conference of the IEEE Engineering in Medicine and Biology Society 2016 EMBC*, 38th Annual International Conference of the IEEE Engineering in Medicine and Biology Society, IEEE, August 16-20, Orlando, USA, pp. 6094-6097

- [5] Handojoseno, A.M.A., Gilat, M., **Ly, Q.T.**, Chamtie, H., Shine, J.M., Nguyen, T.N., Tran, Y., Lewis, S.J.G. & Nguyen, H.T. 2015, 'An EEG Study of Turning Freeze in Parkinson's Disease Patients:The Alteration of Brain Dynamic on the Motor and Visual Cortex', *Proceedings of the 37th Annual International Conference of the IEEE Engineering in Medicine and Biology Society*, 37th Annual International Conference of the IEEE Engineering in Medicine and Biology Society, IEEE, August 25-29, Milano, Italy, pp. 6618-6621

Conference Abstract

- [1] **Ly, Q.T.**, Handojoseno, A.M.A., Gilat, M., S. J. Lewis, and H. T. Nguyen, "Ultilizing ambulatory EEG to explore Gait Initiation Failure in Parkinson's Disease", Australian Biomedical Engineer Conference 2015, November 22-25, Melbourne.

Chapter 2

Literature Review

2.1 PARKINSON'S DISEASE (PD)

Parkinson's disease is one of most common neurodegenerative diseases, affecting approximately 1-2% of the population aged over 60 years. Nearly 70,000 Australian who were reported as living with Parkinson's Disease in 2015; however, more recent research indicates that the actual prevalence is over 108,000 (Parkinson's Australia Submission 2017). Given the tendency that people live longer and that the risk of PD increases with age, the number of people with PD is expected to double by 2030 (Dorsey et al. 2007)

Since the early 1980s, PD has been identified as a degenerative disorder with abnormalities of movement, characterized by dopaminergic depletion in the nigrostriatal pathway (Agid et al. 1989). Dopamine is one of the neurotransmitters in the basal ganglia, which help transmit messages in the striatum to initiate and control movement. The dopamine system undertakes the responsibility to keep the muscles working smoothly. The substantial loss of dopamine in PD makes the muscles overly tense (i.e., rigidity),

causes slow movement (i.e., bradykinesia) and may cause resting tremor (Braak et al. 2004; Jankovic 2008).

PD patients suffered from motor and non-motor symptoms. Some non-motor symptoms such as sensory abnormalities, cognitive impairments, autonomic dysfunction and mood disorder are usually accompanying the patients after several years of PD (Caballol, Martí & Tolosa 2007; Chaudhuri, Healy & Schapira 2006). The motor symptoms by which a patient with PD is diagnosed are bradykinesia, resting tremor, rigidity as well as gait and balance impairments (Jankovic 2008). Bradykinesia or slowness of movement is recorded as the most characteristic feature of PD and observed during behaviors like rapid, sequential movement such as finger tapping. Resting tremor refers to unintended movements at high frequencies (4-6Hz) that mostly appear in the distal extremities. Rigid muscles often appear as an increased resistance to passive flexion, extension or rotation of the limb (Jankovic 2008). Importantly, "freezing" is also a major disabling problem in PD as it is a common cause of falls and injuries (Kerr et al. 2010) (Table 2.1).

Gait disturbance is a cardinal features of this disease and is characterized by short shuffling steps, reduced arm swing and freezing events (Jankovic 2008). The disorder of gait has a negative impact on several domains of activities in PD patient's daily life and causes falls and fall-related psychological issues. As the disease progresses, PD patients often develop FOG, which is described as a sudden inability to walk and patients often feel as though their feet have been 'glued' to the ground (Nutt et al. 2011). FOG often happens when patients are turning or are faced with obstacles, such as narrow doorways, reaching a target and sometimes during straight walking (Schaafsma et al. 2003). Furthermore, FOG can occur when patients initiate the first step, otherwise called gait initiation failure (Schaafsma et al. 2003). FOG is amongst the top symptoms that influence the quality of life (Walton et al. 2015). These disturbances of gait, especially FOG, respond poorly to current therapies and are associated with a high risk for falls and the need for institutional care (Bloem et al. 2004)

Table 2.1: Motor and non-motor symptoms in PD (Magrinelli et al. 2016)

Motor symptoms and signs	
Rest tremor	associated with frequency 4–6 Hz in a tremor; usually involves fingers and hands; sometimes in forearm pronation, jaw and leg.
Rigidity	increased muscle tone involved both flexor and extensor muscles
Postural instability	impaired postural adjustment due to decrease or loss of postural reflexes
Akinesia	reduction, delay, or absence of either voluntary, spontaneous, or associated movement
Hypokinesia	reduced movement amplitude, particularly with repetitive movements
Festination	involuntary gait acceleration with step shortening
Freezing of gait	difficulty in gait initiation (GIF) and unintentional paroxysmal episodes of the motor block during walking or turning.
Akathisia	the feeling of inner restlessness and strong need to be in constant motion associated with the inability to sit or stay still
Non-motor symptoms and signs	
Sensory abnormalities	a condition in which the brain has trouble receiving or interpreting information from the senses
Mood disorders	increased anxiety, apathy or depression symptoms
Cognitive impairment	especially executive dysfunctions, but with disease progression also increasing risk for Parkinson dementia

Moreover, Politis et al. (2010) and others have shown that gait disturbance does not only affect patient's daily activities but is also linked to other negative emotions, such as depression and anxiety (i.e., fear of falling), fatigue, which further decrease the quality of life (Schrag, Jahanshahi & Quinn 2000). This might be a barrier to perform physical activities and be another independent predictor for future falls (Dontje et al. 2013). Therefore, it is clear that novel treatment approaches are required.

2.2 FREEZING OF GAIT (FOG)

Freezing of Gait (FOG) is one of the primary features of gait disturbance in PD. It is a highly disabling symptom that affects approximately half of all Parkinson's disease patients, especially in the advanced stages of the disease (Nutt et al. 2011). Clinically, FOG is defined as a "*brief, episodic absence or marked reduction of forwarding progression of the feet despite the intention to walk*" (Nutt et al. 2011). It commonly occurs in complex environments that necessitate integration of multiple sensory stimuli (Moore, MacDougall & Ondo 2008). Therefore, it is typically seen during turning or going through narrow doorways, reaching a target and sometimes during straight walking (Schaafsma et al. 2003). Furthermore, FOG can occur when patients initiate the first step, otherwise called gait initiation failure (Schaafsma et al. 2003). Importantly, FOG is ranked as one of the symptoms most easily leading to falls and injuries because of its sudden and unpredictable nature, (Giladi & Nieuwboer 2008).

2.2.1 Characterizing of Freezing of Gait in PD

FOG can be characterized as three gait impairments (Giladi & Nieuwboer 2008): a complete akinesia (no limbs or trunk movement), trembling in place (no effective forward), and very small shuffling forward steps. In relation to the character of leg movement, FOG is characterized by four categories such as a profound and incremental decrease in stride length; a highly reduced joint ranges in the hip, knee, and ankle; disordered temporal control of gait cycles; and high-frequency alternate trembling-like leg movements (Nutt et al. 2011).

Based on contexts of behavioural measures in daily life, different types of FOG have been observed including: freezing when turning (Turning FOG-TF); freezing when getting through narrow doorways (Narrow FOG); freezing when reaching a target (Target FOG), freezing when performing dual-tasking; freezing when straight walking or freezing when initiating gait to start movement (GIF) (Schaafsma et al. 2003). Turning FOG appears to be the strongest provoking factor of FOG because it is a complex task that requires difficult inter-limb coordination (Gilat et al. 2015). GIF is followed as the second most common trigger to FOG (Giladi & Nieuwboer 2008) due to failure to initiate the gait (Figure 2.1). Moreover, Snijders et al. (2012); Spildooren et al. (2010) reported that 360 Turning FOG in combination with a dual-task (such as counting number, calling male/female name) is also the most important trigger to FOG.

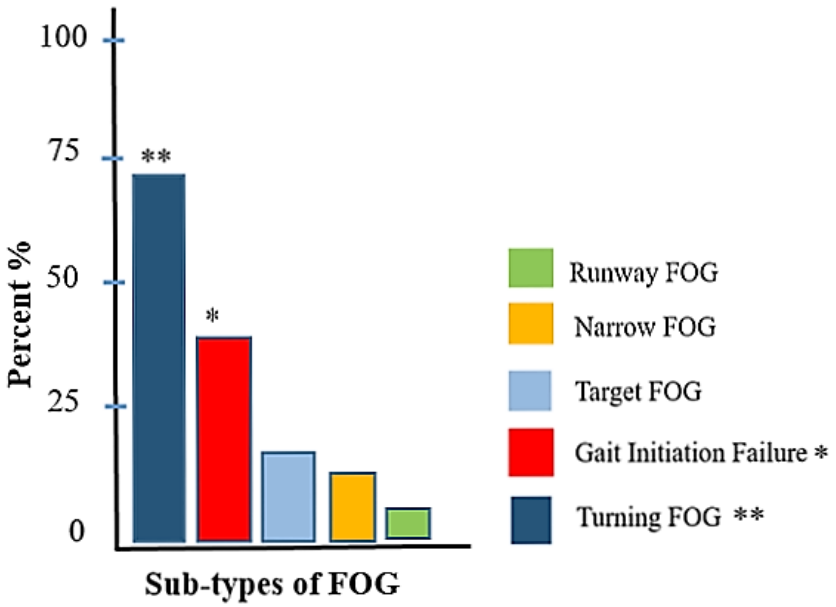

Figure 2.1: The Relative proportion of five sub-types FOG observed during the TUG trials. (Shine et al. 2012; Snijders et al. 2012)

Indeed, in our study to collect FOG data using EEG signals, Turning FOG is recognized to be the most frequent trigger of FOG, totalling 62.7% of all witnessed FOG episodes. Moreover, GIF is also voted as the second common form of FOG, with over 20% of all FOG episodes recorded as being a GIF (Shine et al. 2012; Snijders et al. 2012). These two triggers accounted for more than half of all witnessed FOG, compared to other sub-types of FOG. Therefore, these two common subtypes are selected to test the new advanced algorithm for FOG detection.

2.2.2 Sub-types of FOG

Based on previous research (Schaafsma et al. 2003; Shine et al. 2012), FOG can be distinguished into five sub-types in relation to their clinical situations in which they occurred. Moreover, depending on whether the patient was already walking or just about to start walking, FOG can be divided into two main groups. The first group includes four main subtypes of FOG in which the freezing episodes occurred while the patient was already walking or turning (Nieuwboer & Giladi 2013). These include Turning FOG, narrow FOG, target FOG and runway FOG. The second group is GIF, which considers the freezing episode occurred when the PD patients are just about to start walking. A description is provided below based on (Shine et al. 2012)

- Group 1: patient was already walking or turning

  (i) Turning FOG is the phenomenon in which one or both of the patients' legs failed to take a step during turning as part of all the routines.
  (ii) Target FOG is the phenomenon where FOG occurred upon the arrival to a defined target
  (iii) Narrow FOG is the freezing occurring during the navigation of a narrow portion of the routine (such as a doorway)
  (iv) Runway FOG is the freezing happening when PD experienced normal walking
- Group 2: patient just about to start walking

(v) Gait Initiation Failure (GIF) is the phenomenon where patients were unable to effectively initiate the first step at the start of a TUG task in any of the routines.

2.2.3 Brain location associated with FOG and GIF in PD

To better understand FOG, some research has identified the most affected areas of the brain underlying this phenomenon (Table 2.2). In fact, there are two approaches to investigate on FOG. The first approach studies used function Magnetic Resonance Imaging (fMRI) techniques to compare motor imagery of gait movement disturbances in PD patients (Georgiades et al. 2016; Gilat et al. 2015; Snijders et al. 2011). The second approach studies concentrated on characterizing FOG using Electroencephalography (EEG) signal techniques (Handojoseno, Shine, et al. 2015; Velu et al. 2014).

For fMRI approach, Bakker et al. (2008) revealed in the left and right superior parietal lobule, the right middle occipital gyrus and premotor cortex caudal was associated with FOG due to its increasing cerebral activity in PD patients that experience FOG. Amboni et al. (2008) focused on the executive functions of PD patients and found that FOG correlated with lower scores at frontal locations of early-stage PD patients. Snijders et al. (2011) reported the impact of the right superior parietal lobule underlying the episode of FOG when comparing the activity of motor imagery between walking and freezing in PD patients using fMRI. The frontal-parietal cortex has been noted by Crémers et al. (2012) as the brain location associated with FOG in PD patients because of decreased activity in the SMA being detected during mental imagery of gait.

Regarding the pathophysiology underlying freezing of gait, Shine, Matar, et al. (2013) reported cortical frontal and motor as well as basal ganglia associated with a change in blood oxygen level-dependent response during freezing of gait based on the data of 18 PD patients. These results provide novel insights into the pathophysiology underlying freezing of gait and lend support to models of freezing of gait that implicate dysfunction across coordinated neural networks. Vervoort et al. (2016) demonstrated the impairments between the inferior parietal lobule and premotor cortex (PMC) and between the caudate

and superior temporal lobe. In the combination of fMRI and virtual reality paradigm, Gilat et al. (2015) studied the neural correlates underlying turning episodes in PD patients with and without FOG. Interestingly, the activated inferior frontal regions and visual cortex activation were revealed as the implicated brain regions in PD patient with freezing during turning.

With the understanding that the occurrence of FOG has been related to these brain regions, there are several studies that used portable EEG signals to research actual FOG episodes. Shine, Moustafa, et al. (2013) has reported the motor (Cz) and fronto-parietal network known as the implication of FOG (Figure 2.2). Velu et al. (2014) used portable EEG focused on the occipital (Oz), parietal (P4) and motor (Cz) to examine how visual cues effected freezing across these regions. EEG result from the data of two PD patients suggested there was a significant relationship between visual feedback cues and an occipital-parietal-motor network in FOG. Handojoseno, Shine, et al. (2015) measured EEG power of 16 PD patients with FOG and showed that motor cortex and pre-supplementary motor area (pSMA) had been related to the episode of FOG. Handojoseno, Gilat, et al. (2015) used ambulatory EEG from data of four PD patients to investigate the brain dynamic changes associated with freezing of gait during turning. The occipital and parietal areas have been determined as the most suitable location underlying Turning FOG (Figure 2.3).

2.3 TREATMENT OF FOG

The medical treatment of FOG is complicated due to the multifactorial mechanism related to FOG, and that the pathogenesis of FOG is poorly understood (Nutt et al. 2011). Different stages of the disease and different sub-types of FOG likely need different strategies to treat FOG. Determining the right cue parameters is important for obtaining the best effect on FOG. Dopaminergic medication, rhythmical cueing on gait, exercise training and development of assistive devices have been shown as the compensation strategies to prevent or lessen FOG (Okuma 2014).

Table 2.2: The affected brain locations underlying FOG in PD

Authors	Subjects	Methodology	Affected brain regions
M. Bakker et al., (2008)	16 HC	fMRI on FOG	L Parietal; R Parietal
A.H. Snijders et al., (2011)	13 PD+FOG, 12 PD-FOG	fMRI & EMG on FOG	L Central; L, R, M Parietal; Frontal
J. Créemers et al., (2012)	15 PD , 15 HC	fMRI on FOG	L Central; L, R, M Parietal; L R Frontal
Shine, Matar, et al. (2013)	18 PD patients	fMRI on FOG	L Central; L, R, M Parietal; L R Frontal
D.S. Peterson et al., (2014)	9 PD+FOG; 9 PD-FOG	fMRI on FOG	R Central
J. Youn et al., (2015)	19 PD+FOG, 23 PD-FOG,	fMRI on FOG	M frontal; M central
Gilat et al. (2015)	17 PD+FOG, 10 PD-FOG	fMRI on Turning FOG	L motor; L parietal; L, R frontal; Occipital
Georgiades et al. 2016	54 PD, 15 HC	GIF	Frontal; Primary motor
Vervoort et al. (2016)	17 PD+FOG, 59 PD-FOG,	fMRI on FOG	Prefrontal; Premotor; Parietal
Wu & Hallett (2008)	15 PD, 14 HC	EEG on FOG	Cz
M. Sho et al., (2011)	20 HC, 20 PD	EEG on FOG	Cz
P.D. Velu et al., (2013)	2 PD+FOG; 6 HC	EEG, EMG on FOG	P4, Oz, Cz
J. B. Toledo et al.,2014	22 PD	EEG on FOG	C3, Cz, C4, F3,F4
Shine et al. (2014)	24 PD	EEG on FOG	Cz, Fz
Handojoseno, Shine, et al. (2015)	16 PD or 4 PD	EEG on FOG, Turning FOG	O1, P4, Cz, Fz Or O1, O2, P3, P4

L: Left; R: Right; M: Midline; HC: Healthy Control People; PD: Parkinson's disease Patient; PD+/-FOG: Parkinson's disease Patient with/without FOG;

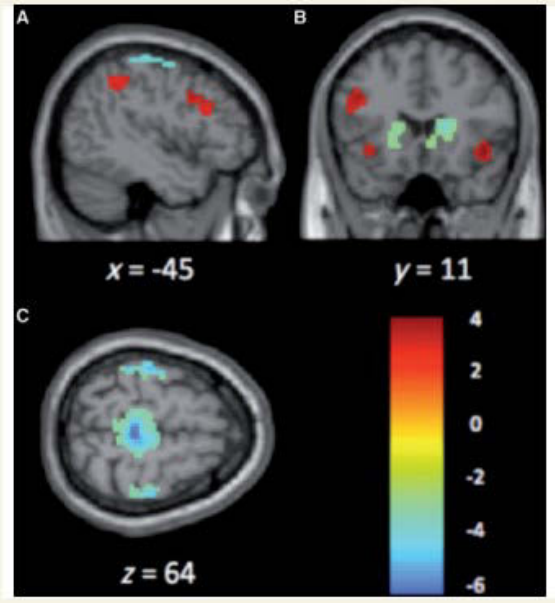

Figure 2.2: Comparison of BOLD activation and deactivation patterns during the contrast of the motor arrests and 'walking' using fMRI (Shine, Matar, et al. 2013)

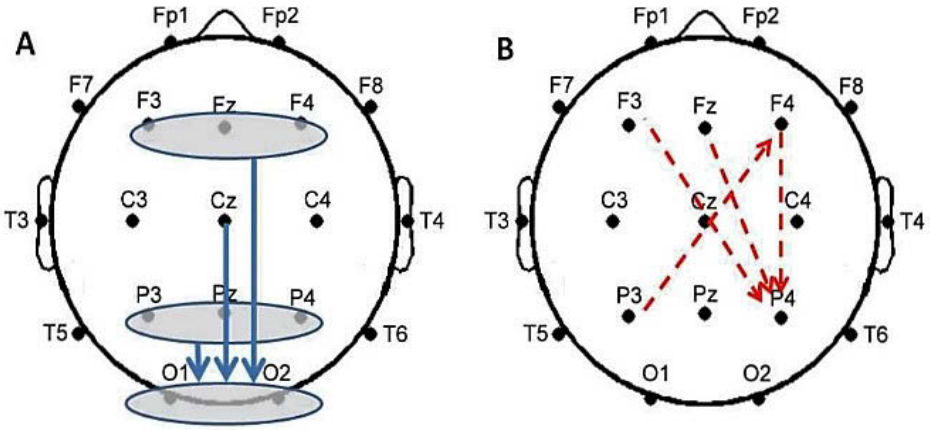

Figure 2.3: The regional analysis reveals an increase of information flow to occipital underlying Turning Freezing using EEG signals (Handojoseno, Gilat, et al. 2015)

2.3.1 Dopaminergic medication

Because widespread dopaminergic loss is a main feature of FOG and GIF, supplying dopaminergic replacement therapy has been chosen as the most effective treatment for PD and aims at restoring dopaminergic transmission. Overall, medication has been shown to improve bradykinesia of the limbs in PD patients (Vaillancourt et al. 2006). The extent of dopaminergic improvement in the treatment of FOG provided improvements in balance and gait tasks, led to faster walking velocity owing to longer steps (McNeely & Earhart 2013).

2.3.2 Cueing techniques

PD patients with FOG increased the length of stride when auditory cues are offered at based line frequency (Willems et al. 2006). Therefore, rhythmical cueing on gait has been chosen as a compensation strategy to break FOG episode in the form of a number of assistive devices. Indeed, specific cueing techniques using rhythmic auditory cues can reduce the severity of FOG by improving step length and walking speed (Nieuwboer 2008b). Over 30% of FOG events can be broken by visual cues when patients pay attention to each step, go upstairs or stamp their feet based on the light direction (Rahman et al., 2008).

Arias & Cudeiro (2010) reported the effect of auditory rhythmic stimulation in 19 PD patients when they performed several tasks in the presence of auditory sensory stimulation. The results showed the existence of auditory rhythmic stimulate could significantly reduce FOG in freezers with 10% compared with the case without cueing. Impressively, auditory stimulation at the frequency proposed has been concluded to avoid freezing episodes in a patient with FOG. However, when the frequency of auditory cueing is too high, patients with FOG do not improve their walking. In addition, cueing is known to lose its beneficial effect over time when constantly applied.

2.3.3 Exercise training

Exercise is known as physical activities that enhance or maintain health in people's lives. It is important to note that addressing balance impairments in PD patients can be solved by training exercise. According to the guideline for Parkinson's disease in the European Physiotherapy, exercise is more likely to be affected directly by the impairment of balanced control in PD such as training them how to walk through a corridor or a narrow door. The regular practice of this movement in PD patients can improve the fluency of motor skills, original motor skills or motor learning skills, which lessen the appearance of FOG in PD.

2.3.4 Assistive devices

To improve the function of non-medication approach, research designed several assistive devices to support the PD patient such as canes or walking sticks, walkers and wheelchairs.

U-step laser walker with a laser beam between the rear is known as one of the useful devices help the patient to overcome FOG or GIF episodes in some patients (Lisette Bunting-Perry PhD et al. 2013).

Furthermore, the combination of a laser light cue with a walker has been confirmed to improve freezing and has been commercialized (Okuma 2014). Janssen et al. (2017) investigated the usability of three dimensions (3D) augmented visual cues delivered by smart glasses in reducing the occurrence of FOG, the percentage of time spent on FOG, and the variability of stride length and cycle time. However, this 3D method did not improve FOG (Figure 2.4).

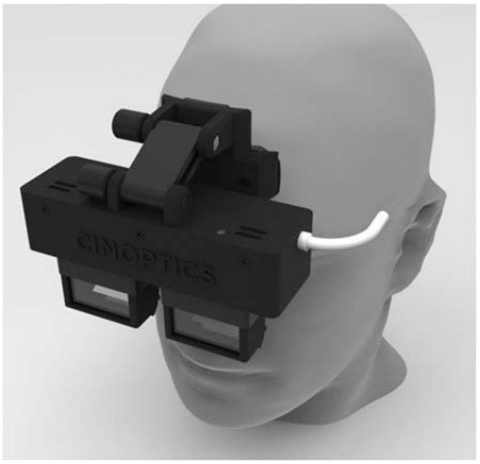

Figure 2.4: A Model of custom-made smart glasses allowing augmented reality visual cues when FOG happened (Janssen et al. 2017)

2.4 CURRENT STRATEGIES FOR FOG DETECTION

FOG has been known to be associated with trembling of the legs. Therefore, there are recent studies using wearable sensors such as accelerometers, goniometers to measure movement signal of the leg as an indicator of FOG detection (Table 2.3 and 2.4). To achieve the best performance, the most effective system also focused on the design of type of sensors, number of sensors, location of the sensors on the body. Sensors were positioned on the shin, waist, chest, insole, lower back and head of the patients to detect FOG (Rodríguez-Martín, Samà, Pérez-López, Català, Arostegui, et al. 2017). There are three approaches to detect FOG in PD. The first approach concentrates on frequency analysis of leg movement. Tri-axial accelerometers, gyroscopes or magnetometers were attached to the body location to measure signals associated with trembling of the leg during FOG events (Moore, MacDougall & Ondo 2008). The second approach is based on the alteration of ECG signal and skin conductance signal of PD patients underlying FOG (Mazilu et al. 2015). The third approach is currently based on the detection of EEG signal to measure changes in the brain activity within FOG episodes (Handojoseno, Shine, et al. 2015).

Table 2.3: **Overview of methods of selected FOG Detection studies (Rodríguez-Martín, Samà, Pérez-López, Català, Moreno Arostegui, et al. 2017)**

Work	PD	Methods	S	Location	Significant results
Rodríguez-Martín et al. (2017)	21	accelerometer	1	waist	sensitivity (74.7%) specificity (79%)
Pham et al. (2017)		accelerometers	3	shank,thigh,lower back, ankle	sensitivity (94%), specificity (84%)
Ahlrichs et al. (2015)	8	accelerometers	1	waist	accuracies >90%
Maidan et al. (2015)	11	infrared spectroscopy	1, 1	head	haemoglobin changed before FOG
Handojoseno et al. (2015)	16	EEG	4	head	sensitivity (86.0%), specificity(74.4%)
Weiss et al. (2015)	28	accelerometer	1	lower back	gait parameters between freezers, non-freezers
Tay et al. (2015)	8	gyroscope	2	waist	variability in gait parameters
Mazilu et al. (2015)	18	ECG	1	chest, fingers	71.3% of success
RodrõÂguez et al. (2014)	10	accelerometer	1	waist	improvement of 5% in specificity
Coste et al. (2014)	4	accelerometer	1	ankle	approach to detect pre-FOG
Djuric-Jovici et al. (2014)	12	accelerometer gyroscope		shin	sensitivity, specificity (>99%)
Takac et al. (2013)	1	depth Sensor accelerometer	1, 1	waist	0.16 m error (RMSE) for human body orientation

PD: number of PD patients
S: number of sensors

Table 2.4: **Overview of methods of selected FOG Detection studies (Rodríguez-Martín, Samà, Pérez-López, Català, Moreno Arostegui, et al. 2017)**

Work	PD	Methods	S	Location	Significant results
Moore et al. (2013)	25	accelerometers	7	lower back, thigh, shank, l	sensitivity, specificity (>70%)
Tripoliti et al. (2013)	5	accelerometers, gyroscopes	6, 2	shank, wrist, chest, abdomen	accuracy (96.11%)
Mazilu et al. (2013)	10	accelerometers	3	shank, thigh, lower back	better performance
Zhao et al. (2012)	8	accelerometers	5	shank, thigh, lower abdomen	sensitivity (81.7%)
Mazilu et al. (2012)	10	accelerometers	3	shank, thight, lower back	sensitivity, specificity (>95%)
Cole et al. (2011)	10	EMG and accelerometers	1, 3	shin. thigh and forearm	sensitivity(83%); specificity(97%)
Niazmand et al. (2011)	6	accelerometers	5	shank, thigh, lower abdomen	sensitivity(88.3%); specificity(85.3%)
Maidan et al. (2010)	10	ECG, insoles, accelerometer	2,2	chest, insole at shoe.	heart rate evolution during FOG
Delval et al. (2010)	10	goniometer, video system	2	knee	sensitivity (75–83%), specificity (>95%)
Jovanov et al. (2009)	2	accelerometers	6	ankle, knee, thigh	the algorithm in real time with fast response
Daphnet (2009–2011)	11	accelerometer	1	left ankle	sensitivity (73.1%), specificity (81.6%)
Zabaleta et al. (2008)	10	accelerometer	1	knee	accuracy (82.7%)
Moore et al. (2008)	11	insole pressure	1	insole at the shoe	accuracy (89.1%)
Han et (2003)	2	accelerometers	2	ankle	frequency response from 6-8Hz in a FOG episode

2.4.1 Measure leg/knee oscillations for FOG detection

Han et al. (2003) used accelerometers to measure the ankle movement underlying FOG from data of two PD patient. This study found a response from patients wearing accelerometers at the ankle associated with the frequency around 6-8Hz. Han et al. (2006) continued their preliminary work by applying 3-dimensional accelerometer with foot pressure system to monitor abnormal activity such as toe-walking and slowness of the patient's movement and a camcorder for observing gait detection.

To detect FOG, Moore, MacDougall & Ondo (2008) used an ankle-mounted sensor array attached to left shank transmitted data wirelessly to a pocket PC at a rate of 100 Hz. A freeze index (FI) was introduced in this study; which calculated by the division of the power in the 'freeze' band and the power in the 'locomotor' band (0.5–3 Hz).

Hausdorff et al. (2003) used two sensors located under the heel and the balls of the feet; placed in the patient's shoe. The data from both sensors were combined before recording to measure the severity of FOG. Djuric-Jovicic et al. (2014) published a proposed method to detect FOG based on data obtained from a 3-D accelerometer, 3-D gyroscope placed laterally along the shank segment of each leg from 12 PD patients.

Mazilu et al. (2016) used wrist-mounted inertial sensors to collect data from eleven PD patients. The sensors were attached to both wrists and both ankles of patients in order to monitor upper limbs movements and detect FOG. Rodríguez-Martín, Samà, Pérez-López, Català, Moreno Arostegui, et al. (2017) used a single tri-axial accelerometer worn at the waist of twenty-one PD patients to evaluate FOG episode at home.

Pham et al. (2017) used three tri-axial accelerometers attached to the shank, thigh, and lower back of the patients using elasticized straps. The data was recorded at 64 Hz, transmitted via a Bluetooth link, and used for FOG detection (Figure 2.5).

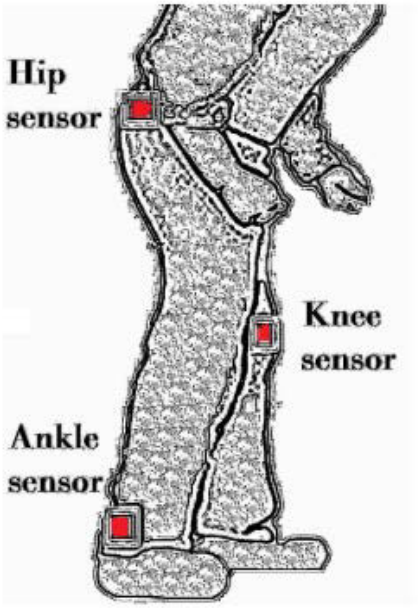

Figure 2.5: Three tri-axial accelerometers were attached to the shank, the thigh, and the lower back (Pham et al. 2017).

2.4.2 Measure ECG signal for FOG detection

To test the hypothesis that heart rate was associated with FOG, Maidan et al. (2010) utilized the ECG data signal from 20 PD with FOG and without FOG in his experiment. Heart rate was measured when patients performed tasks and frequently provoke FOG. The finding showed that heart rate increases during FOG and further increases just prior to FOG based on 120 FOG episodes. Interestingly, present results provided experimental evidence linking between autonomic nervous system and FOG in PD.

Essentially, Mazilu et al. (2015) analysed ECG and skin-conductance (SC) data from 11 PD subjects experienced FOG in their daily activities. Compared to normal walking, ECG was found to change significantly just before the FOG episodes. These significant patterns were used to predict FOG with an accuracy of 71.3% and to help user avoid the gait freeze by external cues (Figure 2.6). However, Mazilu's study was not able to build

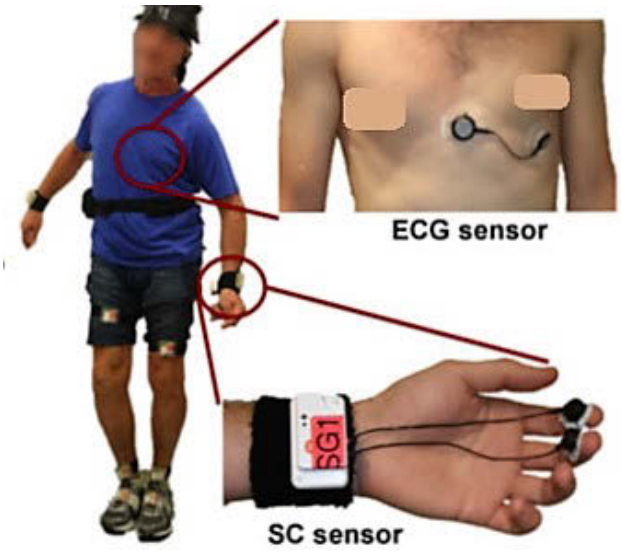

Figure 2.6: FOG detection system with a focus on the ECG and EC sensor systems (Mazilu et al. 2015)

a FOG-prediction model from ECG data because ECG features might not only correlate to FOG, but it could come from the noise associated with ECG from sudden movements of the body during different walking events, e.g. during turning. Furthermore, the sympathetic response captured by ECG may only be associated with FOG in PD patients with a high level of anxiety (Martens, Ellard & Almeida 2014)

2.4.3 Measure EEG signals for FOG Detection

EEG is the electrical potential of brain activity recorded by using electrodes placed on the scalp (Wolpaw et al. 2002). The EEG signal on the scalp is within the range 5-300 μV and the commercial EEG electrodes are usually made from silver/silver-chloride (Ag/AgCl). These scalp electrodes are sensitive for picking up the mixed activity of a large population of neurons, rather than the activity of a single neuron. To keep a good electrical contact in the process of measuring EEG signal, the electrodes are required to have proper connection with the scalp in the specific regions of the brain. The conductive gel is taken to make the electrode wet before the measurement. In fact, there are several artefacts known as non-brain physiological sources (heart activity, eye movements,

muscle activity) which could affect the EEG recording. A power line noise (50/60 Hz) can also contaminate the EEG signal. For these reasons, it is suggested that artefacts be removed from the raw EEG signal before analysing. To conduct measurements with the EEG system, electrodes will be placed on the scalp with even numbered electrodes on the right side and odd number electrodes on the left side of the head.

From 2012 to 2015, Handojoseno et al. (2012) studied the EEG data from sixteen PD patients with significant FOG to detect FOG. EEG data were collected from UTS with sensors located at occipital one (O1-primary visual receiving area), parietal four (P4-navigational movement area), central zero (Cz-primary motor area) and frontal zero (Fz-supplementary motor area) (Figure 2.7). This study demonstrated the potential of the EEG features extracted in both time and frequency domain giving more insight into the pathophysiology of FOG in PD. However, different aspects of the EEG signal, when combined, may provide more significant information, leading to a better classification of the EEG signal.

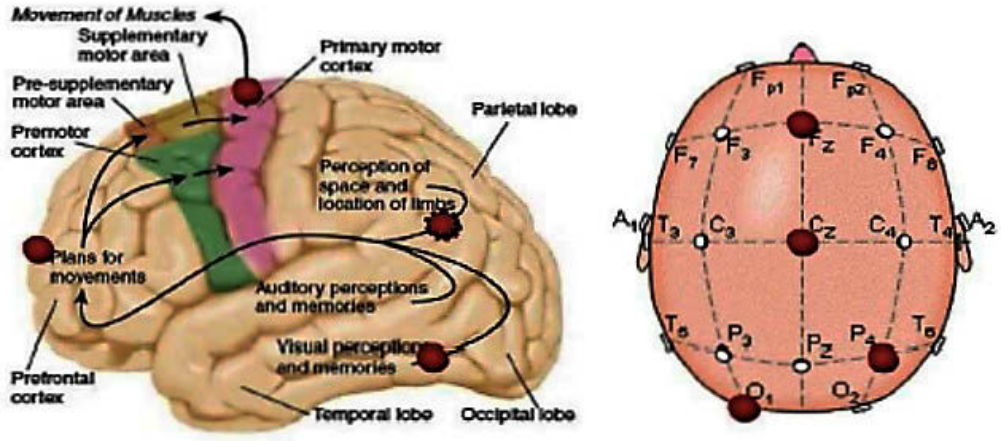

Figure 2.7: Four electrodes related to cortical control of movement in FOG detection system (Handojoseno et al. 2012; Handojoseno, Shine, et al. 2015)

2.4.4 Review on current Computational Intelligence for FOG Detection

Computational intelligence is a fundamental component for FOG detection system in PD. After data is measured from different sensors attached to the PD patients, this is followed by the computational intelligence, including feature extraction block to extract the important features underlying FOG and a classification block to classify the feature vector to detect FOG.

Similar to clinical observations, Han et al. (2003) could detect FOG using two biaxial accelerometers from 2 patients with FOG. Their study found that freezing has a higher main frequency acceleration (6-8Hz) compared with a normal gait (2Hz). Then, FOG, normal gait and resting state were classified by the authors based on the comparison of the wavelet power level on different frequency bands. The group continued their preliminary work by developing the wearable activity monitoring system using a 3-dimensional accelerometer with foot pressure system, and a camcorder for the reference of gait detection (Han et al. 2006). They developed a general gait detection algorithm beyond FOG to detect any abnormality, such as toe-walking and slowness. Based on the subsequent evaluation of gait signal parameter, it has detection accuracies of 94% and 93% for normal and PD gait, respectively.

Zabaleta, Keller & Marti Masso (2008) were able to detect correctly 82.7 % of the FOG episodes based on the significant PSD features during FOG from inertial sensors located at each patient's ankle. Niazmand et al. (2011) employed the hybrid approach which consists of three algorithms for detecting FOG achieving an 88.3% on sensitivity and 85.3% on specificity in 6 PD patients. Tripoliti et al. (2013) used four classification algorithms: Random Tree, Random Forest, Decision Trees and Naïve Bayes in the detection of FOG. The Random Forest classifier was proved as giving the best classification result, with sensitivity (81%), specificity (98%) and accuracy (96%).

Djuric-Jovicic et al. (2014) published a novel method for FOG detection based on the two sections such as the selection of representative stride and the estimation of gait parameters (duration, spectrum, change of orientation and displacement). This proposed method identifies the episode of FOG with excellent results in the range of sensitivity 78% to 100% for the FOG with trembling or completion motor blocks. Mazilu et al. (2012) evaluated a number of supervised classifier algorithms such as Random Forest, C4.5 Decision Trees, Naïve Bayes, multilayer perceptron to detect FOG. Results from 10 PD patients obtained showed higher specificity and sensitivity, with nearly 90%. To continue his work, FOG episodes from data of eleven PD patients were collected and such freezing episodes can be detected by using wrist motion and current machine learning models with an improvement of 95% specificity (Mazilu et al. 2016).

Handojoseno, Shine, et al. (2015) examined 16 PD patients with significant FOG. This research explored and detected FOG based on the various features of EEG, which can be used as indicators of FOG and aimed to introduce the effective features as inputs for the FOG. Importantly, the most effective features achieving the highest performance in EEG study were extracted in the time-frequency domain (wavelet transform). When predicting FOG episode, the classifier resulted in a sensitivity of 86.0%, specificity of 74.4%, and accuracy of 80.2%.

Currently, Rodríguez-Martín, Samà, Pérez-López, Català, Moreno Arostegui, et al. (2017) present a new algorithm to detect FOG with machine learning approach based on Support Vector Machine. Results obtained a mean sensitivity of 84% for detecting FOG at the patient's home, which seems to be significant enough to evaluate FOG. Pham et al. (2017) developed an automated FOG detector for subject-independent. The system applied an anomaly score detector (ASD) with adaptive thresh holding to detect FOG events. The results achieved an improved performance in the classification with a sensitivity of 94% for ankle as an indicator and 89% for back sensors indicator.

2.5 DISCUSSION AND PROPOSED STRATEGY

Because PD is a neural disorder, the brain is the first affected organ. Therefore, both the invasive (DBS) and non-invasive (fMRI, EEG) approaches have been popularly applied in several FOG studies to understand brain mechanism underlying PD. The invasive method requires surgery on patients with obvious disadvantages for safety and the DBS can only provide information of one brain region that is targeted. For the non-invasive methods, these approaches have been ultilized as the common way to understand the brain activities underlying FOG because it is safer for patients and is able to investigate larger areas of the brain involved with FOG. Table 2.5 shows the advantages and disadvantages of FOG detection methods.

Compared to EEG, the neuroimaging techniques, such as fMRI, cannot measure actual FOG in the clinical environment because patients cannot walk inside the scanner to trigger FOG. EEG allows for the investigation of the cortical neural mechanism underlying actual FOG and can be applied in real life environments. As such, this thesis used ambulatory EEG to investigate FOG.

Most of the existing research has used ‘body-worn’ sensors (such as accelerometer, gyroscope, goniometers or ECG sensors) to detect FOG in PD. Compared with these ‘body-worn’ sensors, the advantage of EEG is the ability to measure the earliest onset of FOG in the brain which is the root of FOG. Detecting FOG using ECG provides a sub-optimal time window, whereas EEG records the onset of FOG from where it originates, namely the brain itself. Therefore, EEG can detect FOG quicker than “body-worn” sensors due to the time that the neural signal travels to control the legs. Also, researches using “body-worn” sensors could not detect FOG by different walking styles seen in PD patients such as the complete motor block associated with FOG (Mazilu et al. 2012; Moore, MacDougall & Ondo 2008; Niazmand et al. 2011).

Table 2.5: Overview FOG detection methods, their advantages and disadvantages

Methods	Advantages	Disadvantages
Accelerometers (Han et al. 2006)	portable and wearable fewer artefacts good temporal resolution	not measure brain for medical treatment not identify the episode of motor block
Insole pressure (Moore, MacDougall & Ondo 2008)	portable and wearable reasonable estimate of the duration of stride non-invasive good temporal resolution	not measure brain for medical treatment artefacts interference not identify the episode of motor block
Gyroscope (Delval et al. 2010)	fast and simple to use measure relative orientation on three axes	not measure brain for medical treatment not identify the episode of motor block
Accelerometer Gyroscope (Djuric-Jovicic et al. 2014)	portable and wearable identify the episode of GIF good temporal resolution	not measure brain for medical treatment not identify the episode of shuffle freezing because of the stride length threshold
ECG and Skin Conductance (Mazilu et al. 2015)	good temporal resolution	not measure brain for medical treatment artefacts interference not identify the episode of motor block
EEG (Handojoseno, Shine, et al. 2015)	non-invasive good temporal resolution portable and wearable low cost identify the episode of motor block measure brain for medical treatment	artefacts interference identify the episode of FOG in general not separate the specific sub-types of FOG

For the instrumentation point of view, portability and convenience are important aspects of a FOG detection system. Previous research used four EEG channels preselected based on theory to detect FOG (Handojoseno, Shine, et al. 2015). However, it remains unclear whether these four channels are indeed the most sensitive locations for FOG detection and prediction. As such, this thesis will use 32 channels of EEG positioned over the cortex to detect the most optimal montages. However, a disadvantage of using many channels is that it contributes to the complexity of the instrumentation and likely becomes inconvenient to use by patients on a daily basis. Therefore, using a lower number of EEG channels is important, but the most optimal montage needs to be determined based on data. This would improve portability, convenience, and effectiveness of the system. Therefore, this thesis aims to determine the best montages and the most effective number of channels for detecting FOG using EEG signals among 32 channels.

With regards to the comparison of computational intelligence, several proposed classification algorithms can obtain excellent results with a sensitivity ranging from 95% to 100% for the detection of FOG using 'body-worn' sensors (Djuric-Jovicic et al. 2014; Pham et al. 2017). Online system to identify FOG episode has been proposed using power spectrum, Spatio-Temporal Stride Parameters and Rule-Based classification (Djuric-Jovicic et al. 2014). This system has obtained the sensitivity 100% for FOG detection, using 'body-worn' sensors. However, one of its weaknesses is the error rate achieved up to 16 % in the classification of normal episodes such as standing. Further, an automated FOG detector for subject independence was developed using spectral coherence, Koopman spectral analysis, and intra-class correlations (Pham et al. 2017). This research achieved an improved classification performance with sensitivity, specificity of 94% for FOG indicator. However, it failed to detect FOG in another out-group patient where it reached only 58 % specificity.

Our previous research has used EEG signal to study cortical activities in particular spectral bands and specific location underlying FOG and the transition (5 seconds before FOG) to FOG(Handojoseno, Shine, et al. 2015). This study identified an increase of theta

sub-band activities in the frontal and motor cortex in the transition to FOG episode and was able to detect FOG with sensitivity around 80% (Handojoseno, Shine, et al. 2015). However, these previous studies have focused on episodes of freezing in general without classifying specific sub-types of FOG, potentially limiting its clinical accuracy. Also, they used the predefined four channels. Therefore, there is a need to detect different sub-types of FOG and develop the most optimal montage.

The advantages of EEG is that it is a portable, convenient and safe method that is able to measure actual FOG quicker than "body-worn" sensors. This thesis, therefore, used EEG signal to understand and detect FOG in PD. Overall, the improvements of this research are: (1) collecting EEG data from 32 channels to further explore the neural basis of FOG; (2) dividing sub-types of FOG into two main groups and (3) developing advanced computational intelligence for FOG detection. To assist with the clinical translation, a limited number of EEG channels need to be determined based on our EEG data, which would also improve portability and convenience.

This thesis proposes a new system for detecting FOG using EEG signals. The proposed FOG detection is presented in Figure 2.8. In general, the input of FOG detection is EEG features, which are fed to the classifier which has the output of either FOG or normal states in PD. This thesis focuses on the improvement of pre-processing techniques, feature extracting and classifiers algorithms for the FOG-based EEG detection. Specifically, the advanced pre-processing technique applied is ICA-EMB for improving classification. The feature extractor using frequency (Fast Fourier Transform) and time-frequency (Wavelet Transform, S-Transform) analysis are applied in this thesis. This thesis explores using different classification algorithms, which include Artificial Neural Networks, Support Vector Machine and Bayesian Neural Networks.

This study is one of a small number of original studies in the world to look into the classification and prediction of FOG using real-time EEG signals, so there are not many relevant clinical data available in the literature. Essentially, the method are being

developed the real-time strategies to detect and to predict FOG in the PD patients from the clinic at the Prince Alfred Hospital. Further validation involving a large number of patients in different environments is required before translating our research into a practical and effective FOG detection system. In the near future, we will collaborate with other clinics around the world to improve our detection algorithms collectively.

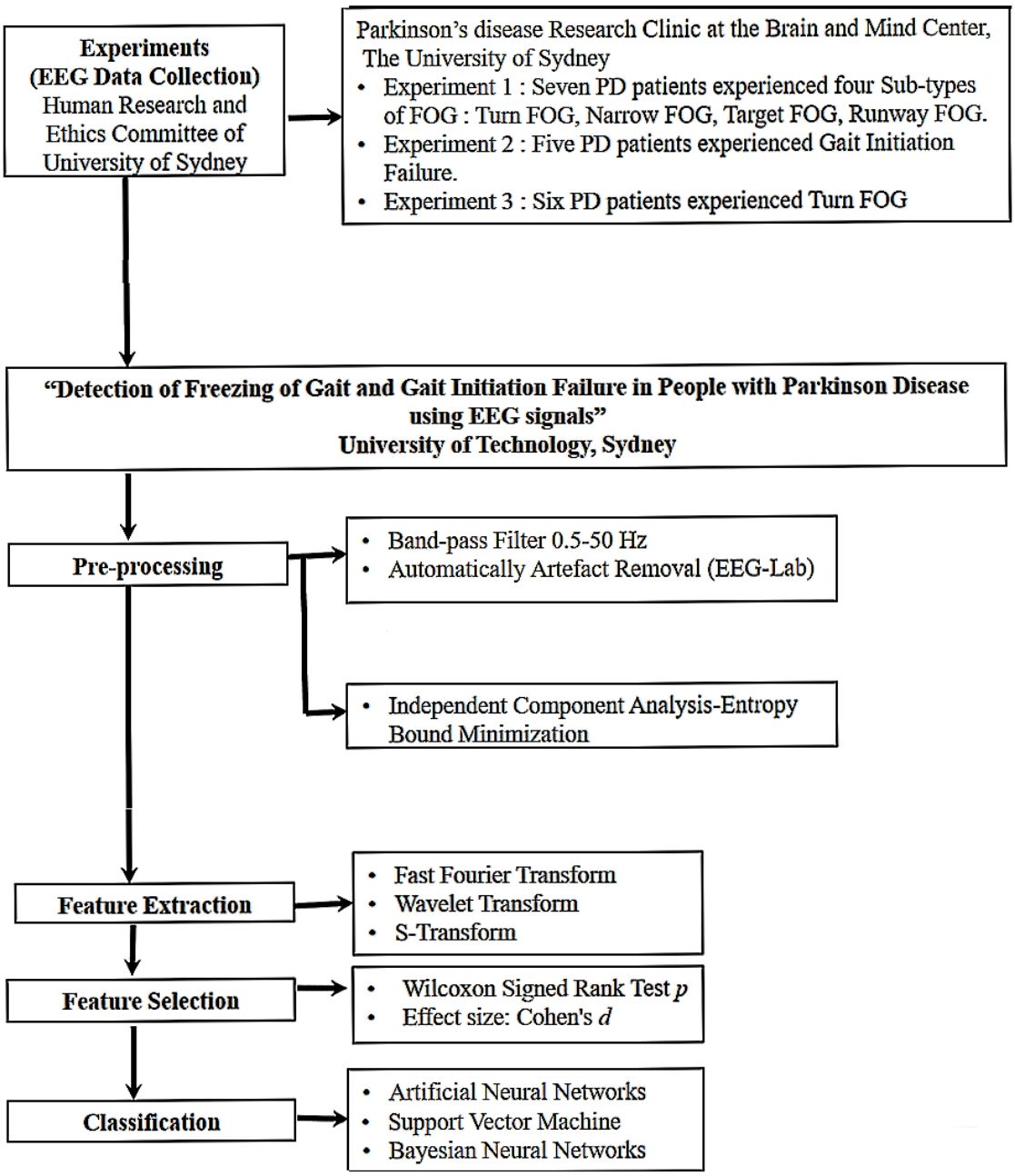

Figure 2.8: Overall EEG-based FOG detection in this thesis

Chapter 3

Detection of Freezing of Gait using EEG and Artificial Neural Networks

3.1 INTRODUCTION

As discussed in chapter 2, FOG was divided into two groups based on whether the PD patient was walking or just starting walking. The first group considers four sub types of FOG which occurred when the patient was already walking. They include Turning FOG, Target FOG, Narrow FOG, and Runway FOG. The second group has gait initiation failure (GIF). This chapter focuses on the detection of the first group compared to the periods of normal conditions (Good Turn, Good Narrow, Good Target and Good Runway). The second group (GIF analysis) will be explored in Chapter 4. For comparison with FOG, the normal conditions were defined by effective forward progression of the feet during

gait, hereafter called 'Effective walking' (EW). The core objectives of this chapter are (1) to build up a computational framework for detecting the episode of FOG; (2) to determine the most optimal locations amongst a 32-channel EEG montage.

For the computational intelligence methods, a Fast Fourier Transform (FFT) algorithm is used as feature extraction in this work. FFT is the most popular method for EEG based feature extraction strategy as it converts the time domain EEG signal into a frequency spectrum. For the classification, artificial neural networks (ANN) was investigated. The ANN as non-linear classification algorithm has been widely used in biomedical applications, especially dealing with EEG signal which contains non-linear and non-stationary properties. The task is on the basis of the measured features, which are extracted from seven patients with PD and FOG during a series of Timed up and Go tasks.

In this chapter, EEG features, including power spectral density, centroid frequency, and power spectral entropy, were used for FOG detection. A feed-forward neural networks with the Levenberg-Marquardt algorithm applied to train the neural network to classify EEG data will be explored. The input of ANN classification consists of the mean, maximum and minimum values of PSD, CF, and PSE which are extracted from EEG signals based on four EEG frequency bands such as theta, alpha, low beta and high beta. The desired output was set at 1 in cases of FOG and 0 in cases of EW. The obtained results showed that even a small number of electrodes suffice to construct a FOG detector with expected performance, which is comparable to the use of a full 32 channels montage. This finding, therefore, progresses the realization of a FOG detection system that can be implemented efficiently on a daily basis for FOG prevention, improving the quality of life for many patients with PD.

3.2 SYSTEM OVERVIEW

The development of FOG detection model based on ANN approach is presented in Figure 3.1.

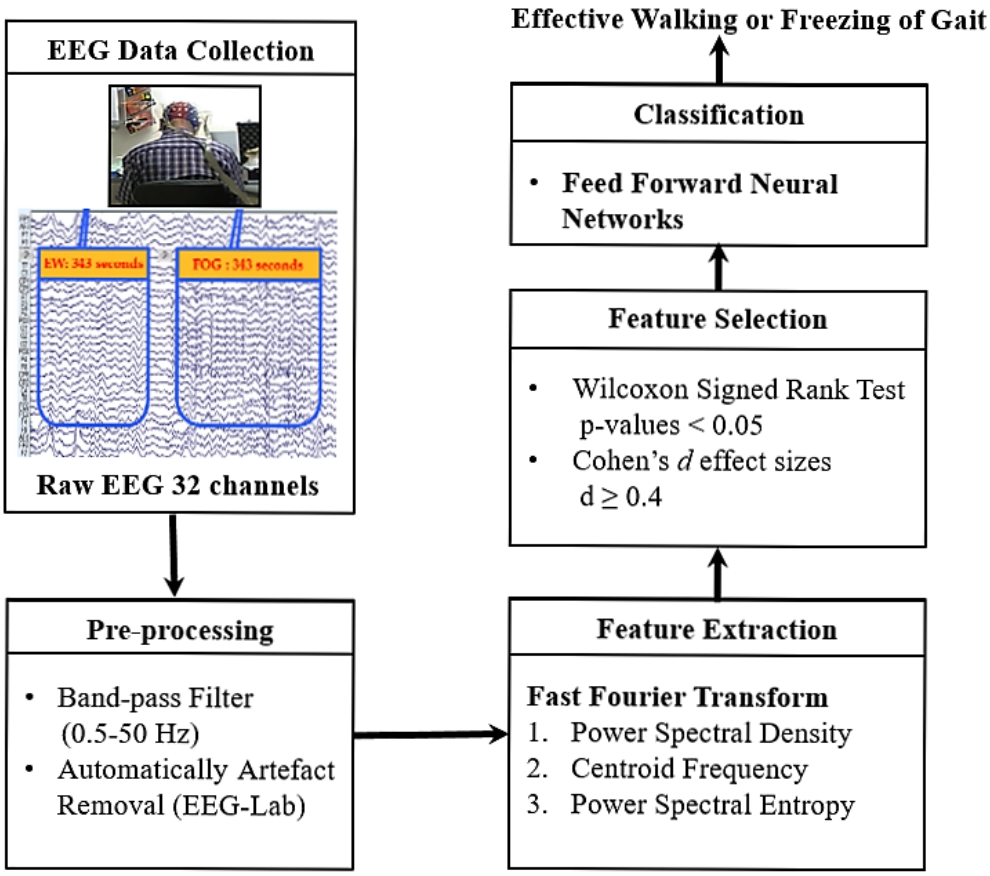

Figure 3.1: Components of EEG-based FOG detection system

There are five main components in the strategy, including EEG data collection, pre-processing, feature extraction and ANN classification. The specific function is elaborated in the following:

- EEG data collection: the brain activity of the PD patient was recorded by using 32 Ag/AgCl scalp electrodes from a Bio-semi ActiveTwo system with the 32 electrodes. The brain signal EEG being measured was amplified, digitized and transmitted for further signal processing.

- Pre-processing: Band-pass filtering and artifacts removal algorithms were applied for enhancing the raw EEG signal.
- Feature extraction: Different EEG parameters in the form of Power Spectral Density (PSD), Centroid Frequency (CF) and Power Spectral Entropy (PSE) were extracted and analyzed to find important features that were significantly changed during FOG
- Feature selection: Wilcoxon Rank Sum Test was used to investigate the significant difference of feature PSD, CF, and PSE between EW and FOG.
- Classification: the significant features from each single channel were then employed as inputs for neural networks to classify patients' conditions during two stages: EW and FOG.

3.3 STUDY, DATA COLLECTION

3.3.1 Study

This study was approved by The Human Research and Ethics Committee, University of Sydney. EEG data were obtained from seven Parkinson's disease patients (six males, one female) with clinically confirmed FOG. They were recruited from the Parkinson's disease Research Clinic at the Brain and Mind Centre, The University of Sydney. These patients were assessed in their practically-defined 'off' state following overnight withdrawal of dopaminergic therapy. The PD patients experienced multiple episodes of FOG during a structured series of Timed Up and Go tasks (walking, turning, going through a narrow doorway and reaching the target).

All patients completed Mini-Mental State Examination (MMSE) (Folstein, Folstein & McHugh 1975). They also underwent a neurological assessment including Movement Disorders Society-Unified Unified PD Rating Scale (UPDRS), Hoehn and Yahr stage (H&Y), and Freezing of Gait Questionnaire (FOGQ) to determine the stage of the disease (Shine et al. 2012).

3.3.2 Data Collection

EEG data was acquired using 32 Ag/AgCl scalp electrodes from a Biosemi ActiveTwo system with the 32 electrodes positioned over the main cortical regions: frontal (motor planning and working memory), central (motor execution), parietal (sensory integration) and Occipital (visual area) (Figure 3.2). These electrodes are over the following specific locations such as:

- Frontal region: FP1, FP2, AF3, AF4, F7, F3, Fz, F4, F8, FC5, FC1, FC2 and FC6.
- Central region: C3, Cz, C4, CP5, CP1, CP2, and CP6.
- Parietal region: P7, P3, Pz, P4, and P8
- Occipital region: O1, O2, and Oz.

The notations are F (frontal), C (central), P (parietal), O (occipital) and z (midline). References were taken by averaging two electrodes placed on the ear lobes. Technically,

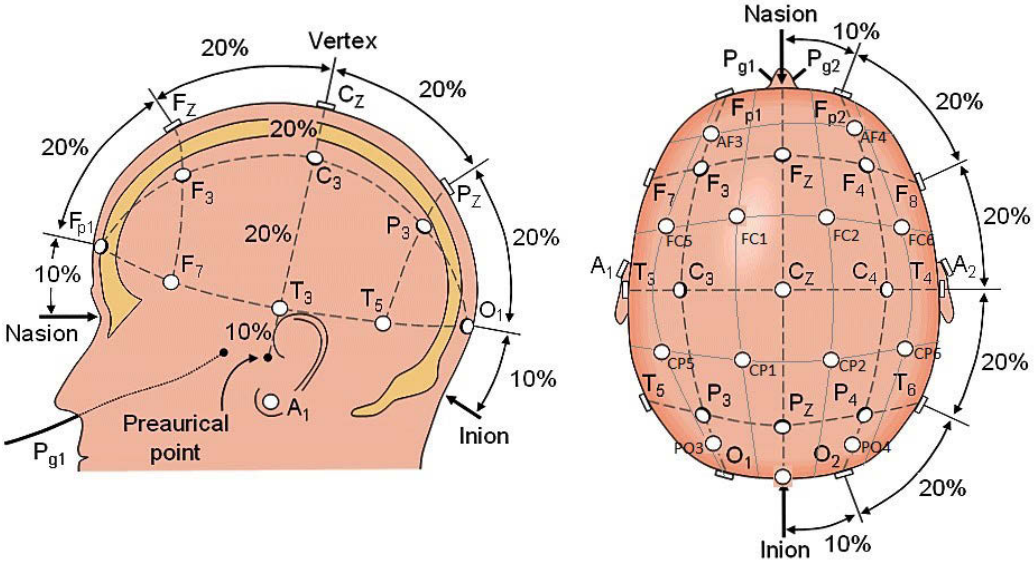

Figure 3.2: **The international ten-twenty (10-20) system for electrode placement**

the EEG signal was amplified with the common-mode rejection ratio >95 dB. They were sampled at a rate of 2048 (2 kHz), and band-pass filtered between 0.15 and 100 Hz. The EEG signals were re-sampled at a rate of 512 Hz for further analysis.

In order to trigger FOG episode data, PD patients were asked to perform a series of Timed "Up-and-Go" (TUG) tasks and were video recorded for assessment. There are four contexts in the TUG experiment aimed at provoking four sub-types of FOG such as Turning FOG, Narrow FOG, Target FOG and Runway FOG. First, the patient sat on a chair, stood up and walked approximately five meters to a target 0.6 m X 0.6 m box marked on the floor and then tried to make a turn around the box (Turning FOG). Second, they were asked to pass a narrow gap of <1 m such as a doorway and then return to the chair (Narrow FOG). Third, patients were asked to imagine trying to catch a bus or pick up a phone in a hurry (Target FOG). Four, freezing events was acquired when PD patients walk (Runway FOG). Four different tasks to triggers four sub-types of FOG are shown in Figure 3.3.

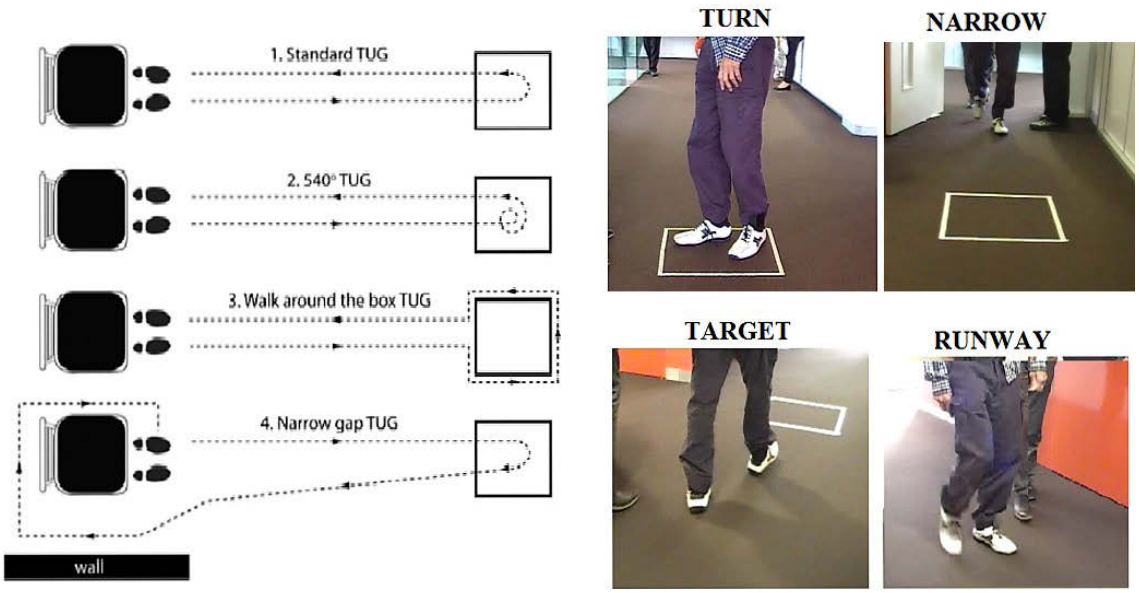

Figure 3.3: **Experiment to provoke FOG episode in PD patients**

Two clinicians labelled the time onset and offset of different sub-types of FOG events based on video recording. The EEG data from EW event was taken based on the time when the patients were able to walk effectivelly. The EEG data FOG events were taken according to the time of onset and offset as scored on the video when the patients felt their feet 'stuck to the floor', they want to walk, but they cannot walk during the TUG tasks. In this study, 343 seconds of EEG data samples of EW and 343 seconds of EEG data samples of FOG from seven PD patients were collected.

3.4 COMPUTATIONAL INTELLIGENCE FOR FOG DETECTION

3.4.1 Signal Pre-Processing

As EEG signals tend to be mixed with artefacts, an automatic artefact removal strategy was used. The EEG signals were filtered using a non-linear IIR band-pass filter with a cut-off frequency lower than 1 Hz and higher than 50 Hz. Ocular, muscular and heart rate signal artefacts were reduced using an automatic artefact removal (AAR) algorithm in the EEGLab (Delorme & Makeig 2004). Figure 3.4 shows EEG data with artefacts filtered or removed.

3.4.2 Feature Extraction Algorithm based on Fast Fourier Transform (FFT)

EEG signals are captured in the time domain and described as a sequence of numbers

$$x(t) = [x(1), x(2), x(3), \dots \dots . x(N)] \quad (3.1)$$

EEG signal can be shown by continuous amplitude and frequency domain using the band power method. FFT is a method to transforms a time-domain into its frequency domain. The EEG signal can be characterized as a sum of a number of amplitude-scaled and time-

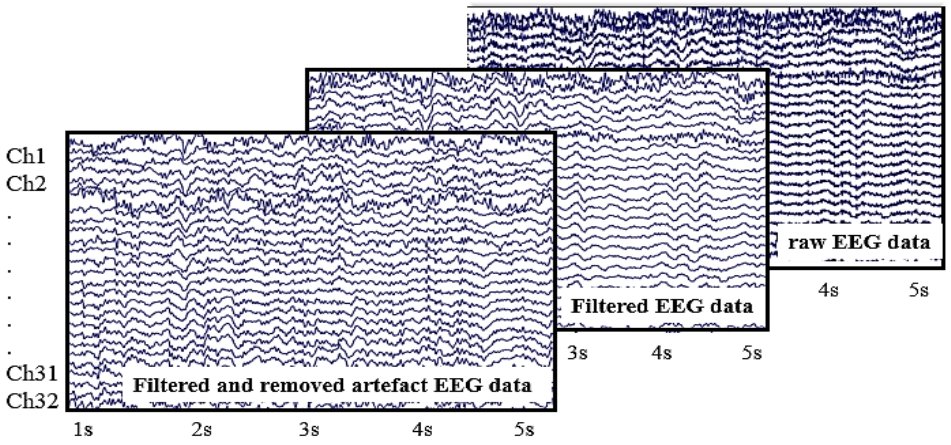

Figure 3.4: **Raw, filtered and removed artifacts EEG data**

shifted sinusoids at specific frequencies. To model continuous signals, it is necessary to adjust the phase and magnitude of each sinusoid. For an arbitrary signal *x*(t), the magnitude (scale) and the phase (shift) of the sinusoid at each frequency ω (radian) = 2πf (Hz) required to represented the arbitrary signal can be determined from the Fourier transform

$$X(\omega) = \int_{-\infty}^{\infty} x(t)\, e^{-j\omega t} dt = \int_{-\infty}^{\infty} x(t)\, [\cos\omega\, t + j\, sin\, \omega t] dt \qquad (3.2)$$

$$= \int_{-\infty}^{\infty} x(t)\, \cos\omega\, t\, dt + \int_{-\infty}^{\infty} x(t)\, \sin\omega\, t\, dt \quad = a(\omega) + jb(\omega)$$

Magnitude and phase of each sinusoidal component are computed as:

$$Magnitude: \ |X(\omega)| = \sqrt{a^2(\omega) + b^2(\omega)} \qquad (3.3)$$

$$Phase: \ \theta = \arg\big(X(\omega)\big) = \ \tan^{-1}\left(\frac{b(\omega)}{a(\omega)}\right) \qquad 3.4)$$

The inverse Fourier transform can compute the magnitude and phase to reconstruct the signal back in the time domain. As a result, the original time-domain signal is reconstructed from the scaled and shifted sinusoids at each frequency, as follows:

$$\text{x(t)} = \int_{-\infty}^{\infty} |X(\omega)|\, \cos(\omega\, t + \theta(\omega)) d\omega \qquad (3.5)$$

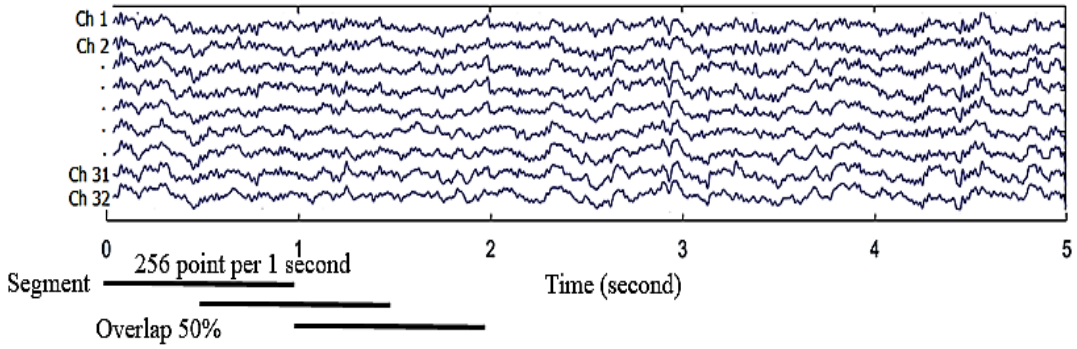

Figure 3.5: **FFT for feature extraction**

In this study, FFT is applied to the EEG signal by applying 256 point FFT to every second width data set and converting into frequency bands of EEG sub-band with an overlap of 50% (Figure 3.5).

Power Spectral Density

Power spectral density (PSD) shows the strength of the energy as a function of frequency. It can be based on the Fourier transform which represents a time series in the frequency domain. It can be defined as the average signal power over the interval [0, T] or as the Fourier transform of the autocorrelation function r_{xx}(t) and in continuous and discrete notation are given by (Semmlow, 2011). It is defined as *P*(f):

$$P(f) = \int_0^T r_{xx}(\tau) e^{-j2\pi f\tau} d\tau \tag{3.6}$$

$$P(f) = \sum_{n-0}^{N-1} r_{xx}\,(n) e^{-j2\pi f_T T_s} \tag{3.7}$$

The direct approach based on Parseval's theorem leads to the FFT, which relates the energy of an analogue signal, x(t), to the magnitude of the signal squared, integrated over time.

$$E = \int_{-\infty}^{\infty} |x_t|^2\, dt = \int_{-\infty}^{\infty} |X_T(f)|^2\, df \tag{3.8}$$

The power spectral density in the direct approach is calculated by

$$P(f) = \frac{|X_T(f)|^2}{T} \tag{3.9}$$

The spectra are calculated via Welch's method using a 256-point Fast Fourier Transform (FFT) and periodic Hamming windows with an overlap of 50%. The duration of the stationary fragments is assumed to be 220 ms with the sampling frequency 512 Hz. To eliminate inter-individual and inter-electrode variance in absolute measurements, power spectra are normalized using z-score normalization:

$$x_{new} = \frac{x_{old} - \mu}{\sigma} \tag{3.10}$$

where x_{old}, x_{new}, μ and σ denotes the original value, the new value, the mean and standard deviation of EEG data, respectively.

Based on our previous work, sub-band delta (1-4 Hz) did not contribute to FOG detection; therefore, in this study we focused on four frequency bands, namely: theta (4-8 Hz), alpha (8-13 Hz), low beta (13-21 Hz), high beta (21-38 Hz) (Handojoseno, Shine, et al. 2015). The beta frequency band was divided into low and high band, based on previous findings showing that high beta frequencies correlate with freezing (Toledo et al. 2014) (Figure 3.6 and Figure 3.7).

Power Spectral Entropy

Single neurons are highly nonlinear elements, and more nonlinearity is found in the neuronal group level with multiple feedback loops at different levels of distributed and interconnected cortical processing. Entropy was used as an index of EEG complexity or irregularly based on Shannon's Information Theory (Shannon 2001).

PSE of EEG signals x is defined as:

$$PSE(x) = -\sum_{i=f_i}^{f_h} P(i)\, logP(i), \tag{3.11}$$

where $P(i)$ is computed by the normalized power density from the signal's spectrum.

Centroid Frequency

Furthermore, we calculate the balance point for the area under the curve representing PSD. CF has been reported as the shift in the center of gravity of a frequency band based on the normalized power spectrum. CF is defined as:

$$CF = \frac{\sum_i f_i * P(f)}{\sum_i P(f)} \qquad (3.12)$$

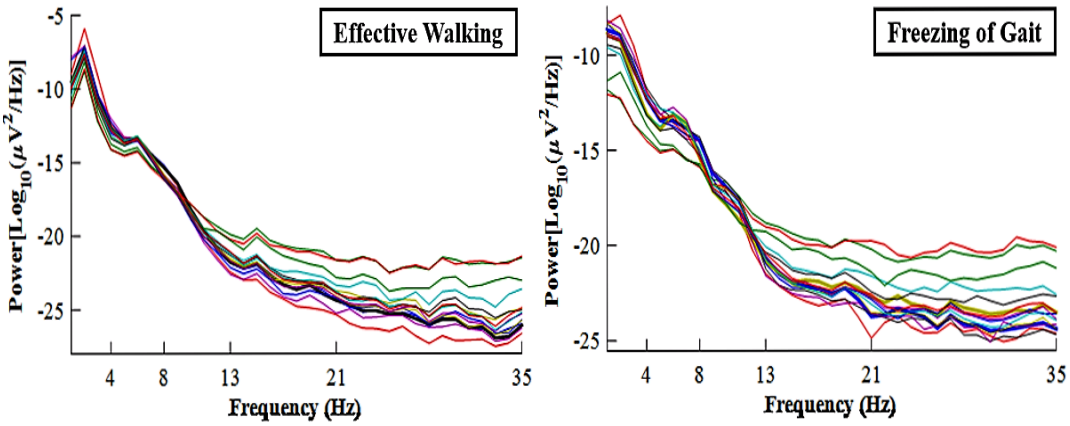

Figure 3.6: **Power Spectral Density of Effective Walking and Freezing of Gait**

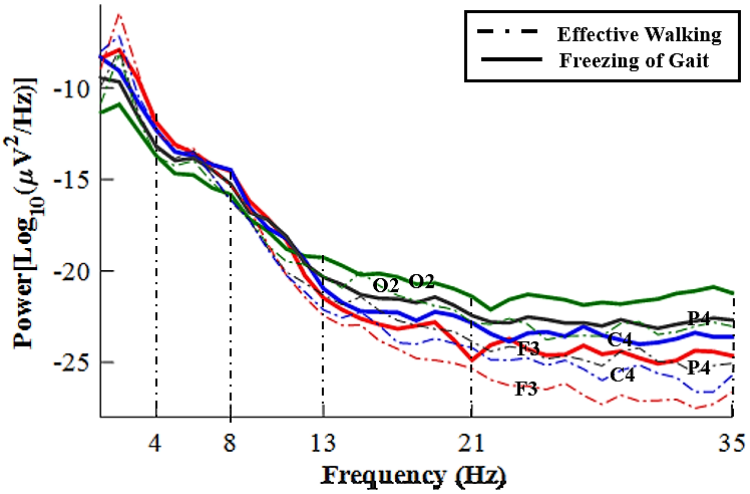

Figure 3.7: **Comparison of PSD between Effective Walking and Freezing of Gait**

3.4.3 Feature Selection

After feature extraction, feature selection is considered as one of the crucial steps in improving performance for our classifier. The purpose is to find the most significant and compact set of features between two different conditions, which steer clear of an excessive number of features affecting the dimensional problem. To compare EEG responses between EW and FOG, a non-parametric statistical analysis named Wilcoxon Sum Rank Test was chosen as feature selection method.

The Wilcoxon rank-sum test is defined as a nonparametric approach to establish significant difference between two sample groups using magnitude-based ranks, based on the two-sample t-test. The Wilcoxon test is based upon ranking the observations of the combined sample. Each observation has a rank: the smallest has rank 1, the 2nd smallest rank 2, and so on. The Wilcoxon rank-sum test statistic is the sum of the ranks for observations from one of the samples. To assess significance, the rank sum value from the dataset with the smallest size is compared to established tables containing p_value associated with rank sum scores. The statistical analysis with p_value ≤ 0.05 was used to investigate significant differences between periods of EW and periods of FOG.

The estimates of effect size are useful for determining the practical or theoretical importance of an effect, the relative contributions of factors, and the power of an analysis. Cohen (1962, 1988) introduced a measure similar to a z-score in which one of the means from the two distributions is subtracted from the other and the result is divided by the population standard deviation for the variables Cohen's d (Fritz, Morris & Richler 2012). Cohen's d effect sizes were also applied to check the most significant difference between EW and FOG conditions with $d \geq 0.4$.

These significant features were used as the main parameters for evaluating the best electrode locations to detect FOG events in PD patients. The mean, maximum and minimum values of PSD, CF, and PSE from 32 electrode's location of four EEG frequency bands were taken to evaluate their strength in detecting freezing.

3.4.4 Classification Algorithm using Artificial Neural Networks (ANN)

The two-layer feed-forward neural networks with 2 to 12 hidden nodes was utilized to classify the pattern into two categories of the disease: FOG and EW (Figure 3.8). In the following section, the structure of neural networks and Levenberg-Marquardt algorithms are discussed further.

Neural Networks Structure

The output of the neural networks is caculated as follows:

$$z(x,w) = f_1\left(b_k + \sum_{j=1}^{m} \bar{w}_{kj}\, f_2\left(b_j + \sum_{i=1}^{n} w_{ji}\, x_n\right)\right) \qquad (3.13)$$

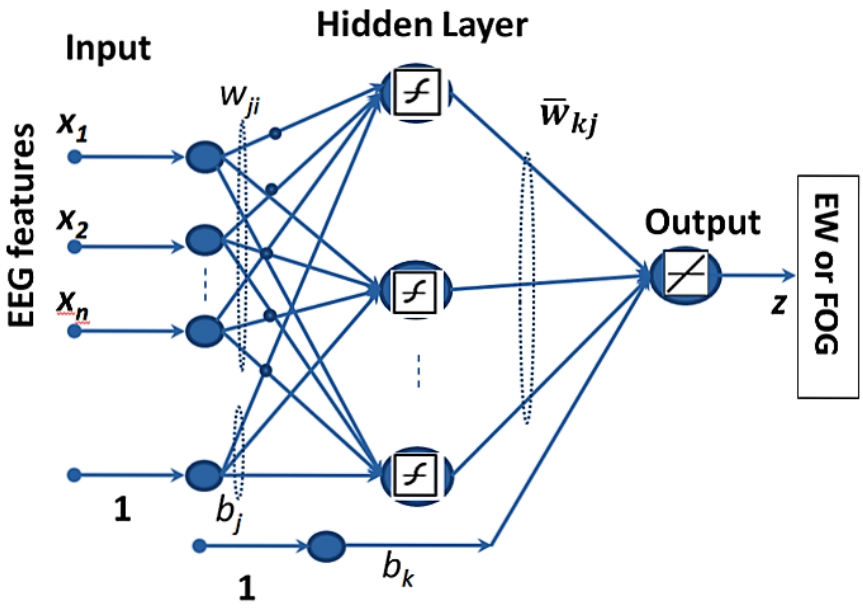

Figure 3.8: **Neural Networks Structure**

where f_1, f_2 is the activation function, *x* presents the input vector, w is the weight matrix vector; w_{ji} is the weight of the link between the *i-th* hidden node and the *j-th* input; $\overline{w}_{kj}$ is the weight of the link between *i-th* hidden node and the output, b_k and b_j are the biases. *m* is the number of outputs; *n* is the number of inputs and the tan-sig function was assigned as the activation function of the hidden layer.

The Levenberg-Marquardt Algorithm of ANN

Levenberg Marquardt algorithm is preferred as a training method due to its stability and speed (Übeyli 2009). Known as an approximation to the Gauss-Newton technique, the Levenberg-Marquardt algorithm is essentially an interactive technique to minimize the objective error function $E(w)$, with $E(w) = (y - t)^2$. This function can be expressed as follows

$$E(w) = \frac{1}{2}\sum_{n-1}^{N}\{y(x^n, w) - t^n\}^2 \quad (3.14)$$

$$= \sum_{n-1}^{N} e^2(w) = e^T(w)e(w) \quad (3.15)$$

where *N* denotes the number of data points of the training set. The aim of the Levenberg-Marquardt algorithm is to compute the network weight vector *w* at which *E(w)* is minimum. To do this, the weight vector w_k+1, will be updated from the previous weight vectorw_k, based on the second-order Tayler series as follows:

$$E(w_{k+1}) = E(w_k + \Delta w_k) \approx E(w_k) + \frac{\sigma E(w_k)}{\sigma w}\Delta w_k + \frac{1}{2}\Delta w_k^T \frac{\sigma^2 E(w_k)}{\sigma w^2}\Delta w_k \quad (3.16)$$

A local minimum of the error function is calculated by taking the gradient of the function with respect to $A(w_k)$, and setting it equal to zero, leading to

$$w_{k+1} = w_k + A_k^{-1} g_k \quad (3.17)$$

where $$g_k = \nabla E(w)|_{w-w_k}, and\ A_k = \nabla^2 E(w)|_{w-w_k} \quad (3.18)$$

we obtain

$$w_{k+1} = w_k - [2J^T(w_k)J(w_k)]^{-1}J^T(w_k)e(w_k) \quad (3.19)$$

In the process of training neural networks, the procedure of the Levenberg-Marquardt algorithm to minimize the cost function E(w) can be presented as the five steps following

1. Computing $E(w_k)$
2. Initialising μ_k with a small value
3. Solving for w_{k+1} to compute $E(w_{k+1})$
4. If $E(w_{k+1}) \geq E(w_k)$ then increase μ_k by a factor of γ(e.g γ=10), then go to step 3
5. If $E(w_{k+1}) \leq E(w_k)$ then decrease μ_k by a factor of γ, then go to step 3

Performance Evaluation of ANN

The significant features were fed into feed-forward neural networks with 2 to 8 hidden nodes to classify the pattern into two categories: EW or FOG. In this study, Levenberg Marquardt's algorithm with early stopping was used to train 34% of the EEG EW-FOG data, followed by 33% of validation and 33% of testing of the total data. The performance of the proposed features was determined using the following statistical measures:

$$Sensitivity = \frac{TP}{TP + FN} \quad (3.20)$$

$$Specificity = \frac{TN}{FP + TN} \quad (3.21)$$

$$Accuracy = \frac{TP + TN}{TP + FN + FP + TN} \quad (3.22)$$

where

- TP (true positive) is the number of inputs which correspond to FOG classified as FOG.

- TN (true negative) is the number of inputs which correspond to EW classified as FOG.
- FP (false positive) is the number of inputs which correspond to EW classified as EW
- FN (false negative) is the number of inputs which correspond to FOG classified as EW

3.5 EXPERIMENTAL RESULTS

3.5.1 Feature Extraction Results

The general PSD pattern of low and high beta band during freezing is shown in Figure 3.9. A comparison of EEG frequency band power during the two conditions EW vs. FOG in these two sub-bands showed that the high beta band stood out as the most affected sub-band during freezing ($p < 0.0001$) regardless of the position of the EEG channel. The low beta band showed the same pattern with a significant increase in frontal and central cortical region during the episode of FOG ($p < 0.0001$).

Specifically, compared to the EW period, FOG was associated with significant shifting in two sub-bands namely low beta and high beta band at locations: frontal F3, F4, F8, FC1, FC2, FC6, central Cz, C3, C4, CP1, CP2, CP6, parietal Pz, P4, P8, PO3, PO4 and occipital O1, Oz, O2. The high beta sub-band continues to increase only in several frontal locations FP1, F7, shifting AF3, F4, and Fz. Also, there were remarkable increases in alpha and theta power in the four main regions of the brain during the period of FOG. The increases of sub-bands theta only appeared in frontal-central and parietal such as at locations of AF3, FC1, FC2, CZ, CP1, CP2, and PZ. Further, the alpha power increased significantly in the four main regions of the brain such as at frontal F3, F4, F8, FC1, FC2, FC6, central C3, Cz, C4, CP5, CP1, CP2, parietal P7, P3, Pz, P4, P8, PO3, PO4 and occipital O1, Oz, O2.

When the effect size *d* was taken into account, the high beta alteration was strongest in frontal F3 (*d*=0.4557) and central C4 (*d*=0.4394), with remarkably increased power in these two locations. In the parietal locations, episodes of freezing were associated with a large increase of power in low-high beta frequency with parietal P4 appearing as the most affected location. In occipital region, O2 (*d*=0.4673) appeared as the location with the largest increase in the high beta band.

In addition, there was significant increases in low beta in occipital O1 (*d*=0.3245), parietal P4 (*d*=0.3333) and central C4 (*d*=0.3081). This pattern is along with the increase of theta in central Cz (*d*=0.2169), frontal FC2 (*d*=0.262). The largest increased alpha activity was found in frontal F3 (*d*= 0.3188), followed by central C3 (*d*= 0.244), parietal P4 (*d*=0.328) and occipital O1 (*d*= 0.3268) (Table 3.1).

The results of our entropy analysis showed that there was an increase of entropy in the frequency high beta in most locations during FOG episodes. The most significant change was detected in PSE high beta in frontal FC1 (*d*=0.4433), central CP6 (*d*=0.4953). There were also significant increases in the regularity of theta, alpha and low beta activity in frontal F3, central C4 and occipital O2 (Table 3.2).

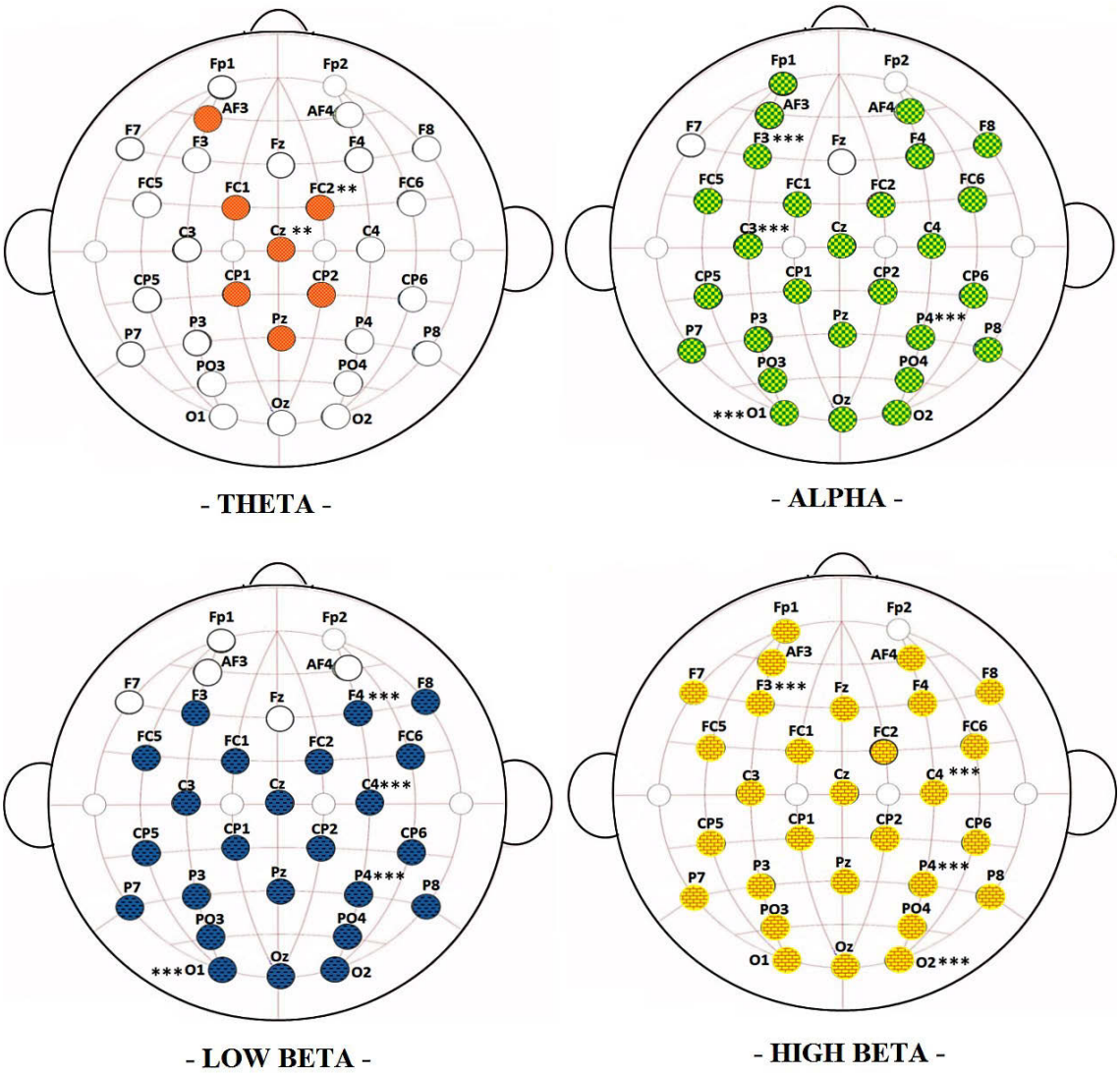

Figure 3.9: **Significant PSD pattern between EW and FOG in theta alpha, low beta and high beta**

Table 3.1: Features analysis of PSD between EW and FOG

Parameter	Band	EW(μV±std)	FOG(μV±std)	p	d	EW vs FOG
PSD-F3	α	0.089 ± 0.08	0.119 ± 0.09	≤0.0001	0.324	**
	lβ	0.038 ± 0.03	0.048 ± 0.03	≤0.0001	0.2776	**
	hβ	0.043 ± 0.03	0.049 ± 0.04	≤0.0001	0.4557	***
PSD-C4	α	0.081 ± 0.07	0.110 ± 0.09	≤0.0001	0.3361	**
	lβ	0.043 ± 0.03	0.055 ± 0.04	≤0.0001	0.3081	**
	hβ	0.050 ± 0.04	0.061 ± 0.05	≤0.0001	0.4394	***
PSD-P4	α	0.080 ± 0.07	0.110 ± 0.08	≤0.0001	0.328	**
	lβ	0.050 ± 0.04	0.062 ± 0.05	≤0.0001	0.3333	**
	hβ	0.050 ± 0.06	0.090 ± 0.08	≤0.0001	0.528	***
PSD-O2	lβ	0.067 ± 0.05	0.083 ± 0.07	0.0091	0.2459	*
	hβ	0.087 ± 0.09	0.137 ± 0.11	≤0.0001	0.4673	***

**: Significant at 0.001 < p ≤ 0.05 and Cohen's d < 0.3*
***: Significant at 0.0001 <p ≤ 0.001 and Cohen's 0.3 ≤ d <0.4*
****: Significant at p≤0.0001 and Cohen's d ≥ 0.4*

Table 3.2: Features analysis of PSE between EW and FOG

Parameter	Band	EW(μV±std)	FOG(μV±std)	p	d	EW vs FOG
PSE-F3	θ	0.866 ± 0.11	0.893 ± 0.09	0.0096	0.2503	*
	lβ	0.900 ± 0.05	0.910 ± 0.05	0.0127	0.1559	*
	hβ	0.911 ± 0.04	0.920 ± 0.04	0.0026	0.2024	*
PSE-C4	θ	0.862 ± 0.12	0.890 ± 0.09	0.0096	0.2870	*
	α	0.890 ± 0.08	0.870 ± 0.09	0.0416	0.1418	*
	hβ	0.917± 0.04	0.990 ± 0.04	0.0447	0.1131	*
PSE-P4	lβ	0.919± 0.05	0.920± 0.05	0.0381	0.0811	*
	hβ	0.910± 0.04	0.920 ± 0.04	0.0072	0.1537	**
PSE-O2	lβ	0.910 ± 0.05	0.920 ± 0.05	0.0029	0.1635	*
	hβ	0.918 ± 0.04	0.926 ± 0.04	0.0037	0.1807	*

**: Significant at 0.001 < p ≤ 0.05 and Cohen's d < 0.3*
***: Significant at 0.0001 <p ≤ 0.001 and Cohen's 0.3 ≤ d <0.4*
****: Significant at p≤0.0001 and Cohen's d ≥ 0.4*

The CF analysis revealed the changes of centroid frequency in theta, low and high beta in almost all of 32 channels during freezing episodes ($p < 0.0001$). The CF high beta stood out as the most affected frequency band from EW episode to FOG episode with the largest shifts in the frontal F3, central C4, followed by occipital O2 and parietal P4.

When compared to the effective walking, episodes of freezing were associated with a significant shift in theta frequency band with the largest shift of CF in frontal and central leads such as F3 and C4 (Figure 3.10). This suggests that frontal-central cortical regions were more affected than the parietal-occipital region in terms of CF features (Table 3.3). This brain pattern is aligned with function Magnetic Resonance Imaging (fMRI) studies in which freezing provoked by a virtual reality gait paradigm was associated with alterations in the pre-supplementary and primary motor areas, presumably as a compensatory strategy to overcome reduced automaticity of gait (Shine, Moustafa, et al. 2013).

Table 3.3: Features analysis of CF between EW and FOG

Parameter	Band	EW (Hz±std)	FOG (Hz±std)	p	d	EW vs FOG
CF-F3	θ	5.493 ± 0.59	5.673 ± 0.06	00002	0.2993	**
	lβ	16.150 ± 0.88	16.419 ± 0.91	≤0.0001	0.3	**
	hβ	27.680 ± 1.81	28.438 ± 1.82	≤0.0001	0.4180	***
CF-C4	θ	5.460 ± 0.59	5.636 ± 0.58	≤0.0001	0.2953	**
	lβ	16.278 ± 0.91	16.526 ± 0.94	0.0002	0.1418	**
	hβ	27.901 ± 1.78	28.620 ± 1.85	≤0.0001	0.3958	***
CF-P4	θ	5.608 ± 0.57	5.729 ± 0.56	0.0187	0.2113	*
	lβ	16.348 ± 0.91	16.491 ± 0.90	0.0116	0.1574	*
	hβ	28.175 ± 1.89	28.897 ± 1.88	≤0.0001	0.3827	***
CF-O2	lβ	16.333 ± 0.93	16.477 ± 0.89	0.0118	0.1569	*
	hβ	28.402 ± 2.00	29.021 ± 1.93	≤0.0001	0.3144	**

**: Significant at $0.001 < p \leq 0.05$ and Cohen's $d < 0.3$*
***: Significant at $0.0001 < p \leq 0.001$ and Cohen's $0.3 \leq d < 0.4$*
****: Significant at $p \leq 0.0001$ and Cohen's $d \geq 0.4$*

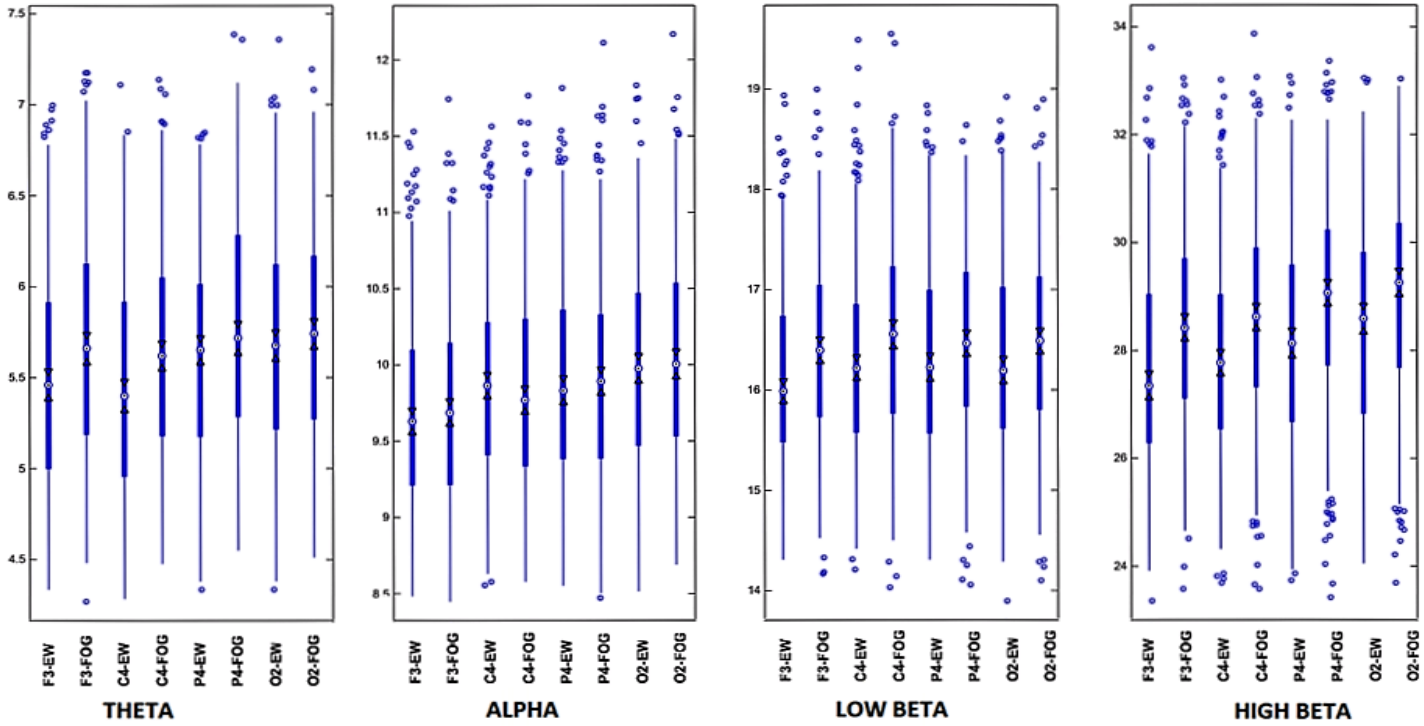

Figure 3.10: **Boxplot of Centroid Frequency of EEG signals between EW and FOG**

3.5.2 Affected EEG Montages Systems underlying FOG

EEG data samples of FOG events were processed and analysed using the EEGLab toolbox. They were categorized separately into three bands: theta, low beta and high beta and summarized into a color-coded map in the form of scalp topography. Figure 3.11 displays the topographic distribution of spectral power represented by the three bands: theta, low beta and high beta underlying FOG episodes. The power values were calculated and transferred into the corresponding values using an interpolation method in order to produce a smooth surface of the scalp topography.

Each oval topography depicts a view of the head from above with frontal areas at the top. For individual scalp topography, each electrode zone is color coded to indicate how much activity it contains compared to other regions, with a blue color indicating reduced power and a red color spectrum indicating increased power. It is observed that the theta power escalation spreads within central and frontal locations while the low-high beta power increased significantly in frontal F3, central C4, parietal P4 and occipital O2 locations. This finding is strongly consistent with multiple studies that have shown a relationship between FOG and impairments within both visual-attention (P4-O2) networks and motor planning-executive network (F3-C4) in the human cortex (Handojoseno, Shine, et al. 2015; Shine, Moustafa, et al. 2013).

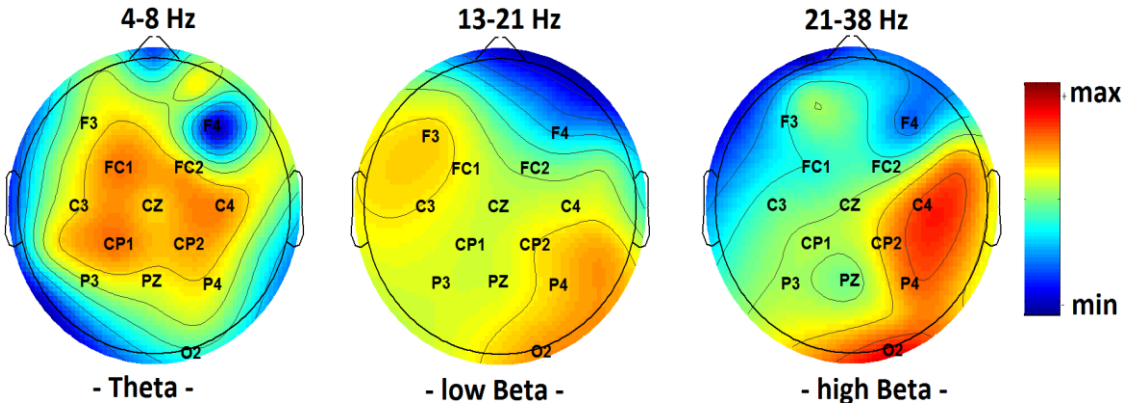

Figure 3.11: **Scalp topography of EEG power activity underlying FOG**

3.5.3 Classification Results

The strength of the alteration of the EEG signal parameters differs from one location to another. Therefore, the following factors were analyzed for their influence on the accuracy of FOG detection. First, a combination of four affected channels representing frontal, central, parietal and occipital regions were analysed. Second, a combination of channels, which experienced similar PSD pattern underlying FOG episodes, were analysed. Therefore, based on the result of feature extraction and classification system using the single channel as input, we designed the three EEG montages systems including 15 EEG channels that might facilitate the identification of FOG arising from four main cortical regions. These systems were also compared with the previous finding to validate that they are the most affected locations of the brain during FOG in many fMRI studies (Snijders 2012). The three EEG Systems were designed as followed:

- EEG System 1: Four most affected channels among 32 channels during FOG. The EEG montages were F3, C4, P4, and O2.
- EEG System 2: Six channels experienced a significant increase in four sub-bands: theta, alpha, low-high beta. The EEG montages were FC1, FC2, Cz, CP1, CP2 and Pz.
- EEG System 3: Seven channels experienced a significant increase in only three sub-bands: alpha, low-high beta. The EEG montages were as follows: F3, F4, C3, C4, P3, P4, and Oz

The neural networks were developed with inputs corresponding to significant data ($p<0.05$) from 1, 2, 3, 4, 6, 7 and 32 EEG channels as shown in Table 3.4 and 3.5. The classification results using input from each single channel location at a time showed that the central regions were the best area for detecting freezing events. Indeed, central C4 seemed to be the best location to detect freezing with 70.88% sensitivity and 69.13% accuracy. Frontal F3 and parietal P4 provided strength as an indicator of FOG, with

70.29% and 69.59%.sensitivity, respectively. These two locations achieved similar accuracy in detecting FOG with 68.93%. The best performance of classifier using a single channel from the occipital region was with O2, which had 70.72% sensitivity and 66.60% accuracy.

The performance of the detection of FOG using the combination of these four different channels was also studied. In the systems using input from two to four locations, central-occipital C4O2 appeared as the best combination of two channels to detect freezing with a sensitivity of 72.54% and an accuracy of 69.71%. The combination from four locations that provided the best indicator of freezing was F3C4P4O2 with 72.29% sensitivity and 70.29% accuracy. As the results are shown in Table 3.5, the neural networks based classifier with inputs obtained from six locations in System 2 provided 70.23% sensitivity and 68.93% accuracy. The sensitivity of the system was improved slightly with 70.94% when using the input from seven locations of System 3. Interestingly, when all the 32 channels were taken as an input, the classification system provided the sensitivity of 72.20%; which is lower than that of the two channels system C4O2.

3.6 DISCUSSION

In this chapter, EEG measures, including power spectral density, centroid frequency and power spectral entropy, were extracted and used as input of our classifier. By applying a feed-forward neural networks, the obtained results showed that even a small number of electrodes suffice to construct a FOG detector with expected performance with the accuracy around 70%, which is comparable to the use of a full 32 channels montage.

The high beta oscillations in the cortex increasing and remaining high across all the brain regions during freezing is consistent with previous studies (Toledo et al. 2014). This finding suggests that high beta frequencies are likely linked to neural communications of a stopping network in which the beta power increases in order to prohibit movements, which could cause FOG in PD (Aron, Robbins & Poldrack 2004).

Table 3.4: **Classification results of FFT based features using ANN in detecting FOG from EW**

Channels	Hidden	Training			Testing		
		Sen (%)	Spec (%)	Acc(%)	Sen (%)	Spec(%)	Acc(%)
F3	2	72.20	70.29	70.92	69.65	67.28	68.93
O2	2	76.42	70.72	74.67	72.73	62.93	66.60
P4	2	73.99	69.59	71.50	68.99	68.11	68.93
C4	3	74.36	70.88	73.21	72.03	67.41	69.13
F3C4	6	75.88	71.97	73.96	71.66	68.09	69.71
F3P4	8	76.73	71.86	74.33	71.04	68.31	69.71
F3O2	7	75.99	78.44	77.25	70.71	69.18	69.90
C4P4	5	74.91	69.95	72.46	71.38	66.94	68.93
C4O2	6	77.99	69.77	73.92	72.54	66.96	69.71
P4O2	2	73.05	72.05	72.54	71.00	68.31	69.71
F3C4P4	7	77.15	72.87	74.96	71.20	68.56	69.90
F3C4O2	5	74.96	72.29	73.63	71.40	67.02	69.13
C4P4O2	2	73.29	72.90	73.08	71.25	67.26	69.13
F3C4P4O2	8	76.19	76.66	76.46	72.29	68.22	70.29

Sen: Sensitivity; Spe: Specificity; Acc: Accuracy

Table 3.5: Comparison of classification results in detecting FOG from EW

Number	Channels	Testing		
		Sen (%)	Spec(%)	Acc(%)
1	C4	72.03	67.41	69.13
2	C4O2	72.54	66.96	69.71
3	F3C4O2	71.40	67.02	69.13
4	F3C4P4O2	72.29	68.22	70.29
6	FC1, FC2, Cz, CP1, CP2, Pz	70.23	67.45	68.93
7	F3, F4, C3, C4, P3, P4, Oz	70.94	67.03	68.93
32	All 32 channels	72.20	70.58	71.46

Sen: Sensitivity; Spe: Specificity; Acc: Accuracy

Fifteen electrodes positioned over the following cortical regions: frontal F3, F4, FC1, FC2 (motor planning and working memory), central C3, C4, CP1, CP2, CZ (motor execution), parietal P3, PZ, P4 (sensory integration) and occipital O1, OZ, O2 (visual area) has been reported as the most affected channels underlying FOG based on our EEG data. Our goal in evaluating differing montages was to find a minimum number of electrodes strategically placed to maximize the identification of FOG. Further, this study revealed that optimal FOG detection was achieved when using an EEG system with only two channels C4-O2 with a sensitivity of 72.54%.

These results are closely aligned with several previous fMRI studies in which the motor lead C4, planning motor lead F3, parietal lead P4, and visual lead O2 are recording over regions that have been implicated in the pathogenesis of FOG in PD (Shine, Handojoseno, et al. 2014; Snijders 2012). This information would greatly assist with the clinical translation of a FOG detection device since fewer sensors will improve computation efficiency, robustness of the classification system and convenience for the use of ambulatory EEG by patients.

Although limited to seven patients, this part of the study demonstrated that FOG would be detected effectively using an EEG system with only two input channels (C4O2). Further studies using larger sample sizes are now required to confirm these preliminary findings and further delineate the specific neural networks to provide a better performance of FOG detection and prediction system.

Chapter 4

Detection of Gait Initiation Failure using EEG and Support Vector Machine

4.1 INTRODUCTION

Gait Initiation is a complex task that requires both motor and cognitive processing to enable the correct selection, timing and scaling of movements (Delval et al. 2015). Gait Initiation Failure (GIF) is clinically important as a trigger for FOG (accounting for 24% of all sub-types of FOG). When PD patients initiate gait, this frequently increases the risk

of falls induced by GIF (Backer 2006). As a result, it can negatively affect the quality of life for patients with PD and can result in injury as well as nursing home placement (Moore, Peretz & Giladi 2007). However, understanding of the neurobiological mechanisms underlying GIF has been limited by difficulties in eliciting and objectively characterizing such gait phenomena in the clinical setting.

Using a computational intelligence strategy, this study investigates abnormal changes in EEG parameters associated with GIF by extracting EEG signals in the time-frequency domain Wavelet Transform (WT). This is then continued by applying Support Vector Machine (SVM) to be used for GIF classification and detection. GIF detection has been performed with different classification methods to achieve the highest performance. Although the traditional logistic regression classification methods can be used for detection as described in some EEG studies (Mumtaz et al. 2015), its drawback is that it requires large sample size and has overfitting issue to achieve stable results. Our ANN and SMV strategies minimise the overfitting issue. In addition, one of the reasons why SVM was used is that EEG signals will be represented in high dimensional features space and it is therefore difficult to interpret. SVM aims to maximize the margin in order to avoid the risk of over-fitting data and minimize the misclassification error. Further, with the goal of developing a faster and better classification system, the current chapter have developed a more advanced strategy which uses Independent Component Analysis (ICA) for EEG source separation, Wavelet Transform (WT) for feature extraction and Support Vector Machine (SVM) for classification, with good sensitivity and specificity performance. It is expected the convolutional neural network strategy would provide a similar result to our research, and will explore this option in our future direction.

The contributions of this chapter are as follows: first, different feature extractors were explored, including FFT, WT to find a better feature extractor. Second, two classifiers were used for detecting GIF, including the ANN and SVM. These optimization techniques combined ICA-EBM as source separation, WT as feature extraction and SVM

as classifier showed the highest classification accuracy between these methods in the detecting of GIF.

4.2 SYSTEM OVERVIEW

An overview of the GIF detection based on SVM approach is illustrated in Figure 4.1. This starts from data collection in which EEG data was measured using a Biosemi ActiveTwo system and was categorized into two events: Good Start (GS) and Gait Initiation Failure (GIF). Next, raw EEG data was filtered and artifacts removed. Different EEG parameters in the form of Wavelet Transform (Wavelet Energy, Wavelet Centroid Scale, Wavelet Energy Entropy) were extracted and analyzed to explore important features that were significantly changed between two events GS and GIF. Regarding the input of the classification, the source separation technique was applied such as ICA-EBM for separating EEG data into independent components before extracting features (ICA-EBM, WT). The feature pattern was examined using the non-parametric Wilcoxon Rank-Sum Test to investigate the significant alteration of these features. Next, the significant features of two events were then employed as inputs for neural networks to classify using SVM.

4.3 STUDY, DATA COLLECTION

4.3.1 Study

EEG data was obtained from five Parkinson's disease patients who were recruited from the Parkinson's disease Research Clinic at the Brain and Mind Centre, The University of Sydney. Patients were tested in their practically-defined 'off' medication state, following overnight (minimum 12 hours since the last dose) withdrawal of dopaminergic therapy. The subjects demonstrated multiple episodes of GIF (40% of gait initiations elicited a GIF) during a structured series of Timed Up and Go tasks.

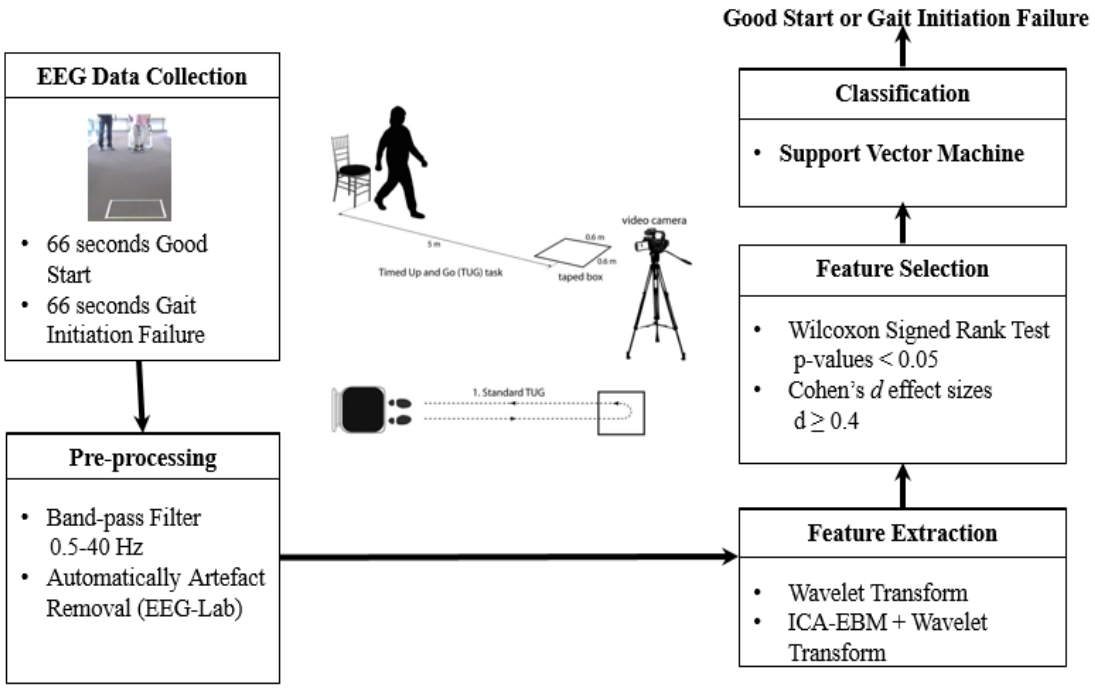

Figure 4.1: **Components of EEG-based GIF detection system**

4.3.2 Data Collection

EEG data was acquired from 15 electrodes using a Bio Semi Active Two system. These electrodes were positioned over the following cortical regions: frontal F3, F4, FC1, FC2 (motor planning and working memory), central C3, C4, CP1, CP2, CZ (motor execution), parietal P3, PZ, P4 (sensory integration) and occipital O1, OZ, O2 (visual area).

References signal was taken by averaging two electrodes placed on the ear lobes. The recording was segmented to 1-second durations and digitized at 512 Hz. In order to provoke GIF data, PD patients were asked to start from a starting position where they were seated in a chair, listen to a simple order 'Ready, go!'. After that, they stood up and started walking along the center of a large open corridor. A video camera was placed on a tripod to evaluate any episode of GIF (Figure 4.2).

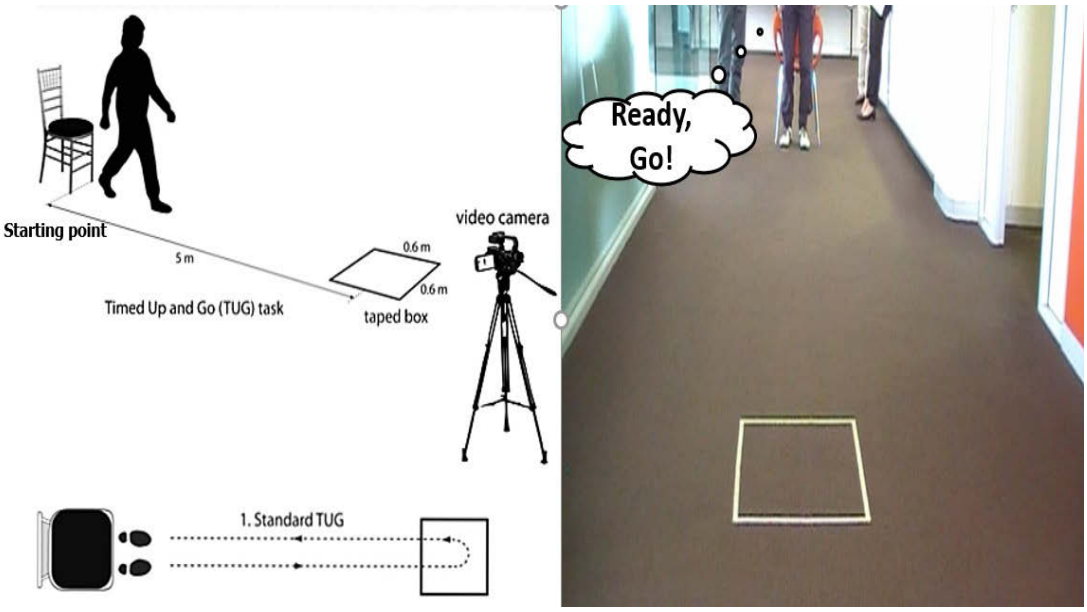

Figure 4.2: **Experiment 2 to provoke GIF episode in PD patients**

Both GS and GIF were determined according to the time onset and offset as scored on the video during the TUG tasks by two clinical experts:

- Good Start (GS) is defined as the 2-second period after the patients were able to take an effective first step in a normal start during the TUG tasks.
- Gait Initiation Failure (GIF) is defined as the period when the patients tried to take first steps, but failed to do so.

4.4 COMPUTATIONAL INTELLIGENCE FOR GIF DETECTION

4.4.1 Signal Pre-Processing

66 seconds of EEG data samples of GS were matched to 66 seconds of data samples of GIF as recorded from five PD patients. Data samples were then filtered using a band-pass

filter at 0.5-50 Hz. Eye movement and heart rate signals artefacts were eliminated using Automatic Artefact Removal (AAR) in the EEGLab from all electrode locations of raw EEG data (Delorme & Makeig 2004).

Figure 4.3 shows the amplitude spectra of representative raw EEG data of one patient that were tracked in the time domain.

Overall, decomposition of the EEG data into theta, alpha and low-high beta bands demonstrated that GIF was associated with high amplitude within a range from 4 to 8 Hz (theta) and 21 to 38 Hz (high beta). In addition, GS was typically characterized by regularly decreased amplitude in these two sub-bands within different brain regions.

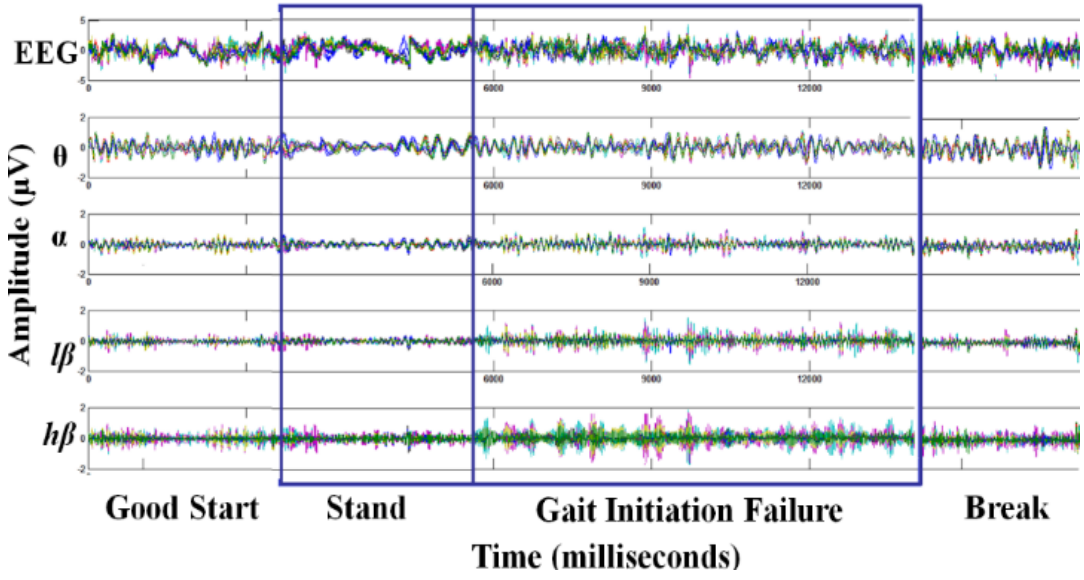

Figure 4.3: **Amplitude spectra of representative raw EEG data of one patient**

4.4.2 Source separation: Independent Component Analysis Entropy Boundary Minimization (ICA-EBM)

Since EEG data is recorded from different locations on the scalp, one of the problems is that its electrical potential was generated as the mixing complex connection from a different component of brain activity. Therefore, the idea of using ICA to separate the linearly mixed neural activities into its constituent independent components (ICs) was applied to solve this problem. Most of ICA algorithms exploit both higher order and second order statistics to minimize the non-Gaussian minimization aspect of the sources. ICA by entropy bound minimization (ICA-EBM) has emerged as an effective source separation technique (Li & Adali 2010).

The algorithm takes both non-Gaussian property and sample correlation into account by minimizing mutual information rates. It is originally introduced as a full Blind Source Separation (BSS), which results in the improved general temporal structure of sources. This chapter uses ICA-EBM as a source separator to our EEG data.

A full BSS algorithm is introduced as

$$x(t) = As(t) \tag{4.1}$$

where $s(t)$ is a zero mean source, calculated as $s(t) = [s_1(t), \dots, s_{N1}(t)]^T$. $s(t)$ is mixed with a mixing matrix A(N x N). The mixture x(t) is obtained as follows $x(t) = [x_1(t), \dots, x_N(t)]^T$ where *T* and *t* denotes the transpose and time index respectively.

The objective of ICA is to separates the mixture calculated as

$$y(t) = Wx(t) \tag{4.2}$$

where y is an independent component (IC) which was calculated as $y(t) = [y_1(t), \dots, y_N(t)]^T$ and *W* is the un-mixing or reparation matrix.

The statistical IC estimations are expressed as a new cost function

$$I(y_1, \ldots \ldots, y_N) = \sum_{n=1}^{N} H(y_n) - \log|\det(W)| - H(x) \qquad (4.3)$$

where $I(y_1, \ldots \ldots, y_N)$ is the mutual information among N random variables $y_n, n = 1, \ldots, N$. $H(y_n)$ represents the entropy of the n[th] individual separated source, and entropy of observation *H(x)* is constant with respect to the un-mixing matrix *W*. However, a new cost function is needed because the current function cannot obtain most of the temporal information of data sources. The new cost function is re-calculated as:

$$I(y_1, \ldots \ldots, y_N) = \sum_{n=1}^{N} H(y_n) - \log|\det(W)| - H_r(x) \qquad (4.4)$$

where $H_r(y_n) = \lim_{t\to\infty} H[y_n(1), \ldots, y_n(t)]\,/t$ is the entropy rate of the n^{th} process of y_n and entropy rate of observation $H_r(x) = \lim_{t\to\infty} H[x(1), \ldots, x(t)]\,/t$ of the observed vector-valued process *x* is constant with respect to the un-mixing matrix *W*. $H_r(x)$ is the entropy rate of the separated process of the individual. Equation is modified using the method proposed by Li & Adali (2010) to obtain new entropy estimator and cost function. The new cost function is explained as:

$$J(W, p_1, \ldots \ldots, p_N) = \sum_{n=1}^{N} H(v_n) - \log|\det(W)| \qquad (4.5)$$

where $v_n(t) = \sum_{q-0}^{p-1} a_n(q) y_n(t-q), y_n = w_n^T x$ is the n^{th} separated source, and $a_n = [a_n(0), \ldots, a_n(p-1)]^T$ are the filter coefficients.

Later, the algorithm is optimized to obtain a new *W*, which minimizes the mutual information rate. The ICs, $\hat{s}(t)$ are recovered using the equation $\hat{s}(t) = W_x(t)$ where *W* and *x(t)* are the un-mixing matrix and recordings (mixtures) respectively.

ICA-EBM was applied to 15 EEG channels for source separation with the aim of improving detection ability of GIF events as compared to the normal initiation of gait

(Good Start) (Figure 4.4). After source separation, the 15 ICs separated data were extracted in the form of WT and fed into our classifier.

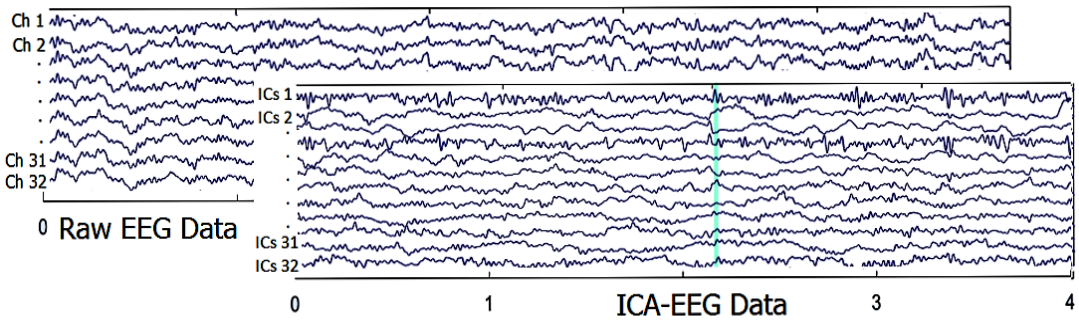

Figure 4.4: **EEG Data and ICA-EEG data**

4.4.3 Feature Extraction using Wavelet Transform (WT)

Due to the strengths in the time-frequency method, WT was chosen to extract the EEG data in the form of Wavelet Energy (WE), Wavelet Centroid Scale (WCS) and Wavelet Energy Entropy (WEE). WT is defined as the convolution between the signal and wavelet function generated by dilations and translations of scaled mother wavelet (Burrus, Gopinath & Guo 1997).

In this research, the discrete wavelet transforms (DWT) based on dyadic scales and positions is used (Burrus, Gopinath & Guo 1997). DWT is computed as

$$DWT(j,k) = \frac{1}{\sqrt{|2^j|}} \int_{-\infty}^{\infty} x(t) \Psi \left(\frac{t - 2^j k}{2^j} \right) dt \qquad (4.6)$$

where 2^j denotes the scale and $2^j k$ denotes the time localization and Ψ denotes the mother wavelet function.The wavelet decomposition for an EEG signal *x(t)* at scales *j*, time point *k* could be calculated as:

$$x(t) = \sum_{k=-\infty}^{\infty} A(k) \varphi_{J,k}(t) + \sum_{j=0}^{\infty} \sum_{k=-\infty}^{\infty} D(j,k) \Psi_{j,k}(t) \qquad (4.7)$$

where $A(k), D(j,k), \varphi_{J,k}, \Psi_{j,k}\ (t)$ denotes approximation coefficients, detail coefficients, scaling function, and wavelet functions, respectively.

Daubechies wavelet of order *4* (*db4*) was selected as the wavelet function since its smoothing feature has been confirmed to work well in discovering changes of EEG signals (Burrus, Gopinath & Guo 1997). For EEG sampled at 512Hz, a six level decomposition (*D1, D2, D3, D4, D5, and D6*) was computed by squaring and summing the wavelet coefficients of the decomposed level. Four levels of coefficients correspond approximately to our four EEG sub-bands. The theta sub-band is reconstructed by the wavelet component at level 6 of the decomposition *(D6)*. The alpha sub-band is reconstructed by the wavelet component at level 5 of the decomposition *(D5)*. The low beta sub-band is reconstructed by the wavelet component at level 4 of the decomposition *(D4)*. The high beta sub-band is reconstructed by the wavelet component at level 3 of the decomposition *(D3)*. They were used for further analysis. Reconstruction of these signals into decompositions is represented in Figure 4.5.

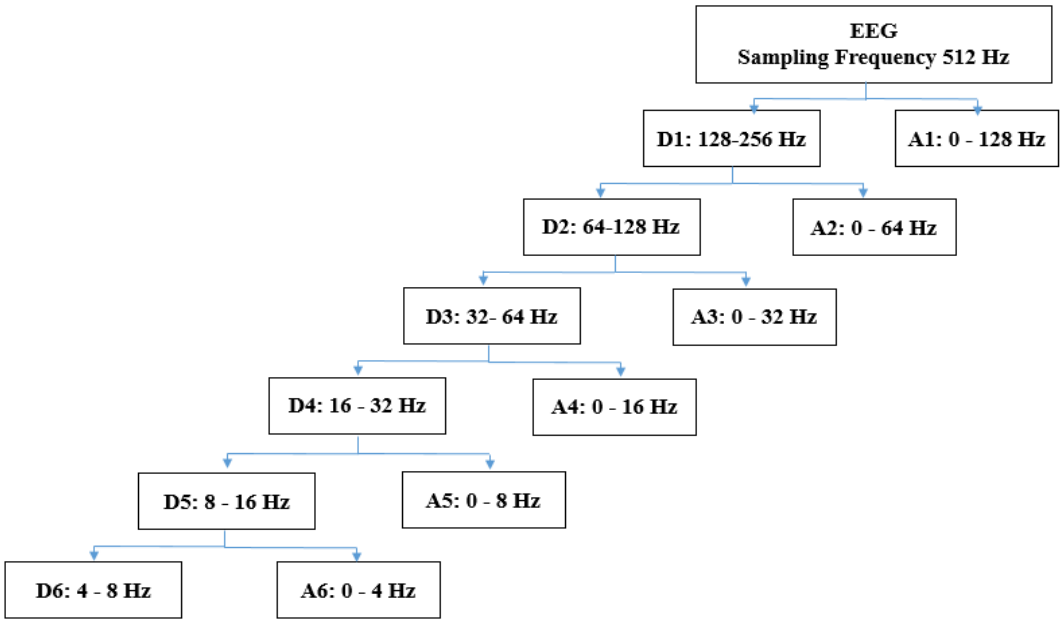

Figure 4.5: **Wavelet decomposition of EEG signal with frequency at 512 Hz**

Wavelet Energy (WE)

According to Parseval's Theorem, in wavelet analysis, the energy of signals which correspond to PSD, WE can be partitioned at different levels of wavelet decomposition ($j = 1, \ldots l$) and is expressed as a function of the scaling and wavelet coefficient:

$$E_T = \int |f(t)|^2 \, \mathrm{dt} = \sum_k \left|C_{J,k}\right|^2 + \sum_k \sum_j \left|C_{J,k}\right|^2 \tag{4.8}$$

The analysis of each detail of decomposed signals also captures the temporal dynamics of the signals in each electrode and frequency band through the calculation of the mean, minimum and maximum values of signals.

Wavelet Centroid Scale (WCS)

The calculation of Wavelet Centroid Scale (WCS), based on the CWT scale-gram, shows the shift of the centre of gravity of the frequency band. The CWT is chosen since it has a better frequency (scale) representation compared to the DWT. The complex Morlet wavelet is used due to its narrow spectral band and its having an extended time domain made it more suitable for extracting information in the frequency domain (Misiti et al. 2013). It is equivalent to a complex sinusoid with a Gaussian envelope and can be written as:

$$\psi_0(t) = \frac{1}{\sqrt[4]{\pi}} e^{2\pi f t} e^{-\frac{t^2}{2}} \tag{4.9}$$

Wavelet Energy Entropy (WEE)

The wavelet energy entropy (WEE) is calculated as

$$P_i = \frac{\mathrm{E}_j}{E_T} \tag{4.10}$$

where E_j refers to the energy of signals at a j^{th} frequency band of decomposition and E_T refers to the energy of all frequency bands of decomposition.

4.4.4 Feature Extraction using Fast Fourier Transform (FFT)

As discussed in Chapter 3 for FFT feature extraction, the EEG data in the time domain was transformed into the frequency domain using Welch's method with a 256 points FFT with 55% overlapping.

The power spectrum $P(f_i)$ was used to analyse into four frequency subbands, namely theta (4-8Hz), alpha (8-13Hz), low beta (13-21 Hz) and high beta (21-38Hz). The PSD, PSE and CF of each frequency band were estimated and chosen as the main parameters for GIF detection.

4.4.5 Classification Algorithm using Support Vector Machine (SVM)

A Wilcoxon signed-rank test with *p-value* ≤ 0.5 was used to investigate significant differences between periods of GS and GIF. The significant mean, maximum and minimum power value of four sub-bands from each electrode taken from two events were chosen as the features to detect GIF.

Support Vector Machine (SVM) was utilized to detect GIF because of its accuracy and ability to deal with a large number of predictors (Yuwono et al. 2014). The significant features were divided into half portions, one for the training set (50%) and the same amount for the testing set (50%). SVM with a Radial Basis Function (RBF) kernel is computed as follows (Yuwono et al. 2014)

$$RBF_{JS}(x, \mu_k, \sigma_k) = \exp\left(-\frac{JS(x||\mu_k)}{2\,\sigma_k^2}\right) \qquad (4.11)$$

where x, k, μ_k and σ_k denote a random vector, support vector index, support vector centroid and support vector radius, respectively. JS denotes the Jensen-Shannon (JS) divergence between x and μ_k.

The *JS* divergence is a symmetrized and smoothed version of the Kullback-Leibler (KL) divergence. *JS* divergence is calculated as

$$JS(P||Q) = \frac{1}{2}KL(P||M) + \frac{1}{2}KL(Q||M) \qquad (4.12)$$

where *P*, *Q* denote discrete probability distribution, *M* = (*P*+Q) / 2 denotes the central probability mass function and *KL* divergence is computed as

$$KL(R||S) = \sum_{x} R(x) \log \frac{R(x)}{S(x)} \qquad (4.13)$$

A particle swarm ensemble clustering algorithm known as Ensemble Rapid Centroid Estimation (ERCE) was used for estimating the parameters for the RBF kernel (Yuwono et al. 2014). When using ERCE, μ_k and σ_k could be inferred from the training data by using the following four steps:

1. Execute *ERCE* to cluster the training set to an arbitrary number based on *JS* distance.

2. Aggregate the ensemble clustering results using average linkage to get the final clustered sets $\mathbb{C}_k$. The corresponding centroid vector μ_k was computed as:

$$\mu_k = E[x|\mathbb{C}_k] = \frac{1}{|\mathbb{C}_k|} \sum_{x \in \mathbb{C}_k} x \qquad (4.14)$$

3. The *RBF* kernel radius σ_k was taken as the square root of conditional *JS* divergence, which is given as follows

$$\sigma_k^2 = E[JS(x||\mu_k)\mathbb{C}_k] = \frac{1}{|\mathbb{C}_k|} \sum_{x \in \mathbb{C}_k} JS(x||\mu_k) \qquad (4.15)$$

The SVM was then trained using the *LS* algorithm

4.4.6 Classification Algorithm using ANN

Two-layer feed-forward neural networks was applied to classify the pattern into two categories: GIF and GS. The input of ANN included WE, WCS and WEE features extracted from the EEG signals. The desired output was set at 1 in cases of GIF and 0 in cases of GS. The Levenberg-Marquardt algorithm was chosen as a training method for its speed and stability. The data set was separated randomly into a training set and test set at 50%, and 50%, respectively.

4.5 EXPERIMENTAL RESULTS

4.5.1 Feature Extraction Results

Figure 4.6. shows the time-frequency distributions in two events GS and GIF in central location C4 from the EEG data of one PD patient using the EEGLab toolbox. In this analysis, we explored the mean event-related changes in spectral power at each time during the epoch and at each frequency in this PD patient. It is observed that significant increase in power occurred at low beta (13-21 Hz) and high beta (21-38 Hz) frequency bands during GIF.

For the feature extraction, 132 seconds from the two events GS and GIF (66 seconds each) from all five PD patients were analysed. Table 4.1 shows the significant maximum amplitude from 15 locations based on four EEG frequency bands activities. A Wilcoxon signed-rank test with p-value ≤ 0.001 and a Cohen's effect size $d \geq 0.4$ were used to investigate significant differences between periods of GS and GIF.

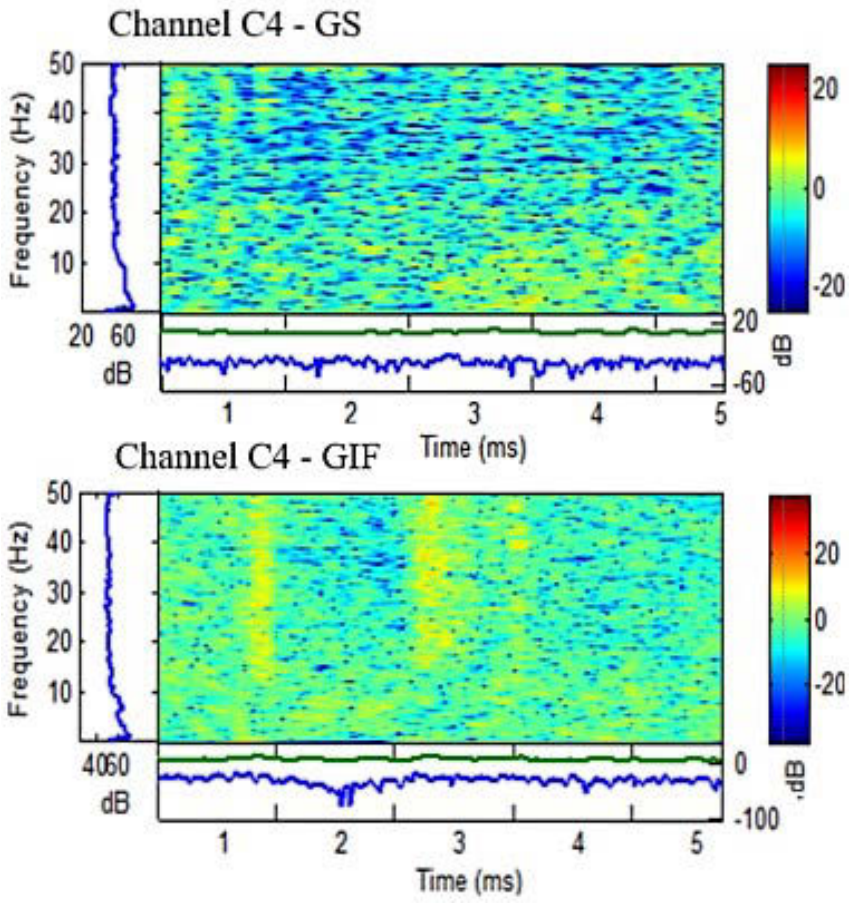

Figure 4.6: **EEG signal during GS and GIF episodes in time-frequency domain in C4**

In Table 4.1, a decrease in WE alpha was found in frontal F4 (*d*=0.2456) and an increase in WE alpha in occipital O2 (*d*=0.3619). However, there was no change in WE alpha in the other locations underlying the GIF episode. Overall, compared to Good start, there was an increase in WE theta in parietal P3 (*d*=0.4529).

In addition, it is apparent that WE high beta increased throughout the cortical brain regions underlying GIF. More specifically, WE high beta experienced the largest significant rise in parietal regions P3 (*d*=0.5013), P4 (*d*=0.5378), central region CP1 (*d*=0.4484) and occipital regions O1 (*d*=0.499), O2 (*d*=0.4577). WE high beta also changed significantly in central locations CP1 (*d*=0.4484) and CP2 (*d*=0.4). There was a slight changes in WE high beta in frontal F3 (*d*=0.1136); however, no change was found

in the opposite side at frontal F4. Low beta increased only in occipital O2 (d=0.2537) in the context of GIF seen in PD patients. This finding is similar to our previous studies using PSD for analysis (Handojoseno, Shine, et al. 2015; Ly et al. 2016). Figure 4.7 shows the comparison in WE theta and WE high beta within frontal-central cortical locations.

The wavelet energy entropy (WEE) measures the temporal regularity of energy of the frequency bands and shows the loss of complexity in most of the frequency bands and electrodes during each event (GIF or GS). The results of entropy analysis in Table 4.2 showed an increase of entropy in most frequency bands and locations during GIF. The WEE low beta appeared as the most affected sub-band underlying GIF, with the strongest increase in central C4 (d=0.5024). There was a slight increase of WEE theta in central Cz (d=0.3625), along with a decrease in occipital O2 (d=0.3878) during GIF episode. The WEE alpha increased only in frontal F3 when PD patients were not able to initiate the gait.

The results of wavelet centroid scale (WCS) show an increase in theta in frontal F4 (d=0.2) and high beta in occipital O1 (d=0.3308) only during GIF episode. There were no changes in two other sub-band alpha and low beta in this episode (Table 4.3).

Table 4.1: Features analysis of WE between GS and GIF

Parameter	Band	GS(μV ± std)	GIF(μV± std)	p	d	GS vs.GIF
WE-F3	α	0160 ± 0.08	0158 ± 0.10	0.4568	0.0201	
	hβ	0.068 ± 0.07	0.076 ± 0.06	0.0453	0.1136	*
WE-F4	α	0.132 ± 0.06	0.113 ± 0.09	0.0026	0.2456	*
	hβ	0.067 ± 0.06	0.068 ± 0.06	0.9655	0.0133	
WE-C3	hβ	0.091 ± 0.07	0.103 ± 0.06	0.0095	0.2205	*
WE-C4	hβ	0.091 ± 0.07	0.107 ± 0.06	0.00219	0.3129	*
WE-CP1	hβ	0.078 ± 0.07	0.119 ± 0.06	0.0008	0.4484	**
WE-CP2	hβ	0.088 ± 0.07	0.119 ± 0.07	0.0058	0.4	*
WE-P3	θ	0.359 ± 0.20	0.377 ± 0.15	0.0178	0.4529	*
	hβ	0.112 ± 0.07	0.150 ± 0.07	0.0015	0.5013	**
WE-PZ	θ	0.283 ± 0.01	0.226 ± 0.01	0.0181	0.4510	
	hβ	0.114 ± 0.07	0.150 ± 0.09	0.0093	0.216	*
WE-P4	θ	0.271 ± 0.01	0.232 ± 0.01	0.1077	0.3149	
	hβ	0.084 ± 0.06	0.115 ± 0.05	0.0055	0.5378	**
WE-O1	α	0.175 ± 0.07	0.191 ± 0.07	0.1801	0.2304	
	hβ	0.203 ± 0.09	0.252 ± 0.09	0.0096	0.315	**
WE-O2	α	0.160 ± 0.07	0.188 ± 0.08	0.0305	0.3619	*
	lβ	0.197 ± 0.11	0.224 ± 0.09	0.033	0.2537	*
	hβ	0.199 ± 0.09	0.242 ± 0.09	0.0065	0.4577	**

**: Significant at $p \leq 0.05$, Cohen's $d < 0.4$; **: Significant at $p \leq 0.001$ and Cohen's $d \geq 0.4$*

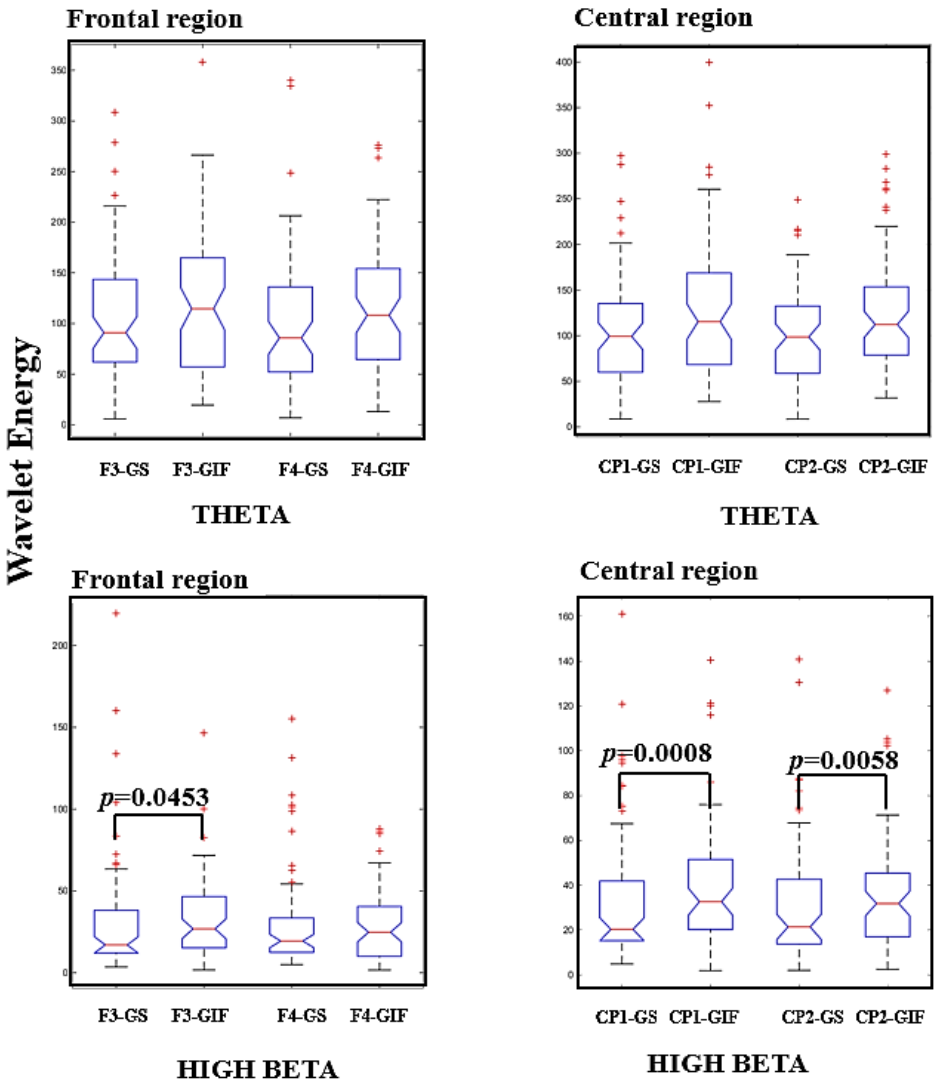

Figure 4.7: Wavelet Energy in Frontal and Central location underlying GS and GIF episodes

Table 4.2: Features analysis of WEE between GS and GIF

Parameter	Band	GS (μV ± sdt)	GIF (μV ± sdt)	p	d	GS vs.GIF
WEE-F3	α	0.731 ± 0.08	0.760 ± 0.07	0.0403	0.3732	*
	lβ	0.770 ± 0.06	0.796 ± 0.03	0.033	0.4725	*
WEE-F4	α	0.739 ± 0.08	0.747 ± 0.07	0.6871	0.1087	
	lβ	0.770 ± 0.06	0.788 ± 0.06	0.0301	0.2839	*
WEE-C3	θ	0.695 ± 0.10	0.711 ± 0.09	0.5648	0.1547	
WEE-C4	θ	0.695 ± 0.11	0.690 ± 0.10	0.8752	0.0453	
	lβ	0.758 ± 0.07	0.791 ± 0.05	0.0014	0.5024	**
WEE-CP1	lβ	0.774 ± 0.05	0.764 ± 0.06	0.2200	0.1593	
WEE-CP2	lβ	0.759 ± 0.07	0.783 ± 0.05	0.0305	0.3656	*
WEE-Cz	θ	0.685 ± 0.09	0.718 ± 0.09	0.044	0.3625	*
	lβ	0.788 ± 0.04	0.768 ± 0.06	0.1472	0.3436	
WEE-P3	α	0.741 ± 0.07	0.760 ± 0.07	0.048	0.2572	*
WEE-P4	α	0.760 ± 0.06	0.766 ± 0.06	0.6409	0.0962	
	lβ	0.778 ± 0.05	0.762 ± 0.07	0.3335	0.2386	
WEE-O1	θ	0.676 ± 0.10	0.700 ± 0.10	0.2431	0.2289	
WEE-O2	θ	0.714 ± 0.09	0.670 ± 0.12	0.046	0.3878	*
	lβ	0.743 ± 0.08	0.742 ± 0.07	0.5285	0.0073	

**: Significant at $p \leq 0.05$ and Cohen's $d < 0.4$; **: Significant at $p \leq 0.001$ and Cohen's $d \geq 0.4$*

Table 4.3: Features analysis of WCS between GS and GIF

Parameter	Band	GS (μV ± sdt)	GIF (μV ± sdt)	p	d	GS vs.GIF
WCS-F3	θ	69.141 ± 6.43	73.115 ± 8.20	0.0483	0.2	*
	hβ	20.176 ± 6.12	20.915 ± 6.93	0.5587	0.1129	
WCS-F4	θ	72.106 ± 7.90	73.974 ± 8.36	0.5405	0.1030	
	hβ	20.176 ± 6.12	20.915 ± 6.93	0.5587	0.1129	
WCS-C3	θ	72.527 ± 8.00	73.547 ± 6.83	0.1409	0.1733	
	hβ	19.914 ± 5.77	21.532 ± 7.90	0.5679	0.2337	
WCS-C4	θ	72.291 ± 9.70	74.734 ± 6.71	0.3026	0.1337	
WCS-P3	hβ	19.469 ± 6.00	21.729 ± 8.47	0.2524	0.3078	
WCS-P4	hβ	19.774 ± 7.02	20.572 ± 7.44	0.6214	0.1102	
WCS-O1	θ	75.887 ± 7.56	76.720 ± 8.66	0.3785	0.2383	
	hβ	19.649 ± 7.57	22.705 ± 7.64	0.045	0.3308	*
WCS-O2	θ	74.856 ± 6.59	76.484 ± 9.82	0.2717	0.2821	
	hβ	20.473 ± 9.13	21.539 ± 9.99	0.3520	0.1059	

**: Significant at $p \leq 0.05$ and Cohen's $d < 0.4$*

4.5.2 Classification Results

Next, the 15 channels EEG data was fed to the ICA-EBM which resulted in the 15 ICs separated sources. These optimized sources were further segmented for feature extraction using wavelet transform. To build a faster and better classification system, only significant statistically different features between two groups of data (p-values < 0.05) were chosen as input for the GIF detection.

Table 4.4 shows the classification result for GIF detection using WT as feature extraction and SVM as classification. For comparison purposes, the performance of the classifier using SVM depends on the input based on different parameters extracted by wavelet analysis. The classification result is from the original 15 EEG channels with different features such as WE, WCS and WEE in the case of with/without using of ICA-EBM. The classification (without ICA-EBM) using the WE, WCS and WEE as an input from 15

channels resulted in a sensitivity of 81.52%, a specificity of 85.45% and an accuracy of 83.48%, while the classification using 15 ICs (with ICA-EBM) resulted in a higher sensitivity of 83.94%, a specificity of 89.39% and an accuracy of 86.67%.

In addition, the performance using WCS and WEE features as input results in 77.12%, 79.24% and 78.18% for sensitivity, specificity, and accuracy, respectively, whereas the WE obtained the better result at 80.70% sensitivity, 80.60% specificity and 80.60% accuracy. The results confirmed that the combination of ICA-EBM as the source separator, WT as feature extraction and SVM as classifier achieved a better performance for detecting GIF.

Table 4.4: **Classification results of WT based features using SVM in detecting GIF from GS**

ICA-EBM	Features	Training			Testing		
		Sen(%)	Spe(%)	Acc(%)	Sen(%)	Spe(%)	Acc(%)
No	WCS,WEE	77.18	79.33	78.25	77.12	79.24	78.18
No	WE	81.00	80.80	80.90	80.70	80.60	80.60
No	WE,WCS,WEE	81.65	85.47	83.56	81.52	85.45	83.48
Yes	WE,WCS,WEE	84.25	89.43	86.84	83.94	89.39	86.67

Sen: Sensitivity; Spe: Specificity; Acc: Accuracy

Further comparisons were carried out between different classifiers (ANN, SVM) and feature extractors (FFT, WT) using ICA-EBM as source separation. Figure 4.8 shows the results in the receiver operating characteristic (ROC) curve and analyses of two classifiers (ANN, SVM) for detecting GIF based on the training data set (accounting for 50% of the total data). By definition, the ROC curve defines the compromise between the true positive rate (sensitivity) versus false positive rate (1-specificity). The ROC curve determines the desired classification performance in the comparison of different methods. In the ROC curve, each point is corresponding to one specific output threshold. The area

under the ROC curve (AUC) is an important value that reveals the performance of classification. The better ROC curve is the one that has the highest number of AUC.

The bold red coloured line represents the ROC curve for the method using ICA-EBM, WT, and SVM for GIF detection. The star blue coloured line represents the technique using ICA-EBM, WT, and ANN. The green coloured line represents the method using ICA-EBM, FFT, and SVM and the black line shows the ROC curve method using ICA-EBM, FFT and ANN. Using the same training data set, the ROC curves demonstrated that the combination of ICA-EBM, WT and SVM produced the highest AUC of 0.9036 for classifying GIF. This value outperforms the method using different classifier (ICA-EBM, WT, ANN) that achieved the AUC at 0.8552. On the same feature extractor FFT, the method using ICA-EBM, FFT, SVM achieved the higher AUC values (AUC= 0.7651) than that using ICA-EBM, FFT, ANN (AUC=0.7355) for detecting GIF.

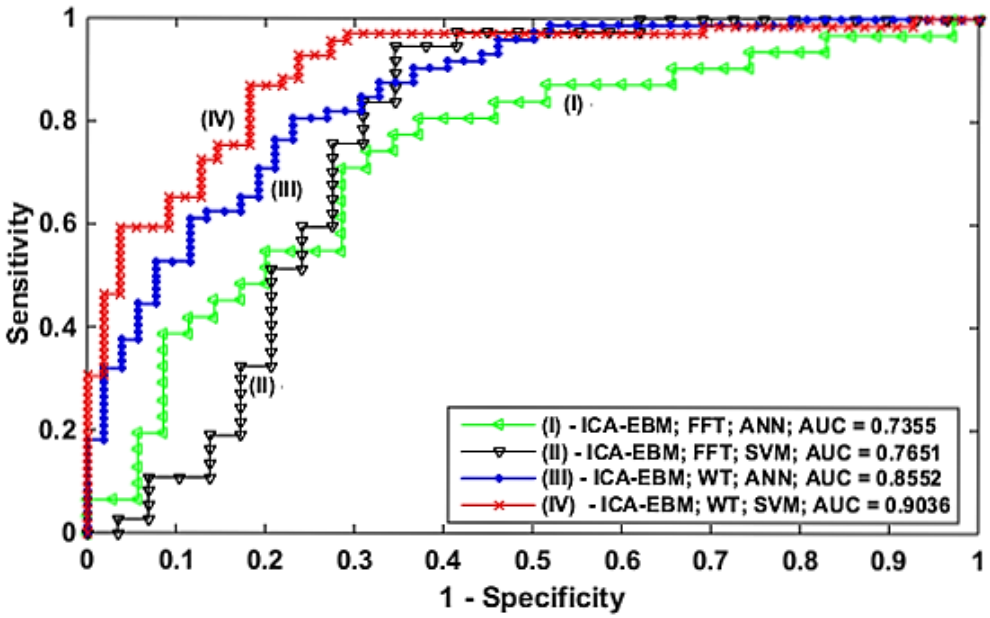

Figure 4.8: **ROC plot**

For the testing data set (accounting for 50% of the rest of the total EEG data), the results of the experiment show that wavelet analysis provided a better result compared to Fourier analysis based on the feature extraction related to power, centroid and entropy and classifiers such as ANN and SVM. When using WT based feature and ANN as a classifier, the 15 ICs data provided better results than using FFT based features and the same classifier. The results show sensitivity, specificity, and accuracy of 83.83%, 85.84%, and 85.00%, respectively. The performance was increased when using WT and SVM, with results of 83.94% sensitivity, 89.39% specificity and 86.67% accuracy (Table 4.5).

Table 4.5 Comparison of classification results in detecting GIF from GS using source separation ICA-EBM

Feature	Classifier	Testing		
		Sen (%)	Spec (%)	Acc(%)
FFT	ANN	80.59	74.52	77.59
FFT	SVM	79.04	78.89	78.81
WT	ANN	83.83	85.84	85.00
WT	SVM	83.94	89.39	86.67

Sen: Sensitivity; Spe: Specificity; Acc: Accuracy

4.6 DISCUSSION

This chapter compared ambulatory EEG during Gait Initiation Failure and Good Start in patients with PD who had GIF. By applying WT for feature extraction, the results showed the fast temporal changes occurring in the brain during GIF associated with an overall increase in high beta activities over frontal, central, parietal and occipital cortical locations underlying GIF. FOG has previously been associated with high beta oscillations in the subthalamic nucleus, which are coherent with both supplementary and primary motor areas (Toledo et al. 2014). Together these may constitute inhibitory control over motor actions when response conflict arises (Georgiades et al. 2016). This could explain the high beta frequencies found in frontal and central cortical regions during GIF in the

current study. High beta oscillation in parietal and occipital locations support the notion that PD patients with GIF suffered from impaired sensory integration and thus had to gain more information from the environment to initiate gait (Georgiades et al. 2016).

Classification results also showed that GIF could be detected using an advanced algorithm for GIF detection that applied ICA-EBM for source separation, wavelet for feature extraction and Support Vector Machine. This method achieved the best performance indicators for GIF detection, with sensitivity increasing by 2.42% (from 81.52% to 83.94%) and accuracy increasing by 3.19 % (from 83.48% to 86.67%) as compared with the case without using ICA-EBM (Table 4.4).

This research has successfully used EEG signals to investigate dynamic brain changes underlying GIF. Furthermore, using this technique, GIF could be detected with high performance using wavelet analysis as feature extraction. The current study provided additional support toward detecting freezing events (in this case GIF) by testing similar technique such as the combination of ICA-EBM (Source Separation), SVM (classifier) with different feature extraction (FFT, WT). The classification results showed the accuracy improved from 78.81% (ICA-EBM, FFT, SVM) to 86.67% (ICA-EBM, WT, SVM) for GIF detection. Finally, this work helps to understand the neurobiology of GIF, showing it is associated with high beta frequencies across the motor and sensory cortices. These results will ultimately promote the development of novel therapies and technologies to assist with the management of FOG in PD.

Chapter 5

Advanced Detection of Turning FOG and Gait Initiation Failure using EEG and Bayesian Neural Networks

5.1 INTRODUCTION: TURNING FOG AND GAIT INITIATION FAILURE

In contrast to chapters 3 and 4, where FFT and WT based feature was used for feature extraction, in this chapter, a time-frequency S-Transform (ST) was applied for feature extraction. One of the advantages of S-Transform technique is the capability to detect and analyse non-stationarity and their related aspects of EEG signals such as trends, breakdown points and discontinuity (Tran et al. 2014). Therefore, the FOG pattern can be characterized in both time and frequency domains. Further improvement focused on

developing an advanced computational intelligence system, in which advanced pre-processing techniques such as ICA-EBM and advanced classifier Bayesian Neural Networks (BNN) were built and applied to FOG detection system using EEG signals. As discussed in Chapter 2, Turning FOG and GIF were recognized to be the most frequent trigger of FOG. In our EEG data collection, Turning FOG and GIF accounted for 62.7% and around 24% of all witnessed FOG episodes, respectively (Schaafsma et al. 2003). Therefore, this chapter testes an advanced detection algorithm on these two common subtypes of FOG.

The main contributions of this chapter are the novel technique that combined ICA-EBM as the EEG source separation technique and EEG feature extraction using ST decomposition. Artificial neural networks optimized by Bayesian inference techniques were used for detecting Turning FOG and GIF. The reason why BNN was used is that Bayesian regularization framework has been proposed to enhance the generalization abilities of neural networks regardless of finite and/or noisy data. The probability distribution of network parameters is considered in Bayesian learning, providing the best generalization of the trained network. Especially, this type of neural network can be trained on all of the available data. Therefore, it is suitable for applications where the dataset is small.

The entropy bound estimation in ICA-EBM was chosen for its flexibility and its ability to approximate sources of a wide range of distributions that fit with the EEG signals, which indeed improved classification performance in previous EEG studies (Chai et al. 2017). The S-Transform was used to track alterations in signal magnitude, frequency and phase of selected EEG sources as it has been shown to outperform classical techniques based on either frequency or time domain (Stockwell, Mansinha & Lowe 1996).

5.2 SYSTEM OVERVIEW

An overview of the advanced Turning FOG/GIF detection based on BNN approach is illustrated in Figure 5.1. This started with data collection and was followed by pre-

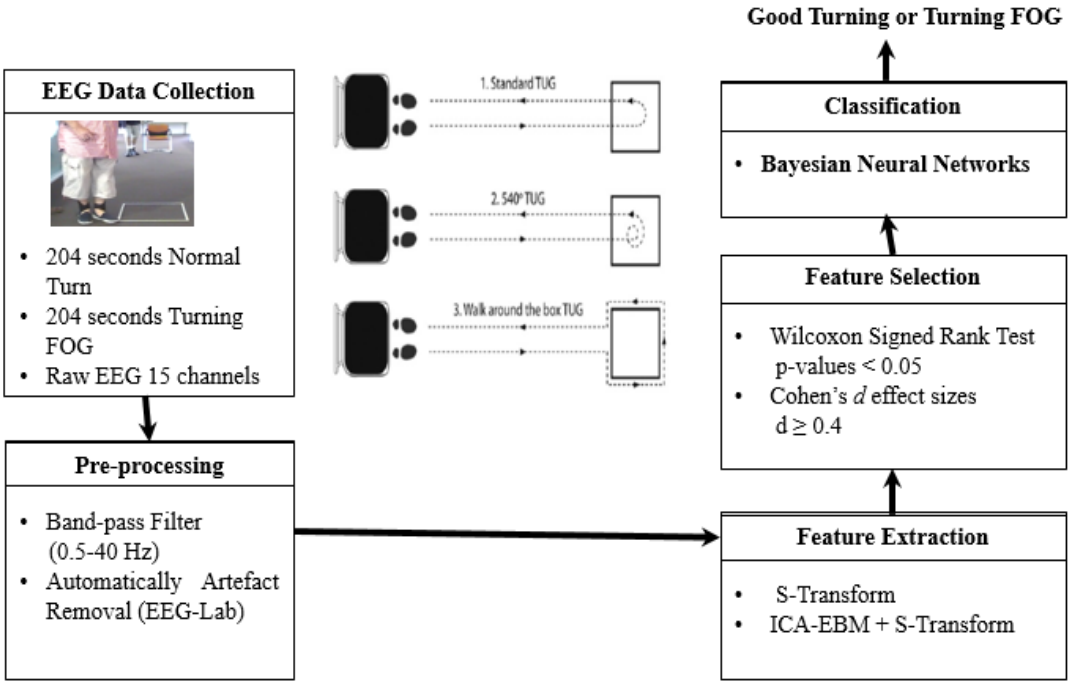

Figure 5.1: **Components of EEG-based Turning FOG detection system**

processing steps (filtered and removed artifacts in EEG signals) and was extracted in the form of S-Transform Decomposition. For input of classifier, the raw EEG signal was separated into Independent Components (ICs) using ICA-EBM and extracted using S-Transform decomposition. Artificial neural networks optimized by Bayesian framework was used for detecting Turning FOG/GIF in PD.

5.3 DATA COLLECTION

EEG data was recorded from 15 locations positioned over the following key cortical regions: F3, F4, FC1, FC2, C3, C4, CP1, CP2, CZ, P3, P4, Pz and O1, O2, Oz. PD patients were asked to perform either a right or a left turn (180 degrees or 540 degrees) inside/outside the taped box on the floor in a TUG task. Two separate conditions were identified for each patient based on video recordings, which was currently used as the golden standard to characterize FOG (Handojoseno, Gilat, et al. 2015) (Figure 5.2).

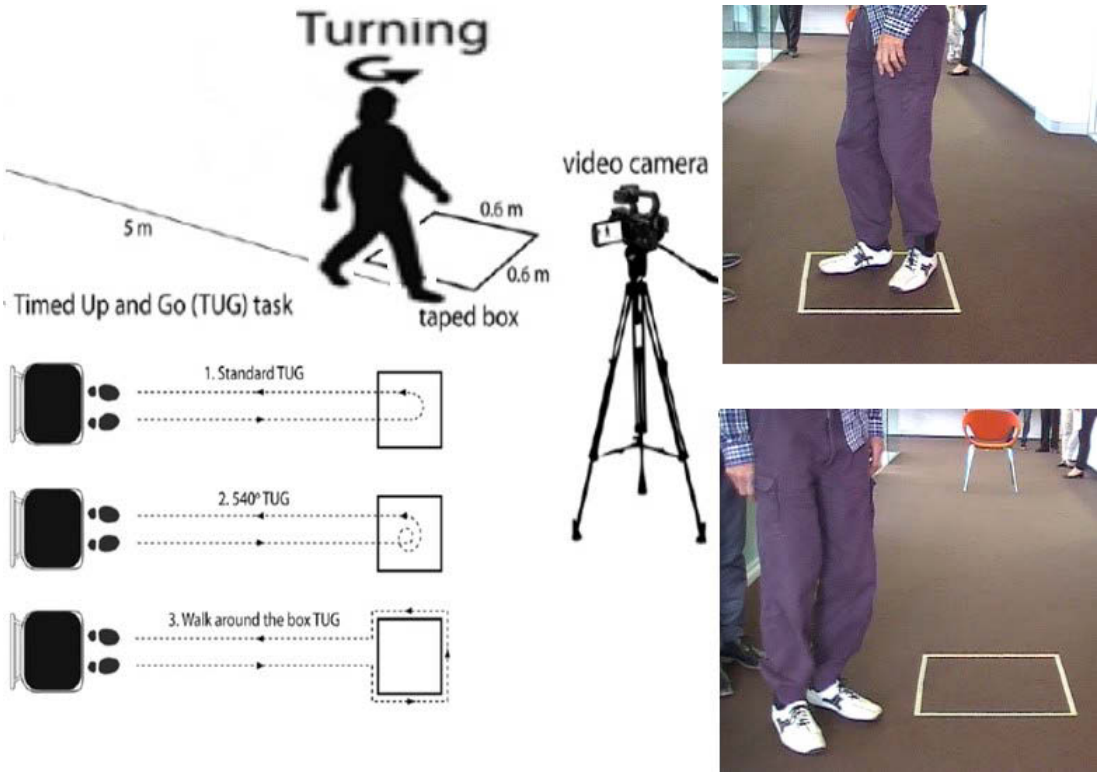

Figure 5.2: **Experiment setup to provoke Turning FOG in PD patients**

- Good Turn (GT): identified as a 2-second epoch of time in which a patient successfully made a right or left turn (180 degrees or 540 degrees) inside a taped $1m^2$ box on the floor.

- Turning FOG (TF): identified as an epoch of time in which patients suddenly became unable to make a turn inside a taped $1m^2$ box on the floor, despite the intention to do so. The duration of FT episodes occurs typically from 2 seconds to 5 seconds.

Raw EEG data from six PD patients resulted in 204 seconds of EEG data samples of Turning FOG (TF), which were matched to 204 seconds of EEG data samples of Good Turn (GT). EEG Data was then filtered using a band-pass filter (0.5-40 Hz). Artefacts such as eye activity movement and heart rate signals were removed by Automatic Artefact Removal (AAR) using the EEGLab toolbox before using the data for further analyses.

5.4 COMPUTATIONAL INTELLIGENCE

5.4.1 Data Pre-processing: Source separation ICA-EBM

As mentioned in chapter 4, ICA-EBM provided flexible density matching through the use of contrast functions based on the maximum entropy principle (Li & Adali 2010). ICA-EBM can separate sources that are both sub- or super-Gaussian distributions using only a small class of nonlinear functions. The algorithm adopted a line search procedure and initially used updates that constrain the ICA de-mixing matrix to be orthogonal for robust performance. Therefore, ICA-EBM was applied as a source separator to EEG data of Turning FOG/GIF in this chapter.

5.4.2 Feature Extraction using S-Transform Decomposition

The S-transform (ST) is a time-frequency analysis technique proposed by Stockwell, Manisinha and Lowe in 1996 (Stockwell, Mansinha & Lowe 1996). The ST was developed on the basis of short time Fourier Transform (STFT) and continuous wavelet transform (CWT) involving direct time-frequency mapping. The advantages of the S-transform are its linearity, lossless reversibility, multi-resolution and good time-frequency resolution. The S-Transform generates a constant relative bandwidth analysis while maintaining a direct link with the Fourier spectrum. In this study, four frequency bands were analysed using ST, namely: theta, alpha, low beta and high beta (Figure 5.3).

Given h(t) is a continuous signal, the S-transform is defined as:

$$S(\tau, f) = \int_{-\infty}^{\infty} h(t) w(\tau - t, f)\, exp(-i2\pi f t)\, dt \qquad (5.1)$$

where $w(\tau - t, f)$ denotes the specific mother wavelet of the signal

$$w(\tau - t, f) = \frac{|f|}{\sqrt{2\pi}} \exp(-0.5(\tau - t)^2 f^2) \qquad (5.2)$$

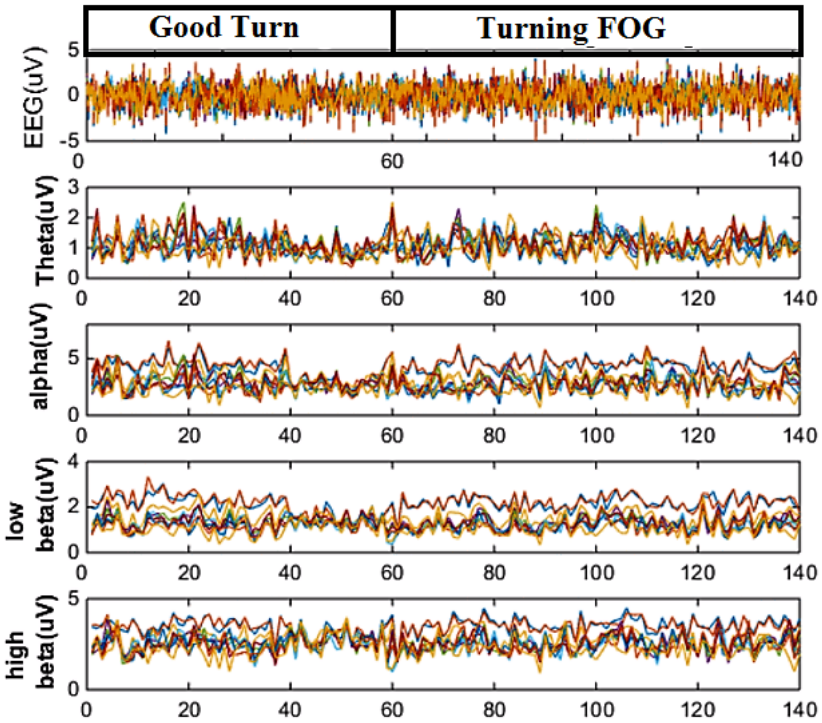

Figure 5.3: S-Transform Decomposition in Good Turn (1-5s), Turning FOG (6-10s) in F4 location

where *f* denotes the frequency, *t* denotes the time and τ denotes the delay with

$$\int_{-\infty}^{\infty} w(t,f)dt = 1 \tag{5.3}$$

Here, two parameters were extracted: the first is the maximum amplitude for each band at a time (t), $ST^{max}(t)$. The second parameter was computed as the mean of the of sum amplitudes within each band at a time (t), $ST^{mean}(t)$. These main features were used to explore the neural correlates underlying the episodes of turning FOG. In this study, a non-parametric statistical analysis, the Wilcoxon Sum Rank Test was chosen as feature selection method. Only useful features with corrected p-values<0.05, as computed by the non-parametric Wilcoxon Sum Rank Test, were employed as input for our classifier.

5.4.3 Feature Extraction using FFT and WT

The FFT feature extractor, which has been discussed and used previously in Chapter 3 and 4, is a frequency domain analysis. The power spectrum was calculated by using established FFT and Hanning window to derive spectral power. The WT feature extractor applied previously in Chapter 4, is obtained by shifting and dilating a mother wavelet function. The decomposition of the signal leads to a set of wavelet coefficients. As a result, the signal could be reconstructed as a linear combination of the wavelet functions weighted by the wavelet coefficients. The key feature of wavelets is the time-frequency localisations, which means that most of the energy of the wavelet is restricted to finite time intervals. Theta, alpha, low beta and high beta were analysed based on FFT and WT for the purpose of comparison detection.

5.4.4 Classification using Bayesian Neural Networks

The next step included a feature extraction module that transformed the pre-processed EEG signal with ICA-EBM into ST decomposition based on four sub-bands. Only useful features with corrected *p-values*<0.05, as computed by the non-parametric Wilcoxon Signed Rank Test, were employed as input for our classifier.

For the classification algorithm, Bayesian neural networks were implemented. Bayesian regularization framework has been proposed to improve the generalization abilities of neural networks regardless of finite and noisy obtainable data (Bishop 1995). Applying Bayesian techniques to neural network training and prediction offers principal methods for determining optimal weight decay coefficients and model selection while making efficient use of training data. The use of the hyper parameters in the cost function can prevent the network from being trapped in poor generalization. As a result, a validation data set is not needed for Bayesian training. BNN is highly suitable for experiments such as ours where a limited set of data is only available for training and testing. The BNN structure uses a 3-layer (input, hidden and output layers) feed-forward structure as follows:

$$z(x,w) = f_1\left(b_k + \sum_{j=1}^{m} \overline{w}_{kj}\, f_2\left(b_j + \sum_{i=1}^{n} w_{ji}\, x_n\right)\right) \quad (5.4)$$

where f_1, f_2 denotes the activation function, x represents the input vector, w denotes the weight matrix vector; w_{ji} indicates the weight of the link between the *i* hidden node and the *j* input; $\overline{w}kj$ denotes the weight of the link between *i* hidden node and the output, b_k and *bj* denote the biases; *m* denotes the number of outputs; *n* denotes the number of inputs.

In the Bayesian framework, the most probable model corresponding to the training data D is found automatically. Based on the Gaussian probability distribution over weight values, the posterior distribution of the weights *w* in network *H* can be calculated using Bayes' theorem as shown below:

$$p(w|D,H) = \frac{p(D|w,H)\, p(w|H)}{p(D|H)} \quad (5.5)$$

where $p(w|D,H)$ is the likelihood which contained information about weight from observations, the prior distribution $p(w|H)$ contains information about background weight set, and the $p(D|H)$ is known as the evidence of the network *H*.

The BNN training modifies the objective function of the networks such as the sum of squared error (*mse*) with the error function is calculated as

$$F = E_d = \frac{1}{I}\sqrt{\sum_{i=1}^{n}(d_i - o_i)^2} \quad (5.6)$$

where d_i is the desired output, and o_i is the actual output.

The regularization improves the model's generalization by adding the sum of squared weight function E_w to the objective function component(w) :

$$F(w) = \beta E_d(\mathrm{w}) + \alpha E_w(\mathrm{w}) \quad (5.7)$$

where β and α are two hyper-parameters which indicate a minimal error, and minimal weights to seek in the learning process. E_d(w) is the error function, and $E_w(w)$ is the sum square of weight function, defined in the following equation:

$$E_w(w) = \frac{1}{2}||w||^2 \tag{5.8}$$

By introducing hyper-parameters in the cost function, neural network weights can be prevented from being too large, which would result in poor generalization for new test cases. As a result, a validation set is not required in a neural network training procedure.

Next, the Bayesian algorithm regularization is applied to revise hyper-parameters as follows

$$\alpha^{MP} = \frac{\gamma}{2E_w(w^{MP})} \tag{5.9}$$

$$\beta^{MP} = \frac{N-\gamma}{2E_D(w^{MP})} \tag{5.10}$$

where $\gamma = n - 2\alpha^{MP} tr(H^{MP})^{-1}$ is called the effective number of parameters, *n* is the total number of parameters in the network, *N* is the total number of errors, and *H* is Hessian matrix of *F(w)* at the minimum point of w^{MP}. The log evidence of model H_i is evaluated by Bayesian framework as follows:

$$\ln p(D|H_i) = -\alpha_{MP}E_W^{MP} - \beta_{MP}E_W^{MP} - \frac{1}{2}ln|A| + \frac{W}{2}ln\,\alpha_{MP} + \frac{N}{2}ln\,\beta_{MP} + \ln M! + 2\ln M + \frac{1}{2}ln\frac{2}{\gamma} + \frac{1}{2}ln\frac{2}{N-\gamma} \tag{5.11}$$

where *W* is the number of network parameters, *M* is the number of hidden nodes, and A is the Hessian matrix of the cost function. A network structure with the highest log evidence value will be selected as the best optimal structure of that network.

This addition was proposed to find the best generalization by optimizing these parameters in the Bayesian framework. To improve the efficiency of the optimization, Bayesian was

added to the Levenberg-Marquardt to be used for the Gauss-Newton approximation to the Hessian matrix, available in this optimization algorithm for learning. For Bayesian neural network classification, a validation set is not required in a neural network training procedure. As a result, the current dataset was randomly divided into a training set and a test set with each containing 50% of the original data from PD patients. For the performance measurement, the well-known performance indicators, including specificity (%), sensitivity (%) and accuracy (%) were calculated based on function 3.20; 3.21 and 3.22 in chapter 3.

5.4.5 Classification Algorithms using ANN and SVM

Two-layer feed-forward neural networks with 2 to 12 hidden nodes was applied to classify the pattern. The input of this classifier included ST features extracted from the EEG signals. The motivation behind the support vector machine (SVM) classification is to map the input into a high dimensional feature space, in which the data might be linearly separable. The training of the SVM is defined in the first place for the case of a binary classification problem, for which a linear decision surface exists that can perfectly classify the training data. The assumption of linear separability means that there exists some hyperplane, which perfectly separates the data. The data set was separated randomly into a training set and test set with the ratio of 50% and 50%, respectively for classification.

5.5 DETECTION OF TURNING FOG USING ICA-EBM (SOURCE SEPARATOR), S-TRANSFORM (FEATURE EXTRACTOR) AND BAYESIAN NEURAL NETWORKS (CLASSIFIER)

Figure 5.4 shows the time-frequency distributions of S-transform based on the above EEG signals from the frontal F4 electrode of one PD patient in two events Good Turn and Turning FOG. The GT segments run from 1 to 5 seconds and the TF segments run from

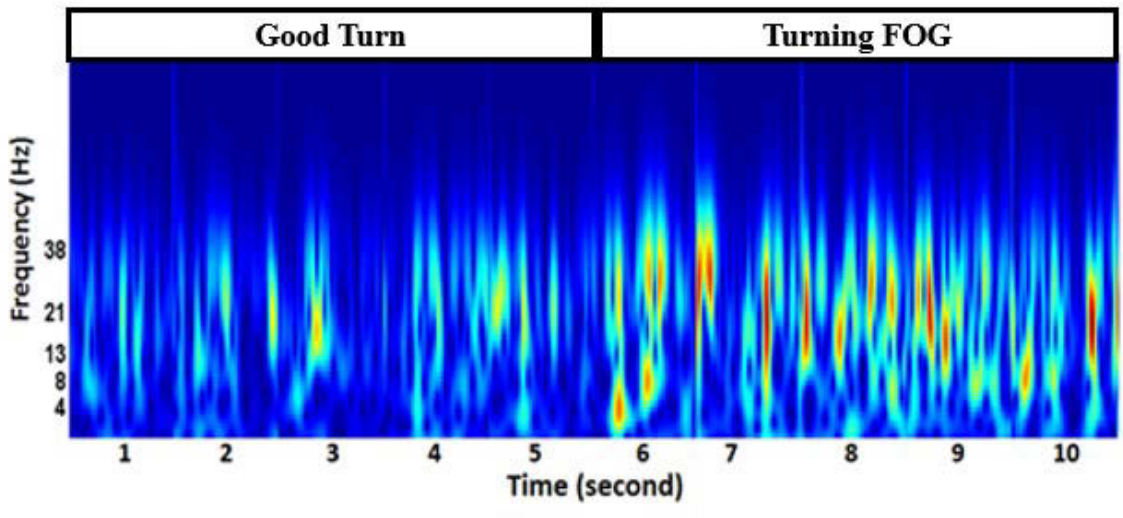

Figure 5.4: **Time-frequency distributions of S-transform in Good Turn (1-5s), Turning FOG (6-10s) in F4 location**

6 to 10 seconds. As clearly demonstrated, there are significant increases during TF across theta, alpha, low beta and specifically high beta frequency bands.

To investigate significant differences between periods of GT and periods of TF, a Wilcoxon Signed-Rank Test was conducted on the sample of 6 patients. Table 5.1 and Table 5.2 shows the significant maximum amplitude ($ST^{max}(t)$) in the four sub-bands between periods of GT and TF. Smaller p-values (p-values ≤0.0001) and larger Cohen's *d* (*d*≥0.4) indicated the biggest differences in features between the two conditions.

The most considerable significant increase in activity was found in low beta and high beta bands across the brain regions during TF. The most substantial maximum differences were found in high beta activity from frontal F4 (*d*=0.6143) and occipital O2 (*d*=0.5919) locations. Moreover, maximum alpha band activity increased significantly only in occipital locations O1 (*d*=0.3731), Oz (*d*=0.3911) and O2 (*d*=0.3089) during TF stages. Theta band increased remarkably just in occipital locations O1 (*d*=0.3202), O2 (*d*=0.2043) and the low beta increased in F3 (*d*=0.3777), O1 (*d*=0.508), O2 (*d*=0.483) and Oz (*d*=0.4647) during TF.

Table 5.1: Feature analysis of ST (ST^{max}) based feature between GT and TF in Frontal, Central and Parietal

Parameter	Band	GT(μV± std)	TF(μV ± std)	p	d	GTvs. TF
ST-F3	θ	0.233 ± 0.12	0.213 ± 0.11	0.1354	0.1702	
	α	0.302 ± 0.12	0.335 ± 0.11	0.0067	0.2278	*
	lβ	0.261 ± 0.09	0.296 ± 0.09	0.0002	0.3777	**
	hβ	0.292 ± 0.10	0.343 ± 0.08	≤0.0001	0.4994	***
ST-F4	θ	0.213 ± 0.14	0.191 ± 0.11	0.8782	0.0937	
	lβ	0.224 ± 0.09	0.262 ± 0.09	0.0004	0.3993	**
	hβ	0.262 ± 0.10	0.322 ± 0.09	≤0.0001	0.6143	***
ST-FC1	lβ	0.295 ± 0.09	0.302 ± 0.10	0.2185	0.1768	
	hβ	0.323 ± 0.09	0.362 ± 0.09	0.0004	0.3818	**
ST-FC2	lβ	0.262 ± 0.09	0.283 ± 0.10	0.0851	0.1958	
	hβ	0.302 ± 0.09	0.353 ± 0.09	≤0.0001	0.5354	***
ST-C3	θ	0.222 ± 0.13	0.192 ± 0.10	0.1572	0.2212	
	hβ	0.334 ± 0.09	0.371 ± 0.09	≤0.0001	0.4938	***
ST-C4	lβ	0.241 ± 0.10	0.278 ± 0.10	0.0017	0.3234	*
	hβ	0.27 ± 0.09	0.310 ± 0.09	0.0001	0.4295	**
ST-CP1	lβ	0.321 ± 0.11	0.337 ± 0.12	0.5677	0.1072	
	hβ	0.329 ± 0.09	0.376 ± 0.09	0.0001	0.4556	**
ST-CP2	hβ	0.320 ± 0.09	0.362 ± 0.08	0.0001	0.4729	**
ST-P3	lβ	0.302 ± 0.14	0.302 ± 0.12	0.4401	0.0347	
	hβ	0.362 ± 0.11	0.415 ± 0.10	0.0002	0.4397	**
ST-P4	lβ	0.220 ± 0.13	0.194 ± 0.10	0.1572	0.2212	
	hβ	0.332 ± 0.10	0.373 ± 0.09	0.0011	0.3654	**
ST-Pz	lβ	0.383 ± 0.13	0.372 ± 0.14	0.5780	0.0242	
	hβ	0.359 ± 0.10	0.402 ± 0.09	≤0.0001	0.4427	***

**: Significant at $0.001 < p \leq 0.05$ and Cohen's $d < 0.3$*
***: Significant at $0.0001 < p \leq 0.001$ and Cohen's $0.3 \leq d < 0.4$*
****: Significant at $p \leq 0.0001$ and Cohen's $d \geq 0.4$*

Table 5.2: Feature analysis of ST (ST^{max}) based feature between GT and TF in Occipital

Parameter	Band	GT(μV± std)	TF(μV ± std)	p	d	GTvs. TF
ST-O1	θ	0.302 ± 0.12	0.332 ± 0.08	0.0081	0.3202	*
	α	0.582 ± 0.22	0.662 ± 0.18	0.0007	0.3731	**
	lβ	0.513 ± 0.21	0.593 ± 0.16	≤0.0001	0.4304	***
	hβ	0.444 ± 0.15	0.514 ± 0.12	≤0.0001	0.508	***
ST-Oz	α	0.595 ± 0.23	0.671 ± 0.18	0.0002	0.3911	**
	lβ	0.516 ± 0.21	0.602 ± 0.15	≤0.0001	0.4647	***
	hβ	0.433 ± 0.14	0.502 ± 0.11	≤0.0001	0.5063	***
ST-O2	θ	0.302 ± 0.12	0.321 ± 0.10	0.0079	0.2043	*
	α	0.588 ± 0.25	0.657 ± 0.20	0.0055	0.3089	*
	lβ	0.481 ± 0.22	0.586 ± 0.17	≤0.0001	0.483	***
	hβ	0.402 ± 0.15	0.488± 0.11	≤0.0001	0.5919	***

**: Significant at 0.001 < p ≤ 0.05 and Cohen's d < 0.3*
***: Significant at 0.0001 <p ≤ 0.001 and Cohen's 0.3 ≤ d <0.4*
****: Significant at p≤0.0001 and Cohen's d ≥ 0.4*

Table 5.3 and 5.4 shows the significant mean of the S-Transform decomposition $ST^{mean}(t)$ in the four sub-bands within frontal, central and parietal regions between periods of GT and TF. The results show that theta and high beta oscillations increase and remain high during the TF in these four regions. When compared to the period of GT, the TF are associated with the largest significant increase in theta in frontal FC1 (*d*=0.5894), parietal P1 (*d*=0.6018), Pz (*d*=0.6042) and occipital O1 (*d*=0.594). There is a high beta increase underlying the TF episodes seen in PD patients, with the most significant increase in frontal F4 (*d*=0.526), central Cz (*d*=0.53), parietal P4 (*d*=0.4858) and occipital O2 (*d*=0.6388). In addition, there are significant increases in low beta in frontal F4 (*d*=0.4476), central C4 (*d*=0.3034), parietal P4 (*d*=0.3947) and occipital O1 (*d*=0.5927), along with alpha activity in frontal F3 (*d*=0.5523). Overall, occipital regions stand out as the most affected locations during the episode of TF with the smallest *p* (p-values ≤0.0001) and largest Cohen's *d* (d≥0.4).

Table 5.3: Feature analysis of ST (ST^{mean}) based features between GT and TF in Frontal and Central

Parameter	Band	GT(μV±std)	TF(μV ±std)	p	d	GTvs.TF
ST-F3	θ	1.161 ± 1.07	2.101 ± 2.15	0.0021	0.5523	**
	α	2.312 ± 0.96	2.471 ± 0.77	0.006	0.1863	*
	lβ	1.072 ± 0.32	1.132 ± 0.32	0.0003	0.384	**
	hβ	2.163 ± 0.60	2.316 ± 0.53	≤0.0001	0.4586	***
ST-F4	θ	2.165 ± 2.44	1.182 ± 1.26	0.048	0.5042	*
	lβ	0.851 ± 0.38	1.021 ± 0.36	≤0.0001	0.4476	***
	hβ	1.841 ± 0.68	2.181 ± 0.60	≤0.0001	0.526	***
ST-FC1	θ	1.160 ± 1.06	2.048 ± 1.93	≤0.0001	0.5894	***
	lβ	1.112 ± 0.29	1.215 ± 0.32	0.0173	0.3051	*
	hβ	2.391 ± 0.59	2.615 ± 0.56	0.0011	0.37	**
ST-FC2	θ	2.083 ± 2.01	1.133 ± 1.11	≤0.0001	0.5836	***
	lβ	1.010 ± 0.36	1.125 ± 0.37	0.0142	0.2909	*
	hβ	2.260 ± 0.67	2.467 ± 0.59	0.0012	0.3701	**
ST-C3	θ	2.281 ± 2.22	1.254 ± 1.16	≤0.0001	0.5777	***
	lβ	1.232 ± 0.33	1.321 ± 0.33	0.0328	0.2496	*
	hβ	2.471 ± 0.64	2.713 ± 0.58	0.0003	0.3852	**
ST-C4	θ	2.174 ± 2.24	1.202 ± 1.20	0.008	0.5366	**
	lβ	0.901 ± 0.46	1.049 ± 0.44	0.004	0.3034	**
	hβ	1.912 ± 0.74	2.193 ± 0.69	≤0.0001	0.3965	**
ST-CP1	θ	1.218 ± 1.17	2.332 ± 2.16	≤0.0001	0.6018	***
	hβ	2.423 ± 0.69	2.641 ± 0.60	0.007	0.3261	**
ST-CP2	θ	2.253 ± 2.15	1.251 ± 1.18	≤0.0001	0.5778	***
	lβ	1.183 ± 0.41	1.292 ± 0.41	0.0062	0.2787	*
	hβ	2.361 ± 0.69	2.601 ± 0.61	0.0009	0.3672	**
ST-Cz	θ	1.912 ± 1.78	1.082 ± 0.98	≤0.0001	0.5724	***
	lβ	1.122 ± 0.32	1.292 ± 0.33	≤0.0001	0.4929	***
	hβ	2.351 ± 0.63	2.682 ± 0.58	≤0.0001	0.53	***

Table 5.4: Feature analysis of ST (ST^{mean}) between GT and TF in Parietal and Occipital

Parameter	Band	GT(µV± std)	TF(µV ± std)	p	d	GTvs.TF
ST-P3	θ	2.510 ± 2.45	1.362 ± 1.30	≤0.0001	0.5862	***
	α	2.691 ± 0.83	2.548 ± 0.86	0.0511	0.1748	
	lβ	1.442 ± 0.46	1.583 ± 0.40	0.0072	0.3133	*
	hβ	2.721 ± 0.79	2.991 ± 0.64	0.0005	0.4109	**
ST-Pz	θ	2.311 ± 2.07	1.292 ± 1.17	≤0.0001	0.6042	***
	α	2.339 ± 1.42	2.164 ± 1.08	0.2220	0.1847	
	lβ	1.253 ± 0.39	1.361 ± 0.37	0.0077	0.2862	*
	hβ	2.452 ± 0.69	2.629 ± 0.60	0.0007	0.3655	**
ST-P4	θ	2.546 ± 2.37	1.408 ± 1.25	≤0.0001	0.601	***
	α	2.397 ± 1.42	2.161 ± 1.08	0.2220	0.1847	
	lβ	1.421 ± 0.43	1.588 ± 0.36	0.0005	0.3947	**
	hβ	2.622 ± 0.68	2.927 ± 0.55	≤0.0001	0.4858	***
ST-O1	θ	1.541 ± 1.30	2.799 ± 2.69	≤0.0001	0.594	***
	α	3.843 ± 1.14	4.225 ± 0.82	0.0018	0.3737	*
	lβ	1.791 ± 0.58	2.079 ± 0.39	≤0.0001	0.5699	***
	hβ	3.032 ± 0.87	3.536 ± 0.55	≤0.0001	0.6115	***
ST-O1	θ	1.561 ± 1.25	2.776 ± 2.59	≤0.0001	0.591	***
	α	3.902 ± 1.19	4.297 ± 0.86	0.0015	0.3727	**
	lβ	1.792 ± 0.56	2.079 ± 0.37	≤0.0001	0.5927	***
	hβ	3.091 ± 0.87	3.550 ± 0.56	≤0.0001	0.6369	***
ST-O2	θ	1.572 ± 1.34	2.719 ± 2.52	≤0.0001	0.5613	***
	α	3.901 ± 0.54	3.681 ± 1.21	0.0706	0.1791	
	lβ	1.674 ± 0.62	1.988 ± 0.46	≤0.0001	0.5517	***
	hβ	2.913 ± 0.93	3.429 ± 0.64	≤0.0001	0.6388	***

**: Significant at $0.001 < p \leq 0.05$ and Cohen's $d < 0.3$*
***: Significant at $0.0001 < p \leq 0.001$ and Cohen's $0.3 \leq d < 0.4$*
****: Significant at $p \leq 0.0001$ and Cohen's $d \geq 0.4$*

For Source Separator ICA-EBM and classification results, EEG data was fed into the ICA-EBM, which resulted in ICA separated sources of EEG data. Based on our previous findings, the additional optimal systems comprised four locations, frontal F3, central C4, parietal P4 and occipital O2, which were selected for TF detection (Ly et al. 2016). These optimized ICA data sources were further segmented for feature extraction using the S-Transform. The input included the maximum amplitude $ST^{max}(t)$ and the mean amplitude $ST^{mean}(t)$ obtained from the EEG signals based on four sub-bands from two events (GT and TF). These significant features with p-values ≤ 0.05 were used as the main parameters for detecting TF events in PD patients. In comparison, the features were extracted by S-Transform in both cases, with ICA-EBM and without ICA-EBM were used for classification. The desired output was set at 1 in case of TF and 0 in the cases of GT.

Figure 5.5 shows the results in the receiver operating characteristic (ROC) curve and analyses. The bold red coloured line represents the ROC curve for the method using the source separation of ICA-EBM. The star blue coloured line represents the technique without source separation.

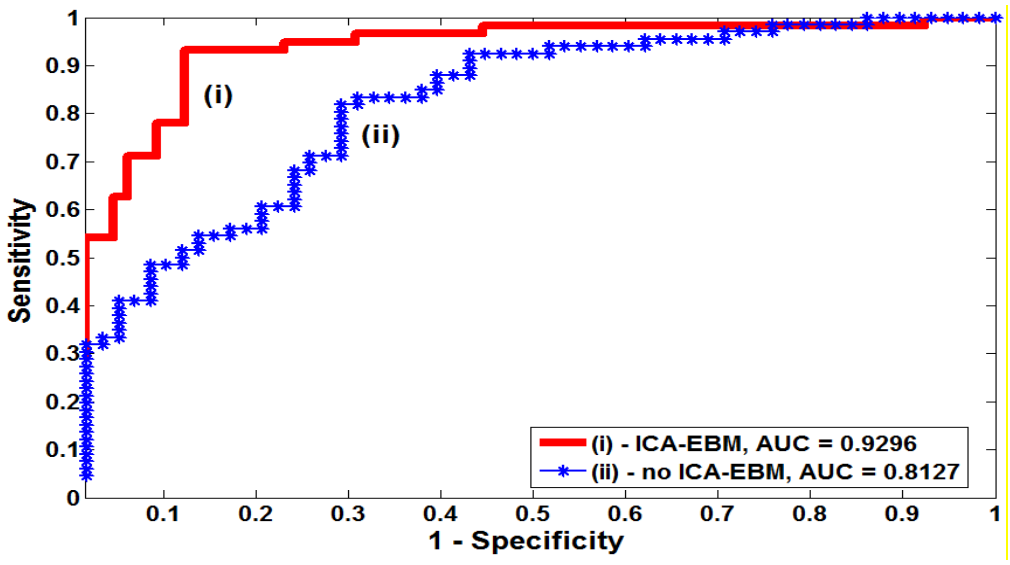

Figure 5.5: **ROC plot**

The areas under the curve (AUC) of ROC were also calculated to evaluate classification performance quantitatively. It can be seen that the method 1 (ICA-EBM, ST, BNN) using the inclusion of the source separation of ICA-EBM had a higher AUC of 0.9296 compared to the method 2 (ST, BNN) without inclusion of the source separation, which had an AUC of 0.8127.

Classification results for TF events detection using S-Transform decomposition as the feature methods and Bayesian neural networks as the classifier are shown in Table 5.5. The outcome indicated that the S-Transform based feature extraction provided respectable results for TF detection, with 79.1% of sensitivity, 77.1% of specificity and 78.2% of accuracy for the test set. Interestingly, further improvements were obtained when using the combination of ICA-EBM as the source separator before extracting feature, which improved outcomes to a sensitivity of 83.0%, a specificity of 87.6% and an accuracy of 85.4% in detecting TF.

The ST based features extracted from the three occipital locations (O1O2Oz) provided good results at 81.47%, 80.98%, and 84.47% of sensitivity, specificity, and accuracy, respectively in the case of using ICA-EBM, comparing with results at 75.93%, 76.72%,

Table 5.5: **Classification Results of ST based features using BNN in detecting TF from GT**

Input	ICA	H	Training			Testing		
			Sen(%)	Spe(%)	Acc(%)	Sen(%)	Spec(%)	Acc(%)
15 Channel	No	4	79.80	78.70	79.20	79.10	77.10	78.20
15 ICs	Yes	4	84.60	88.00	86.30	83.00	87.60	85.40
O1O2Oz	No	10	77.54	73.18	76.12	75.93	76.72	75.27
O1O2Oz	Yes	5	84.03	84.82	8128	81.47	80.98	84.47
F3C4P4O2	No	7	76.30	72.30	74.20	75.70	70.30	73.30
F3C4P4O2	Yes	7	85.80	88.00	86.80	84.20	88.00	86.02

H: Hidden Node; ICA: ICA-EBM; Sen: Sensitivity; Spe: Specificity; Acc: Accuracy

and 75.27% of sensitivity, specificity, and accuracy, respectively in the case of without using ICA-EBM. Moreover, as we expected, the best performance for TF detection was achieved when using our predefined regions of interest (F3C4P4O2) plus ICA-EBM for pre-processing. For this combination (ICA-EBM, ST, BNN), the results were a sensitivity of 84.2%, a specificity of 88.0% and an accuracy of 86.2%.

Further Comparison Classifiers and Feature Extractors for Detecting Turning FOG

Table 5.6 shows the comparision of classification results for TF detection. The classifier BNN with the optimization methods in this study provided the best result compared to the classifier ANN and SVM methods. The ST as the feature extractor has resulted in a more accurate method compared to FFT and WT. The result shows the ANN classifier provided an accuracy of: 74.92% using the FFT, 76.60% using the WT, 82.83% using the ST. The accuracies are slightly improved across different feature extractors (FFT, WT, and ST) when using the SVM classifier with the accuracy of: 76.81% using the FFT, 81.79% using the WT, 83.11% using the ST. The BNN classifier improved the most, with the accuracy of 79.54% using FFT, 81.81% using WT, 85.40% using ST.

Table 5.6: **Comparison of classification results in detecting TF using source separation ICA-EBM**

Feature	Classifier		Testing	
		Sen (%)	Spec (%)	Acc(%)
FFT	ANN	77.67	72.17	74.92
	SVM	78.14	75.49	76.81
	BNN	79.79	78.20	79.54
WT	ANN	79.77	77.26	78.60
	SVM	81.42	82.16	81.79
	BNN	81.44	80.91	81.81
ST	ANN	81.48	83.75	82.83
	SVM	82.89	83.33	83.11
	BNN	83.00	87.60	85.40

5.6 DETECTION OF GAIT INITIATION FAILURE USING ICA-EBM (SOURCE SEPARATOR), S-TRANSFORM (FEATURE EXTRACTOR) AND BAYESIAN NEURAL NETWORKS (CLASSIFIER)

GIF was analysed using 66 seconds of GIF compared to 66 seconds of GS from all five PD patients, extracted using the S-Transform in Table 5.7 and Table 5.8. A Wilcoxon signed-rank test with p-value threshold of ≤ 0.001 and a Cohen's effect size $d \geq 0.4$ were used to investigate the significant mean of S-Transform decomposition $ST^{mean}(t)$ between periods of GS and GIF. When compared to the GS episode, GIF episodes were associated with increased theta, alpha, low and high beta band frequencies in frontal, central, parietal and occipital areas.

Compared to GS, the most significant change of theta activity during GIF was found in frontal F3 (d=0.3026), central C4 (d=0.3089), and occipital O1 (d=0.3439). Furthermore, there was a significant increase of alpha activity in central C4 (d=0.4384), parietal P3 (d=0.4889) and occipital O1 (d=0.5029) and O2 (d=0.5007) as well as high beta activities increases in central CP2 (d=0.341), occipital O2 (d=0.5559) and Oz (d=0.493). The low beta activities demonstrated a similar pattern with an increases in occipital O2 (d=0.4681) and Oz (d=0.4225) during GIF.

Fifteen channels of EEG data were fed into the ICA-EBM, which resulted in 15 ICs separated sources. To localize the source of ICs, "Component maps 2D", a plug-in in EEGLab toolbox was used to plot the IC scalp topographies. Figure 5.6 shows the ten mean ICs scalp maps across five PD patients with a contribution to both events (i.e., GS and GIF). For each IC scalp map, the electrode zone is colour coded to indicate how much activity it contributed to the left/right frontal, central, parietal and occipital locations. The blue colour indicates low contribution and a red colour indicates a high contribution to either GS or GIF.

Table 5.7: **Feature analysis of ST (ST^{mean}) between GS and GIF in Frontal, Central and Parietal**

Parameter	Features	GS(μV±std)	GIF(μV±std)	p	d	GSvs GIF
ST-F3	θ	0.167 ± 0.10	0.201 ± 0.11	0.047	0.3026	*
	α	0.257 ± 0.14	0.301 ± 0.13	0.0093	0.319	**
	hβ	0.242 ± 0.09	0.247 ± 0.09	0.8968	0.0019	
ST-C3	θ	0.194 ± 0.11	0.225 ± 0.10	0.0143	0.2862	*
	α	0.313 ± 0.15	0.370 ± 0.13	0.0021	0.3953	*
	hβ	0.288 ± 0.11	0.302 ± 0.11	0.4486	0.1188	
ST-CP2	θ	0.182 ± 0.10	0.215 ± 0.10	0.039	0.3089	*
	α	0.298 ± 0.14	0.347 ± 0.13	0.0072	0.352	*
	lβ	0.264 ± 0.13	0.295 ± 0.13	0.1325	0.2376	
	hβ	0.268 ± 0.10	0.304 ± 0.11	0.0092	0.341	**
ST-C4	θ	0.202 ± 0.13	0.242 ± 0.13	0.0275	0.2988	*
	α	0.321 ± 0.15	0.389 ± 0.16	0.0058	0.4384	***
	hβ	0.284 ± 0.10	0.328 ± 0.12	0.0386	0.3798	*
ST-Cz	θ	0.174 ± 0.10	0.207 ± 0.10	0.0465	0.3157	*
	α	0.282 ± 0.12	0.335 ± 0.14	0.0176	0.3987	*
	hβ	0.286 ± 0.09	0.311 ± 0.11	0.1938	0.2694	
ST-P3	θ	0.217 ± 0.12	0.251 ± 0.09	0.0066	0.2943	*
	α	0.372 ± 0.16	0.450 ± 0.15	0.0021	0.4889	***
	hβ	0.313 ± 0.12	0.353 ± 0.13	0.0900	0.2935	
ST-P4	α	0.381 ± 0.15	0.443 ± 0.17	0.0212	0.3751	*
	lβ	0.338 ± 0.14	0.381 ± 0.14	0.0611	0.3044	
	hβ	0.313 ± 0.11	0.353 ± 0.12	0.0326	0.3419	*

**: Significant at $0.001 < p \leq 0.05$ and Cohen's $d < 0.3$*
***: Significant at $0.0001 < p \leq 0.001$ and Cohen's $0.3 \leq d < 0.4$*
****: Significant at $p \leq 0.0001$ and Cohen's $d \geq 0.4$*

Table 5.8: **Feature analysis of ST (ST^{mean}) between GS and GIF in Occipital**

Parameter	Features	GS(μV±std)	GIF(μV±std)	p	d	GSvs GIF
ST-O1	θ	0.268 ± 0.10	0.302 ± 0.09	0.0094	0.3439	**
	α	0.537 ± 0.18	0.629 ± 0.18	0.002	0.5029	***
	lβ	0.493 ± 0.16	0.577 ± 0.18	0.0049	0.4817	**
	hβ	0.420 ± 0.12	0.477 ± 0.14	0.0183	0.4128	*
ST-O2	θ	0.270 ± 0.11	0.289 ± 0.08	0.0496	0.1945	*
	α	0.536 ± 0.18	0.629 ± 0.18	0.0016	0.5007	***
	lβ	0.487 ± 0.17	0.571 ± 0.18	0.0039	0.4681	***
	hβ	0.4 ± 0.13	0.475 ± 0.13	0.0004	0.5559	***
ST-Oz	θ	0.278 ± 0.11	0.272 ± 0.07	0.8076	0.0683	
	α	0.558 ± 0.18	0.631 ± 0.19	0.0174	0.3853	*
	lβ	0.497 ± 0.16	0.570 ± 0.18	0.0098	0.4225	***
	hβ	0.402 ± 0.12	0.464 ± 0.124	0.0014	0.493	***

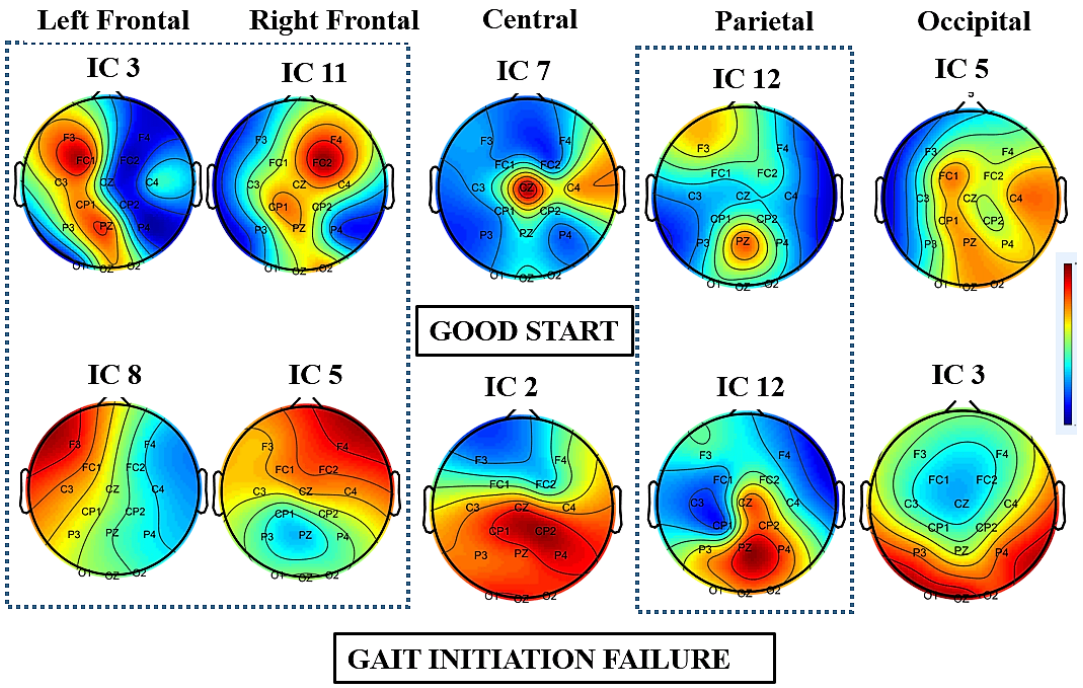

Figure 5.6: **IC scalp maps underlying Good Start and Gait Initiation Failure**

During GS, the red zone spread around the bilateral frontal and central regions, illustrating that these regions may be activating in an attempt to control the muscle and joints in PD patients for movement. However, during the GIF, the red zone spreads significantly around this bilateral frontal and central regions compared with the GS. It might be that due to the inadequate input from motor regions, these freezers might need to use more of their visual system (occipital) to gain information about what is happening (parietal) in order to break GIF (frontal) and send this information to the primary motor regions (central) to initiate walking again (Shine, Matar, et al. 2013).

For the Bayesian framework, the plot of the log evidence against the optimum number of hidden neurons of the Bayesian neural network training is shown in Figure 5.7, which includes: (i) the S-Transform feature extractor without the ICA-EBM with ten hidden nodes which resulted in the best classification evidence; (ii) using the S-Transform feature extractor with the ICA-EBM with seven hidden nodes which produced the best classification evidence.

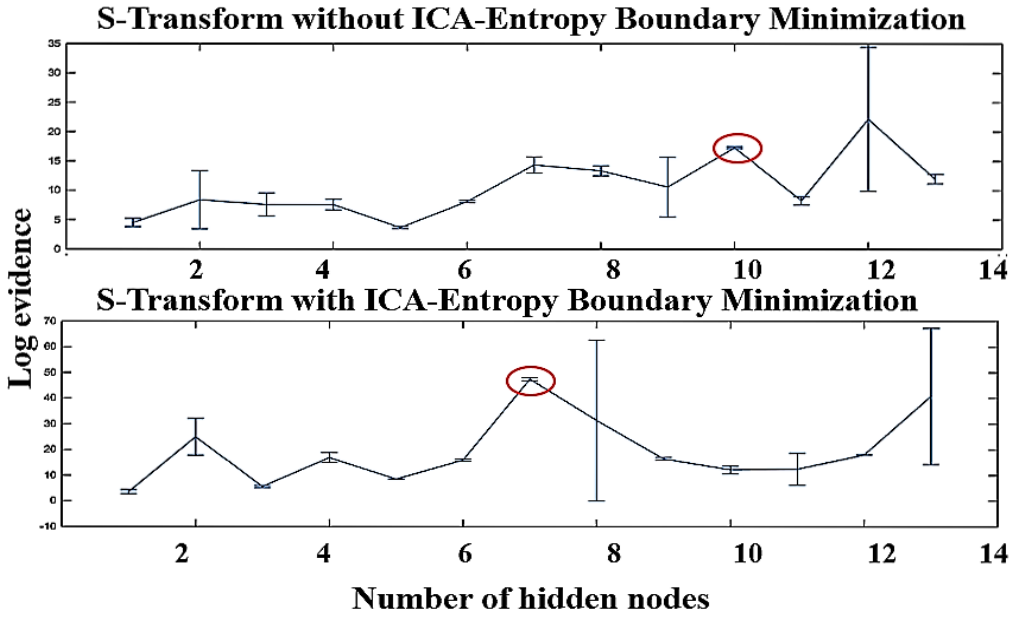

Figure 5.7: The log evidence against the optimum number of hidden nodes

For the input of classification, 15 optimized ICA data sources were further segmented for feature extraction using the S-Transform. The mean and maximum amplitude from four EEG frequency bands (theta, alpha, low beta and high beta) of each location were used to evaluate their ability in detecting GIF. These significant features with p-values ≤ 0.05 were used as the main parameters for detecting GIF events in PD patients. Classification results for GIF events detection using S-Transform decomposition as the feature methods and Bayesian neural networks as the classifier are shown in Table 5.9.

The outcome indicated that the S-Transform based feature extraction of 15 EEG channels provided respectable results for GIF detection, with 85.24% sensitivity, 83.06% specificity and 84.30% accuracy for the test set. When using the combination of ICA-EBM, the classification improvements were obtained, which had the outcome to a sensitivity of 88.96%, a specificity of 90.26% and an accuracy of 89.50% in detecting GIF. Feature extracted from occipital region provides the high sensitivity of 83.98%, specificity of 88.06% and accuracy of 84.00%. The central-frontal locations obtained the lower sensitivity for detecting GIF, with a sensitivity of 81.75%, a specificity of 78.32% and an accuracy of 78.50%. Moreover, the performance for ten dominant ICs shown in Table 5.9 was calculated with a sensitivity of 84.61%, a specificity of 86.17% and an accuracy of 84.40% for detecting GIF.

Table 5.9: Classification Results of ST based features using BNN in detecting GIF from GS using ICA-EBM

Input	ICA	H	Training			Testing		
			Sen (%)	Spec(%)	Acc(%)	Sen (%)	Spec (%)	Acc(%)
15 Channel	No	3	86.06	84.82	85.46	85.24	83.06	84.30
O1O2Oz	Yes	6	87.08	89.10	88.39	83.98	88.06	84.00
Cen-Fro	Yes	7	86.03	79.82	83.30	81.75	78.32	78.50
10 ICs	Yes	9	88.32	88.84	88.80	84.61	86.17	84.40
15 ICs	Yes	7	90.34	91.15	90.73	88.96	90.26	89.50

ICA: ICA-EBM; H: Hidden Node; Sen: Sensitivity; Spe: Specificity; Acc: Accuracy

Further comparison Classifier and Feature Extractors for Detecting GIF

Three proposed methods with different feature extractor namely FFT, WT and ST with several classifiers such as ANN, SVM and BNN are compared and analysed in Table 5.10.

From the results of the GIF detection, using the BNN as classifier and FFT as the feature extractor achieved the sensitivity at 80.87%, specificity at 87.42% and accuracy at 83.50% for the testing set. The system with WT based feature and BNN provided an improved performance with a sensitivity at 84.44%, a specificity at 89.75% and an accuracy at 86.96%. The results of GIF detection using ST as feature extraction and BNN as classifier achieved the highest performance with the testing set leading to 88.96% sensitivity, 90.26% specificity and 89.50% accuracy.

Table 5.10: **Comparison of classification results in detecting GIF using source separation ICA-EBM**

Feature	Classifier		Testing	
		Sen (%)	Spec (%)	Acc(%)
FFT	ANN	80.59	74.52	77.59
	SVM	79.04	78.89	78.81
	BNN	80.87	87.42	83.50
WT	ANN	83.83	85.84	85.00
	SVM	83.94	89.39	86.67
	BNN	84.44	89.75	86.96
ST	ANN	83.46	88.15	86.85
	SVM	89.88	89.16	88.50
	BNN	88.96	90.26	89.50

Sen: Sensitivity; Spe: Specificity; Acc: Accuracy

5.7 DISCUSSION

Turning FOG was found to be associated with a remarkable increase in high beta activity across the cortex. This finding is in accordance with our previous work using FFT (Handojoseno, Gilat, et al. 2015; Ly et al. 2016). Gilat et al. (2015) hypothesized that the subthalamic nucleus (STN) of PD patients with freezing, which has been shown to shut down motor activity using high beta frequencies (Toledo et al. 2014), likely underlies the trigger of TF. Indeed, deep brain stimulation of the STN, specifically when using lower 60Hz frequencies can often alleviate FOG in PD. The STN has projections with the frontal cortex as part of stopping network (Aron, Robbins & Poldrack 2004), thus the high beta of frontal regions in the present study could further implicate the recruitment of a putative stopping network that worsens freezing behaviour as proposed by Gilat et al. (2015).

As in chapter 3 and 4, this GIF study again showed high beta oscillations over frontal, central, parietal and occipital cortical locations, which may relate to stopping network that inhibits motor output and can cause FOG in PD (Aron, Robbins & Poldrack 2004; Georgiades et al. 2016).

For classification, the source separation using ICA-EBM improved the classification performance as compared to the case without source separation. Further, the result shows that the combination of the ICA-EBM (source separator) and the S-Transform (feature extraction) significantly improved the sensitivity and specificity of TF detection. The distinctive frequency-based features of selected independent components of EEG were extracted using S-Transform and classified using Bayesian Neural Networks. This is because the BNN classifier handles only noisy data, which are significantly responsible for the variation of EEG data. This may lead to an increased likelihood of correct identification of FOG events. Therefore, optimal EEG variables are still utilised in the proposed method using BNN to achieve high classification performance.

It can be seen in Table 5.6 that the accuracy of TF detection using this technique (ICA-EBM, ST, BNN) is much higher than that of the others using different feature extractors More specifically, the accuracy performance increased from 79.54% (ICA-EBM, FFT, BNN) to 81.81% (ICA-EBM, WT, BNN) and then jumped to 85.40 (ICA-EBM, ST, BNN) for TF detection. For the GIF detection, the accuracy performance increased from 83.50% (ICA-EBM, FFT, BNN) to 86.96% (ICA-EBM, WT, BNN) and then 89.50% (ICA-EBM, ST, BNN) when using the similar source separator ICA-EBM, classifier BNN and different feature extractors (FFT, WT, ST).

With regard to the affected locations underlying freezing event, the classification results suggest that occipital cortex regions (O1, O2 and Oz) could be the location for detecting TF/GIF in PD patients with the accuracy around 84%. This indicates that the PD patients are 'over-relying' on visual information during freezing. Especially during a period of freezing, due to the inadequate input from motor regions, the response of the muscles and joints in PD patients are different to what they are expected to be. Therefore, these freezers might need to use more of their visual system to gain the information about what is happening in order to break freezing by getting primary motor regions to activate again.

In terms of computation time of classifiers, it is estimated by MATLAB's built-in tic/toc functions whereas the tic function was called before the program and the toc afterwards on the computer (Intel(R) Core(TM) i7-7600 CPU @ 2.80GHz, 16.0 GB RAM). In terms of the classification/execution time, all classifiers were able to complete the task in less than a second. The program developed in MATLAB takes more computational time compared to C language with significantly faster training time. Furthermore, the priority is the classification accuracy in terms of sensitivity and specificity in our study. Although the algorithms are highly efficient, they are obtained off-line and the parameters will be implemented in real-time. If convolutional neural networks (CNN) are to be used, it is expected that the off-line computational time associated with CNN will be longer than our current algorithms.

This research has successfully utilized EEG signals to investigate brain dynamic changes underlying the specific sub-types of FOG and detected these events with high performance. The current studies provided additional support toward detecting a freezing event by using the combination of ICA-EBM, time-frequency analysis of S-Transform and advanced classifier of BNN. This method (ICA-EBM, ST, BNN) improved classification results in detecting TF and GIF in PD. This novel methodology will help the development of a real-time detection device for different sub-types of FOG in PD. Also, the understanding of underlying neuroscience will ultimately promote the development of novel therapies and technologies to assist with the management of FOG in PD.

Chapter 6

Conclusion and Future Work

6.1 CONCLUSION

This thesis used EEG to understand and detect freezing of gait in people with Parkinson's disease. The core objective of this thesis is to introduce a computational intelligence of detecting FOG based on EEG signals. Two main tasks have been implemented throughout the thesis: (1) extracting and finding significant EEG features underlying freezing episodes, in comparison with the normal episodes; (2) detecting freezing events using several classifiers based on input as EEG features are extracted in the frequency and time-frequency domains. The investigation showed using BNN as classifier and ST as feature extraction, optimized by ICA-EBM, provides an advanced detection method with high accuracy in detecting FOG events.

Throughout the research, EEG was able to better understand FOG with three main findings. The first important finding in this thesis is that fifteen channels are reduced from 32 channels based on our EEG data and classifiers to be determined as the most optimal locations underlying FOG. They are positioned on the four main regions of the cortex; including frontal (F3, F4, FC1, FC2), central (C3, C4, CP1, CP2, Cz), parietal (P3, Pz, P4) and occipital (O1, Oz, O2) (Figure 6.1). The second important finding is that the high beta (21 -38 Hz) has identified the most affected EEG sub-band underlying FOG among four sub-bands (theta alpha, low beta and high beta) in three clinical experiments. The final finding is the advanced computational intelligent for FOG detection. By extracting EEG signal based time-frequency techniques and classifying freezing events using several classifiers, the combination of source separation ICA-EBM for improving classification performance, S-Transform and BNN have proved to be a very effective method for FOG detection. Table 6.1 shows the significant results underlying freezing episodes in Chapters 3, 4 and 5.

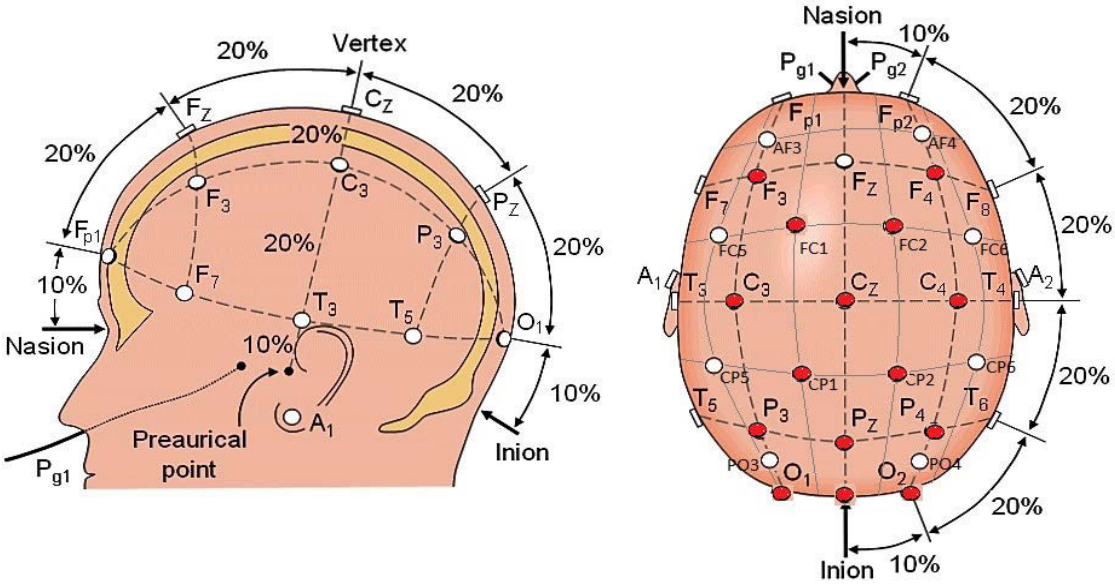

Figure 6.1: **Fifteen affected channels underlying FOG based on our EEG data**

Table 6.1: Significant results underlying Freezing events in this thesis

Work	Summary
Chapter 3: Events: EW vs. FOG Method: - Feature extraction: FFT - Classification: ANN	Feature extraction: - Increase in PSD theta in Cz, FC2. - Increase in PSD alpha in F3, C3, P4 - Increase in PSD low beta in O1, P4, C4. - Increase in PSD high beta in F3, C4, P4, O2. - Fifteen channels are reduced from 32 channels including frontal F3, F4, FC1, FC2; central C3, C4, CP1, CP2, Cz; parietal P3, Pz, P4 and occipital O1, Oz, O2. Classification: - Sensitivity at 72.20% - Specificity at 70.58%
Chapter 4: Event: GS vs. GIF Method: - Feature extraction: WT - Classification: SVM	Feature extraction: - Decrease in WE alpha in F4, increase in O2. - Increase in WE theta in P3. - Increase in WE low beta in O2. - Increase in WE high beta in F3, CP1, CP2, P3, P4. O1, O2. Classification: - Sensitivity at 83.94% - Specificity at 89.39%
Chapter 5: Event: GT vs. TF Method: - Feature extraction: ST - Classification: BNN	Feature extraction: ST - Increased in ST theta in O1, O2 - Increased in ST alpha in O1, O2, Oz. - Increase in ST low beta in F3, O1, O2, Oz. - Increase in ST high beta in F4 and O2. Classification: - Sensitivity at 83.00% - Specificity at 87.60%
Chapter 5: Event: GS vs. GIF Method: - Feature extraction: ST - Classification: BNN	Feature extraction: ST - Increase in ST theta in F3, C4, O1 - Increase in ST alpha in C4, P3, O1, O2. - Increased in ST low beta in O2, Oz - Increase in ST high beta in CP2, O2, Oz Classification: - Sensitivity at 88.96% - Specificity at 90.26%

Chapter 3 was about the comparison of the period of EW and FOG from seven PD patients. For the computational intelligence, the feature extraction was based on Fast Fourier Transform and the FOG events were classified using a feed-forward artificial neural networks trained with the Levenberg-Marquardt algorithm. The high beta alteration was strongest in frontal F3, central C4, parietal P4 and occipital O2. The classification result for FOG detection reached the sensitivity at 72.20% and specificity at 70.58%.

Chapter 4 described the work for the detection of GIF episode from GS episode based on EEG data of five PD patients. The GIF detection system used Wavelet Transform as the feature extractor and Support Vector Machine as the classifier. In the context of GIF, the results showed that the high beta activity experienced the largest significant rise in frontal F3, F4, central CP1, CP2, parietal P3, P4 and occipital regions O1, O2. The results for GIF detection showed that the combination of ICA-EBM as source separation, WT for feature extraction and SVM for classifier achieved the sensitivity at 83.94% and specificity at 89.39%.

Chapter 5 applied the advanced techniques in two studies: GIF detection and Turning FOG detection. This technique used ICA-EBM as source separation, ST as feature extraction and BNN as a classifier. For the Turning FOG, the investigation of significant differences between periods of GT and periods of TF shows the most substantial maximum differences were found in high beta activity from frontal F4 and occipital O2 locations. For the GIF study, GIF episodes were associated with the high beta activities increases in CP2, O2 and Oz.

For the advanced computational intelligence for FOG detection, the improvement of pre-processing techniques, feature extraction methods and classification algorithms were applied for the TF and GIF detection and are shown in Figure 6.2 and Figure 6.3. For TF detection, the advanced method (ICA-EBM, ST, BNN) reached the accuracy at 85.4%; which is the highest result comparing with the other methods (Figure 6.2). The

classification for GIF detection (ICA-EBM, ST, BNN) reached the highest performance with the accuracy at 89.5% (Figure 6.3).

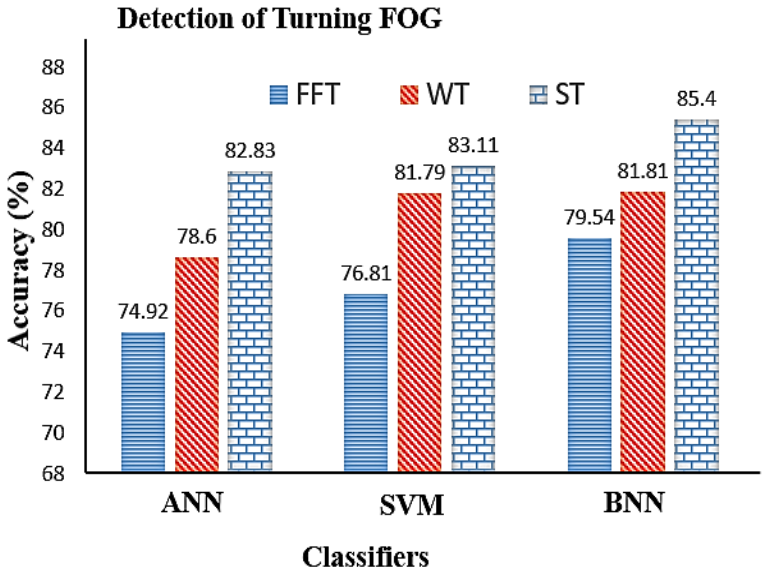

Figure 6.2: **Best performances of proposed methods for detecting TF**

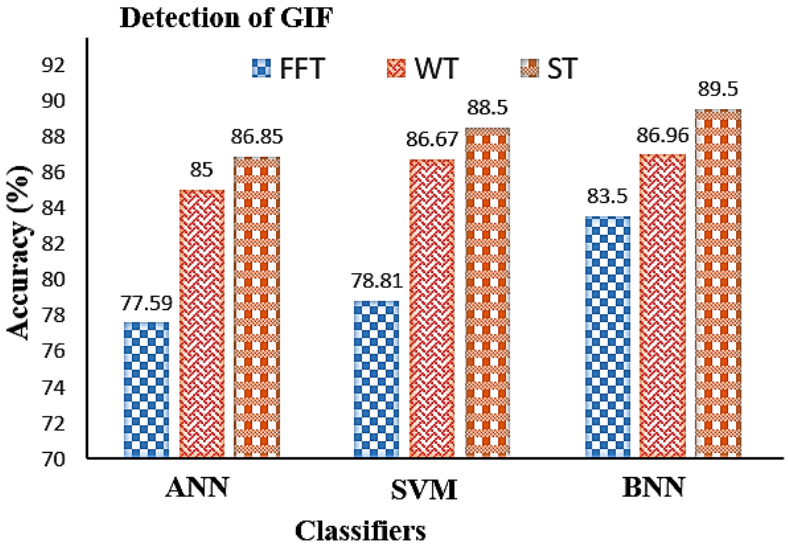

Figure 6.3: **Best performances of proposed methods for detecting GIF**

6.2 FUTURE WORK

In terms of the hardware, an improvement can be further done for the instrumentation, particularly with the EEG electrodes. A dry and contactless sensor technology can be preferred to apply in the real-time FOG detection's instrumentation because the gels used with the EEG electrodes usually dry out after a long period. In addition, the EEG measurement method could be improved by using a wireless embedded system or standalone detection.

In terms of the data collection, larger sample sizes will be required to confirm the findings in this thesis. For the five sub-types of FOG detection, the current research had focused on two specific sub-types GIF and Turning FOG and the four sub-types in general (group 1). Different mechanisms are responsible for different subtypes of FOG and might reflect different pathophysiology. Therefore, it is expected to have enough data for the study and detection of two more sub-types of FOG in group 1 based on their trigger factors: Narrow FOG, Target FOG. Moreover, we did not use a high-threat condition to elicit anxiety-related FOG (Martens, Ellard & Almeida 2014). Future work should assess larger samples to investigate whether the EEG signals change as a function of disease progression and other clinical variables, including dopaminergic medication intake, cognitive performance and mood - all features of PD that likely contribute to the development and severity of FOG (Nonnekes et al. 2015; Nutt et al. 2011).

This study covers various levels of FOG, and we have shown that reasonable classification accuracies have been achieved. Nevertheless, more advanced feature extraction and neural network strategies could be further developed to improve the performance of FOG prediction. For our future work, we will also aim to increase our understanding strategy of the underlying neurobiology associated with PD to promote better FOG prediction performance.

Also, the number of EEG channels could be reduced based on this current finding. For the computational intelligence, another method of feature extraction can be explored as

well, such as Hilbert-Huang transform (HHT) for time-frequency analysis or p-burg for autoregressive time analysis. The classifier such as self-organizing map and deep learning could be used. It is hoped that an increased understanding of underlying neurobiology will ultimately promote the development of novel therapies and technologies to assist the management of FOG in PD.

Appendix A

Research Ethics Clearance

HREC RESPONSE 141125

HREC – 2014/255

NHMRC APP1062319 LEWIS

Dear Applicant

[External Ratification: University of Sydney HREC - 2014/255 - 23/04/2014-23/04/2018]

The UTS Human Research Ethics Expedited Review Committee reviewed your application titled, "Understanding and predicting freezing of gait in Parkinson's Disease", and agreed that the application meets the requirements of the

NHMRC National Statement on Ethical Conduct In Human Research (2007). I am pleased to inform you that your external ethics approval has been ratified.

Your approval number is UTS HREC REF NO. 2014000723

Please note that the ethical conduct of research is an on-going process. The National Statement on Ethical Conduct in Research Involving Humans requires us to obtain a report about the progress of the research, and in particular about any changes to the research which may have ethical implications. This report form must be completed at least

annually, and at the end of the project (if it takes more than a year). The Ethics Secretariat will contact you when it is time to complete your first report.

I also refer you to the AVCC guidelines relating to the storage of data, which require that data be kept for a minimum of 5 years after publication of research. However, in NSW, longer retention requirements are required for research on human subjects with potential long-term effects, research with long-term environmental effects, or research considered of national or international significance, importance, or controversy. If the data from this research project falls into one of these categories, contact University Records for advice on long-term retention.

You should consider this your official letter of approval. If you require a hardcopy please contact Research.Ethics@uts.edu.au.

To access this application, please follow the URLs below:

* if accessing within the UTS network:

http://rmprod.itd.uts.edu.au/RMENet/HOM001N.aspx

* if accessing outside of UTS network:

https://remote.uts.edu.au , and click on "RMENet -

Appendix B

Publications

Detection of Turning Freeze in Parkinson's Disease based on S-transform Decomposition of EEG signals

Quynh Tran Ly[a], *Student Member, IEEE*, A.M. Ardi Handojoseno[a,c,†], Moran Gilat[b], Rifai Chai[a], Kaylena A. Ehgoetz Martens[b], Matthew Georgiades[b], *Member, IEEE,* Ganesh R. Naik[a], Yvonne Tran[a], Simon J.G.Lewis[b,*], Hung T Nguyen[a,*], *Senior Member, IEEE*

Abstract— **Freezing of Gait (FOG) is a highly debilitating and poorly understood symptom of Parkinson's disease (PD), causing severe immobility and decreased quality of life. Turning Freezing (TF) is known as the most common sub-type of FOG, also causing the highest rate of falls in PD patients. During a TF, the feet of PD patients appear to become stuck whilst making a turn. This paper presents an electroencephalography (EEG) based classification method for detecting turning freezing episodes in six PD patients during Timed Up and Go Task experiments. Since EEG signals have a time-variant nature, time-frequency Stockwell Transform (S-Transform) techniques were used for feature extraction. The EEG sources were separated by means of independent component analysis using entropy bound minimization (ICA-EBM). The distinctive frequency-based features of selected independent components of EEG were extracted and classified using Bayesian Neural Networks. The classification demonstrated a high sensitivity of 84.2%, a specificity of 88.0% and an accuracy of 86.2% for detecting TF. These promising results pave the way for the development of a real-time device for detecting different sub-types of FOG during ambulation.**

I. Introduction

Freezing of gait (FOG) are episodes where Parkinson's disease (PD) patients suddenly become unable to walk and often feel as though their feet have been 'glued' to the ground. Based on contexts of behavioral measures, different types of FOG have been observed including: start hesitation (Gait Initiation Failure), freezing whilst passing through narrow gaps, target hesitation, freezing when dual-tasking, freezing on an open runway and turning freezing (TF) [1]. TF is defined as the phenomenon in which the feet of PD patients appear to become stuck whilst usually making a tight turn. Importantly, TF is recognized to be the most frequent trigger of FOG, totaling 62.7% of all witnessed FOG episodes [1]. Turning is a complex motor task requiring motor and cognitive processing to support the correct selection, timing and scaling of movement. TF has clinical importance as it increases the risk for falls and falls related to injuries [1]. However, the pathophysiological basis for these effects is not well known [2].

[a] Faculty of Engineering and Information Technology, University of Technology, Sydney, Broadway, NSW 2007, Australia.

[b] Parkinson's Disease Research Clinic, Brain and Mind Center, University of Sydney, Level 4, Building F, 94 Mallet Street, Camper down, NSW, 2050, Australia.

[c] Faculty of Science and Engineering, Sanata Dharma University, Paingan, Sleman, Yogyakarta, 55281, Indonesia.

[*] Dual senior authorship.

[†] Deceased April 8, 2017.

Our group has previously developed an algorithm that could detect TF by analyzing energy power and brain effective connectivity of EEG signals with an averaged sensitivity around at 68% [3]. This EEG approach offers the potential to identify and detect freezing during turning due to its ability to track the dynamic physiological changes through the brain in real time. In addition, optimal EEG detection would allow for treatment options to be implemented in a timely manner to overcome and preferably prevent TF. As a result, it is critical that these detection methods will need to obtain high classification accuracies. With the goal of improving classification accuracy, the current paper aims to further explore the computational intelligence for EEG signals during TF by applying source separation technique (independent component analysis by entropy bound minimization, ICA-EBM) and S-Transform decomposition as feature extraction methods. The entropy bound estimation in ICA-EBM was chosen for its flexibility and its ability to approximate sources of a wide range of distributions that fit with EEG signals; which indeed improved classification performance in previous EEG studies [4]. The S-Transform was used to track alterations in signal magnitude, frequency and phase of selected EEG source as it has been shown to outperform classical techniques based on either frequency or time domain [5]. It is expected that, early TF detection can help to minimize the affectation of TF through visual cues in treatment of PD.

The main contributions of this paper are the novel technique that combined source separator ICA-EBM and EEG feature extraction using S-Transform decomposition. Artificial neural networks classified these extracted features, which were optimized by Bayesian inference techniques. The results of this study suggest that our proposed methodology is a promising non-invasive approach for improving Turning Freeze classification accuracy during ambulation in PD patients.

II. METHODS

A. Data Collection and Pre-processing

EEG data was collected from six PD patients with clinically confirmed freezing of gait in a structured series of Timed Up and Go (TUG) tasks. The patients were recruited from the Parkinson's Disease Research Clinic, Brain and Mind Center, The University of Sydney. This study was approved for by The Human Research and Ethics Committee of the University of Sydney. Assessments were performed in the practically-defined "off" state, with patients having been withdrawn from dopaminergic replacement therapy for more than twelve hours before testing. All subjects demonstrated multiple episodes of freezing during turning in the TUGs

(66.3% of turns elicited a TF on average). The EEG was recorded from 15 locations by Ag/AgCl scalp electrodes of a Bio-semi Active-Two system. These fifteen locations of interest were chosen based on our previous findings, which were reported as the most affected channels underlying Freezing of Gait in PD patients [7]. These electrodes were positioned over the following key cortical regions: F3, F4, FC1, FC2, C3, C4, CP1, CP2, CZ, P3, P4, PZ and O1, O2, OZ (F=frontal, C=central, P=parietal, O=occipital and Z=midline). The references were taken by averaging the two electrodes A1 and A2, which were placed on the ear lobes. The recording was segmented to 1-second durations and the sampling rate was 512 Hz.

Two separate conditions were identified for each patient based on video recordings of the TUGs, which is currently used as the golden standard to characterize FOG [3]

i) Normal Turning (NT): identified as a 2 second epoch of time in which a patient successfully made a right or left turn (180 degrees or 540 degrees) inside a taped 1m^2 box on the floor.

ii) Turning Freezing (TF): identified as an epoch of time in which patients suddenly became unable to make a turn inside a taped 1m^2 box on the floor, despite the intention to do so. The duration of TF episodes normally occur from 2 seconds to 5 seconds.

In this study, data from six PD patients resulted in 204 seconds of EEG data samples of TF which were matched to 204 seconds of EEG data samples of NT to be used for further analyses. Data were filtered using band-pass filter (0.5-40 Hz). Artifacts such as eye activity movement and heart rate signals were removed by Automatic Artifact Removal (AAR) using the EEGLab toolbox. In order to control inherent differences between electrodes and individual subjects, a Z-transformation was applied to normalize EEG data.

B. Feature Extraction using S-Transform

The S-transform is a time-frequency analysis technique proposed by Stockwell, Manishina and Lowe in 1996 [5]. The S-transform was developed on the basis of short time Fourier Transform (STFT) and continuous wavelet transform (WT) involving direct time-frequency mapping. The advantages of the S-transform are its linearity, lossless reversibility, multi-resolution and good time-frequency resolution. The S-Transform generates a constant relative bandwidth analysis while maintaining a direct link with the Fourier spectrum. In this study, four frequency bands were analyzed, namely: theta (4-8 Hz), alpha (8-13 Hz), low beta (lβ, 13-21 Hz) and high beta (hβ, 21-38 Hz).

Given h(t) is a continuous signal, the S-transform is defined as:

$$S(\tau,f)=\int_{-\infty}^{\infty} h(t)w(\tau-t,f)\,exp(-i2\pi ft)\,dt \qquad (1)$$

where $w(\tau-t,f)$ denotes the specific mother wavelet of the signal

$$w(\tau-t,f)=\frac{|f|}{\sqrt{2\pi}}\exp(-0.5(\tau-t)^2f^2) \qquad (2)$$

where f denotes the frequency, t denotes the time and τ denotes the delay with

$$\int_{-\infty}^{\infty} w(t,f)dt=1 \qquad (3)$$

Here, two parameters were extracted: the first is the maximum amplitude for each band at a time (t), $A^{max}(t)$. The second parameter was computed as the sum of amplitude of the each band at a time (t), $A^{sum}(t)$. These main features were used to explore the neural correlates underlying the episodes of turning freezing.

C. Source separation using ICA-EBM and input for classification

For improving classification results for TF detection, several pre-processing steps were performed prior to feeding the data to our classifier. ICA-EBM was chosen as a source separator to our EEG data because it has been shown to improve classification result in some previous EEG studies [4]. At first, our EEG data were fed to the source separation ICA-EBM for further analysis. Its aim is to separate the mixed information into independent components. ICA-EBM provides flexible density matching through the use of contrast functions based on the maximum entropy principle [6]. ICA-EBM can be applied to separate sources that are both sub- or super-Gaussian distributions using only a small class of nonlinear functions. The algorithm adopted a line search procedure and initially used updates that constrain the ICA de-mixing matrix to be orthogonal for robust performance [6]. The next step included a feature extraction module that transformed the pre-processed EEG signal into S-Transform decomposition based on 4 sub-bands. Only useful features with corrected *p-values*<0.05, as computed by the non-parametric Wilcoxon Signed Rank Test, were employed as input for our classifier.

D. Classification

For the classification algorithm, Bayesian neural networks (BNN) were implemented. Bayesian regularization framework has been proposed to improve the generalization abilities of neural networks regardless of finite and noisy obtainable data [4]. Applying Bayesian techniques to neural network training and prediction offers principle methods for determining optimal weight decay coefficients and model selection while making efficient use of training data. The use of the hyper parameters in the cost function can prevent the network from being trapped in poor generalization. As a result, a validation data set is not needed for Bayesian training. This is highly suitable for experiments such as ours where a limited set of data is only available for training and testing.

The BNN structure uses a 3-layer (input, hidden and output layers) feed-forward structure as follows:

$$z(x,w)=f_1\left(b_k+\sum_{j=1}^{m}\overline{w}_{kj}\,f_2\left(b_j+\sum_{i=1}^{n}w_{ji}\,x_n\right)\right), \qquad (4)$$

where f_1, f_2 denotes the activation function, x presents the input vector, w denotes the weight matrix vector; w_{ji} i denotes the weight of the link between the i hidden node and the j input; $\widetilde{w}_{ij}$ denotes the weight of the link between i hidden node and the output, b_k and b_j denote the biases; m denotes the number of outputs; n denotes the number of inputs.

The BNN training modifies the objective function of the networks such as the sum of squared error (mse)

$$F = E_d = \frac{1}{I}\sqrt{\sum_{i=1}^{n}(d_i - o_i)^2} \qquad (5)$$

where E_d is the error function, d_i is the desired output, and o_i is the actual output.

The regularization improves the model's generalization by adding the sum of squared weight function E_w to the objective function component (w) :

$$F(w) = \beta E_d + \alpha E_w \qquad (6)$$

where β and α are two hyper-parameters which indicate minimal error, and minimal weights to seek in the learning process.

This addition is proposed to find best generalization by optimizing these parameters in the Bayesian framework [4, 6]. To improve the efficiency of the optimization, Bayesian was added to the Levenberg-Marquardt and to be used for the Gauss-Newton approximation to the Hessian matrix, available in this optimization algorithm for learning.

For Bayesian neural network classification, a validation set is not required in a neural network training procedure. As a result, the current dataset was randomly divided into a training set and a test set with each containing 50% of the original data from all six patients. The input included the sum amplitude $A^{sum}(t)$ and the maximum amplitude $A^{max}(t)$ obtained from the EEG signals based on four sub-bands from two events (NT and TF). In comparison, the features were extracted by S-Transform in both cases, with ICA-EBM and without ICA-EBM were used for classification. The desired output was set at 1 in cases of TF and 0 in cases of NT. This system is expected to test with the new patients in the future.

III. RESULTS

A. Feature Extraction Results

Figure 1 show the time-frequency distributions of S-transform based on the above EEG signals from the frontal F4 electrode of one PD patient. The NT segments in run from 0 to 5 seconds and the TF segments run from 6 to 10 seconds. As clearly demonstrated, there are significant increases during TF across theta, alpha, low beta and specifically high beta frequency bands.

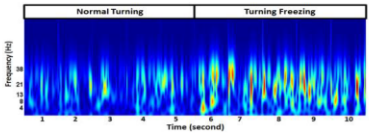

Figure 1. Time-frequency distribution in NT(1-5s), TF (6-10s) in F4.

TABLE I. FEATURE EXTRACTION

Location	Band	Normal Turning $A^{mean}(t) \pm$ std	Turning Freezing $A^{mean}(t) \pm$ std	Significant
F3	lβ	0.26±0.09	0.29±0.09	**
	hβ	0.29±0.10	0.34±0.08	***
F4	lβ	0.22±0.09	0.26±0.09	**
	hβ	***0.26±0.10***	***0.32±0.09***	***
FC1	hβ	0.32±0.09	0.36±0.09	**
FC2	hβ	0.30±0.09	0.35±0.09	***
C3	hβ	0.33±0.09	0.37±0.09	***
C4	lβ	0.24±0.10	0.27±0.10	*
	hβ	0.27±0.09	0.31±0.09	**
CP1	hβ	0.32±0.09	0.37±0.09	**
CP2	hβ	0.32±0.09	0.36±0.08	**
CZ	lβ	0.29±0.09	0.33±0.10	**
	hβ	0.32±0.09	0.37±0.10	***
P3	hβ	0.36±0.11	0.41±0.10	**
P4	hβ	0.33±0.10	0.37±0.09	**
Pz	hβ	0.35±0.10	0.40±0.09	***
O1	θ	0.30±0.12	0.33±0.08	*
	α	0.58±0.22	0.66±0.18	**
	lβ	0.51±0.21	0.59±0.16	***
	hβ	0.44±0.15	0.51±0.12	***
OZ	α	0.59±0.23	0.67±0.18	**
	lβ	0.51±0.21	0.60±0.15	***
	hβ	0.43±0.14	0.50±0.11	***
O2	θ	0.30±0.12	0.32±0.10	*
	α	0.58±0.25	0.65±0.20	*
	lβ	0.48±0.22	0.58±0.17	***
	hβ	***0.40±0.15***	***0.48±0.11***	***

*: *Significant at $0.001 < p \leq 0.05$ and Cohen's $d < 0.3$*
**: *Significant at $0.0001 < p \leq 0.001$ and Cohen's $0.3 \leq d < 0.4$*
***: *Significant at $p \leq 0.0001$ and Cohen's $d \geq 0.4$*

To investigate significant differences between periods of NT and periods of TF, a Wilcoxon Signed-Rank Test was conducted on the sample of 6 patients. Table 1 shows the significant maximum amplitude ($A^{max}(t)$) in the four sub-bands between periods of NT and TF. Smaller p-values (*p-values ≤ 0.0001*) and larger Cohen's d ($d \geq 0.4$) indicated the biggest differences in features between the two conditions.

The largest significant increase in activity was found in low beta and high beta across the brain regions during TF. The strongest maximum differences were found in high beta activity from frontal F4 (d=0.6143) and occipital O2 (d=0.5919) locations. Moreover, maximum alpha band activity increased significantly only in occipital locations O1, O2 and Oz during TF stages. Theta band increased remarkably only in occipital locations O1, O2 during TF.

B. Source Separator ICA-EBM and Classification results

In this stage, EEG data was fed into the ICA-EBM, which resulted in ICA separated sources of EEG data. Based on our previous finding, the additional optimal systems comprised four locations F3, C4, P4 and O2, which were selected for TF detection [7]. These optimized ICA data sources were further segmented for feature extraction using the S-Transform. The mean and maximum amplitude from four EEG frequency bands of each location were used to evaluate their ability in detecting TF. These significant features with *p-values* ≤ 0.05 were used as the main parameters for detecting TF events in PD patients.

Classification results for TF events detection using

TABLE II. CLASSIFICATION RESULTS

Cha	ICA	H	Training			Testing		
			Sen	Spe	Acc	Sen	Spec	Acc
15	No	4	79.8%	78.7%	79.2%	79.1%	77.1%	78.2%
15	***Yes***	4	***84.6%***	***88.0%***	***86.3%***	***83.0%***	***87.6%***	***85.4%***
4	No	7	76.3%	72.3%	74.2%	75.7%	70.3%	73.3%
4	***Yes***	7	***85.8%***	***88.0%***	***86.8%***	***84.2%***	***88.0%***	***86.2%***

Cha: Number of Channels; ICA: ICA-EBM; H: Hidden Node; Sen: Sensitivity; Spe: Specificity; Acc: Accuracy

S-Transform decomposition as the feature methods and Bayesian neural networks as the classifier are shown in Table II. The outcome indicated that the S-Transform based feature extraction provided respectable results for TF detection, with 79.1% of sensitivity, 77.1% of specificity and 78.2% of accuracy for the test set. Interestingly, further improvements were obtained when using the combination of ICA-EBM as the source separator before extracting feature, which improved outcomes to a sensitivity of 83.0%, a specificity of 87.6% and an accuracy of 85.4% in detecting TF. Moreover, as we expected, the best performance for TF detection was achieved when using our predefined regions of interest (4 locations) plus ICA-EBM for pre-processing. For this combination the results were a sensitivity of 84.2%, a specificity of 88.0% and an accuracy of 86.2%.

Figure 2 shows the results in the receiver operating characteristic (ROC) curve and analyses. The bold red colored line represents the ROC curve for the method using the source separation of ICA-EBM. The star blue colored line represents the method without source separation. The ROC curve is a plot of the true positive rate versus the false positive rate utilizing different threshold ratios as a sweeping variable. The areas under the curve (AUC) of ROC were also calculated to quantitatively evaluate classification performance [4]. It can be seen that the method using the inclusion of the source separation of ICA-EBM had a higher AUC of 0.9296 compared to the method without inclusion of the source separation, which had an AUC of 0.8127.

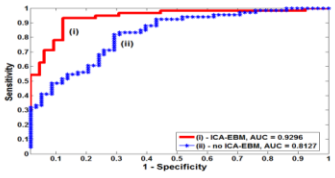

Figure 2. AUC plot

IV. DISCUSSION

In this paper, TF was found to be associated with a remarkable increase in high beta activity across the cortex. The most prominent results were found for high beta in the frontal F4 and occipital O2 locations. These findings are in accordance with our previous work using FFT and functional magnetic resonance imaging for analyzing turning behavior in PD patients [2, 3]. Based on these results, we hypothesize that the subthalamic nucleus (STN) of PD patients with freezing, which has been shown to shut down motor activity using high beta frequencies, likely underlies the trigger of TF [2]. Indeed, deep brain stimulation of the STN, specifically when using lower 60Hz frequencies can often alleviate FOG in PD [2]. The significant increase in high beta of frontal regions could further implicate the recruitment of a putative stopping network that worsens freezing behavior.

In terms of classification, the application of source separation using ICA-EBM improved the classification performance as compared to the case without source separation. Altogether, the result shows that the combination of the ICA-EBM (source separator) and the S-Transform (feature extraction) significantly improved the sensitivity and specificity of TF detection.

V. CONCLUSION

During turning freezing, PD patients showed an increase in beta activities across regions that implicate involvement of the STN and a potential recruitment of a hyper-direct stopping network, which may be manifested pathologically as a freeze as sensorimotor processing becomes more complex. The current study provided additional support toward detecting freezing during turning by using the combination of ICA-EBM, S-Transform analysis and BNN. This method improved classification results in detecting TF in PD. This novel methodology will help the development of a real-time detection device for different sub-types of FOG in PD. Also, the understanding of underlying neurobiology will ultimately promote the development of novel therapies and technologies to assist with the management of FOG in PD.

ACKNOWLEDGMENT

The authors would like to dedicate this work to the memory of Dr A.M. Ardi Handojoseno who contributed significantly to our research in Parkinson's disease. His intellect, kindness and compassion will always remain deeply in our hearts.

REFERENCES

[1] J. D. Schaafsma, Y. Balash, T. Gurevich, A. L. Bartels, J. M. Hausdorff, and N. Giladi, "Characterization of freezing of gait subtypes and the response of each to levodopa in Parkinson's disease," European Journal of Neurology, vol. 10, pp. 391-398, 2003.

[2] M. Gilat, J. M. Shine, C. C. Walton, C. O'Callaghan, J. M. Hall, and S. J. G. Lewis, "Brain activation underlying turning in Parkinson's disease patients with and without freezing of gait: a virtual reality fMRI study," *Npj Parkinson's Disease*, vol. 1, p. 15020, 2015

[3] A. M. A. Handojoseno, M. Gilat, Q. T. Ly, H. Chamtie, J. M. Shine, T. N. Nguyen, *et al.*, "An EEG study of turning freeze in Parkinson's disease patients: The alteration of brain dynamic on the motor and visual cortex," in *2015 37th Annual International Conference of the IEEE Engineering in Medicine and Biology Society (EMBC)*, 2015, pp. 6618-6621

[4] R. Chai, G. Naik, T. N. Nguyen, S. Ling, Y. Tran, A. Craig, *et al.*, "Driver Fatigue Classification with Independent Component by Entropy Rate Bound Minimization Analysis in an EEG-based System," *IEEE Journal of Biomedical and Health Informatics*, vol. PP, pp. 1-1, 2016

[5] R. G. Stockwell, L. Mansinha, and R. P. Lowe, "Localization of the complex spectrum: the S transform," *IEEE Transactions on Signal Processing*, vol. 44, pp. 998-1001, 1996.

[6] X. L. Li and T. Adali, "Independent Component Analysis by Entropy Bound Minimization," *IEEE Transactions on Signal Processing*, vol. 58, pp. 5151-5164, 2010

[7] Q. T. Ly, A. M. A. Handojoseno, M. Gilat, N. Nguyen, R. Chai, Y. Tran, H. T. Nguyen *et al.*, "Identifying montages that best detect the electroencephalogram power spectrum alteration during freezing of gait in Parkinson's disease patients," in *2016 38th Annual International Conference of the IEEE Engineering in Medicine and Biology Society (EMBC)*, 2016, pp. 6094-6097

Detection of Gait Initiation Failure in Parkinson's disease based on Wavelet Transform and Support Vector Machine

Quynh Tran Ly[a], *Student Member, IEEE*, A.M. Ardi Handojoseno[a,c,†], Moran Gilat[b], Rifai Chai[a], Kaylena A. Ehgoetz Martens[b], Matthew Georgiades[b], *Member, IEEE,* Ganesh R. Naik[a], Yvonne Tran[a], Simon J.G.Lewis[b,*], Hung T Nguyen[a,*], *Senior Member, IEEE*

Abstract— **Gait initiation Failure (GIF) is the situation in which patients with Parkinson's disease (PD) feel as if their feet get "stuck" to the floor when initiating their first steps. GIF is a subtype of Freezing of Gait (FOG) and often leads to falls and related injuries. Understanding of neurobiological mechanisms underlying GIF has been limited by difficulties in eliciting and objectively characterizing such gait phenomena in the clinical setting. Studies investigating the effects of GIF on brain activity using EEG offer the potential to study such behavior. In this preliminary study, we present a novel methodology where wavelet transform was used for feature extraction and Support Vector Machine for classifying GIF events in five patients with PD and FOG. To deal with the large amount of EEG data, a Principal Component Analysis (PCA) was applied to reduce the data dimension from 15 EEG channels into 6 principal components (PCs), retaining 93% of the information. Independent Component Analysis using Entropy Bound Minimization (ICA-EBM) was applied to 6 PCs for source separation with the aim of improving detection ability of GIF events as compared to the normal initiation of gait (Good Starts). The results of this analysis demonstrated the correct identification of GIF episodes with an 83.1% sensitivity, 89.5% specificity and 86.3% accuracy. These results suggest that our proposed methodology is a promising non-invasive approach to improve GIF detection in PD and FOG.**

I. Introduction

Freezing of gait (FOG) is defined as a brief, episodic absence or marked reduction of forward progression of the feet despite the intention to walk [1]. In our Timed Up and Go experiment, different types of FOG were distinguished relating to the clinical situation in which they occurred, such as gait initiation failure (GIF), freezing whilst passing through a narrow space, freezing whilst dual-tasking, freezing on an open runway and freezing during turning [1]. GIF is a very common situation in which patients with PD experience FOG when initiating their first step. The prevalence of GIF ranges from 21% to 24% of all witnessed FOG in PD [1, 2]. Behavioral manifestations during GIF can be observed like as trembling in place, shuffling with minimal forward movement, or complete akinesia [1]. Gait Initiation is a complex task which requires both motor and cognitive processing to enable the correct selection, timing and scaling of movements [3]. From a functional perspective, GIF is clinically important as a trigger for FOG because initiating gait is frequently attempted every day. The increased risk of falls induced by GIF negatively affects the quality of life for patients with PD and can result in injury as well as nursing home placement.

In recent years, a number of researches have reported the detection of FOG based on the leg oscillations using accelerometer, gyroscope and goniometers. However, using such sensors based FOG detection systems could not identify GIF periods which are not associated with the trembling of the legs. Our group previously studied the brain activity underlying GIF by analyzing energy power of surface ambulatory EEG signals underlying this event [2, 4]. However, as data was derived from a large number of channels, computational complexity was increased for performing further signal processing methods. With the goal of developing a faster and better classification system, the current paper sought to analyze EEG features to detect GIF using principal component analysis (PCA) for data dimensional reduction, Independent Component Analysis with Entropy Bound Minimization (ICA-EBM) for source separation, Wavelet Transform (WT) decomposition for feature extraction and Support Vector Machine (SVM) for classification. PCA is used to transform a high dimensional EEG dataset to a low dimensional orthogonal feature set while retaining the maximum information of the original high dimensional dataset [5]. ICA-EBM was developed to separate the EEG data source to improve the classification [6].

The main contributions of this paper are the novel techniques applied, in which PCA is used for reducing data dimension, ICA-EBM for source separation, WT decomposition for feature extraction and SVM for classification; which has not been explored previously to detect GIF in PD. These results suggest that our proposed methodology is a promising non-invasive approach for improvement of GIF detection.

II. METHODS

A. Data Collection and Pre-processing

EEG data was obtained from five Parkinson's disease patients who were recruited from the Parkinson's disease Research Clinic at the Brain and Mind Center, The University of Sydney. This study was approved for by The Human Research and Ethics Committee, University of Sydney. They were tested in their practically-defined 'off' medication state, following overnight (minimum 12 hours

[a] Faculty of Engineering and Information Technology, University of Technology, Sydney, Broadway, NSW 2007, Australia.
[b] Parkinson's Disease Research Clinic, Brain and Mind Center, University of Sydney, Level 4, Building F, 94 Mallet Street, Camper down, NSW, 2050, Australia.
[c] Faculty of Science and Engineering, Sanata Dharma University, Paingan, Sleman, Yogyakarta, 55281, Indonesia.
[*] Dual senior authorship.
[†] Deceased April 8, 2017.

since last dose) withdrawal of dopaminergic therapy. The subjects demonstrated multiple episodes of GIF (40% of gait initiations elicited a GIF) during a structured series of Timed Up and Go tasks. Good Starts (GS) is defined as the 2-second period after the patients were able to effectively initiate the first step. GIF is defined as the period when the patients tried to take a first steps but failed to do so. Both were determined according to the time onset and offset as scored on the video during the TUG tasks.

Based on our previous FOG findings, EEG data was acquired from 15 electrodes using a Bio semi Active Two system [4]. These electrodes positioned over the following cortical regions: frontal F3, F4, FC1, FC2 (motor planning and working memory), central C3, C4, CP1, CP2, CZ (motor execution), parietal P3, PZ, P4 (sensory integration) and occipital O1, OZ, O2 (visual area). References signal was taken by averaging 2 electrodes placed on the ear lobes. The recording was segmented to 1-second durations and digitized at 512 Hz.

In this study, 66 seconds of EEG data samples of GS were matched to 66 seconds of data samples of GIF as recorded from five PD patients. Data samples were then filtered using band-pass filter at 0.5-50 Hz. Eye movement and heart rate signals artifacts were eliminated using Automatic Artifact Removal (AAR) in the EEGLab from all electrode locations of raw EEG data [4].

B. Feature Extraction

Due to the strengths in time-frequency method, WT was chosen to extract the EEG data. WT is defined as the convolution between the signal and wavelet function generated by dilations and translation of scaled mother wavelet [7]. In this research, the discrete wavelet transforms (DWT) based on dyadic scales and positions is used [7]. This is computed as

$$DWT(j,k) = \frac{1}{\sqrt{|2^j|}} \int_{-\infty}^{\infty} x(t) \Psi \left(\frac{t - 2^j k}{2^j} \right) dt \quad (1)$$

where 2^j denotes the scale and $2^j k$ denotes the time localization and Ψ denotes the mother wavelet function.

The wavelet decomposition for an EEG signal x (t) at scales *j*, time point *k* could be calculated as:

$$x(t) = \sum_{k=-\infty}^{\infty} A(k) \varphi_{j,k}(t) + \sum_{j=0}^{\infty} \sum_{k=-\infty}^{\infty} D(j,k) \Psi_{j,k}(t) \quad (2)$$

where $A(k), D(j,k), \varphi_{j,k}, \Psi_{j,k}(t)$ denotes approximation coefficients, detail coefficients, scaling function, and wavelet functions, respectively.

Daubechies wavelet of order 4 (db4) were selected as the wavelet function since its smoothing feature has been confirmed to work well in discovering changes of EEG signals [7]. For EEG sampled at 512Hz, a six level decomposition (d1, d2, d3, d4, d5, d6) were computed by squaring and summing the wavelet coefficients of the decomposed level. Four levels of coefficients were corresponded approximately to our four EEG sub-band, d6 (theta: 4-8 Hz), d5 (alpha: 8-13 Hz), d4 (low beta: 13-21 Hz), d3 (high beta: 21-38 Hz); which were used for further analysis. In order to eliminate differences between electrodes and individual subjects, a Z-transformation was applied to normalize EEG data.

C. Principal Component Analysis (PCA) for dimensional reduction

The computational complexity increases with a higher dimensional dataset. Therefore, PCA was applied to decrease the dimension dataset into a lower dimension dataset that still covers enough information [5, 9].

Given a raw EEG dataset x_t and $\sum_{k=1}^{M} x_k$, with M denoting the number of EEG samples, the covariance matrix C of PCA was computed as:

$$C = \frac{1}{M} \sum_{j=1}^{M} x_j x_j^T \quad (2)$$

where $x_j x_j^T$ denotes a vector of N x N matrix, with N denoting the number of EEG channels. PCA calculated the eigenvector as

$$\lambda \mu = C \mu \quad (3)$$

where μ denotes the eigenvectors of C and λ denoted the eigenvalues. The principal component of S_t as the orthogonal transformation of x_t is calculated as followings

$$S_t = \mu^T x_t \quad (4)$$

Principal components contain the maximum variance in the data. The origin of the new coordinate system is located in the center of the data points. The first PC points in the direction of highest variance, the second PC points in the direction of second highest variance and so on. The variances captured for the corresponding PCs were calculated as well. The eigenvectors are ranked in a descending order of eigenvalues. By choosing only the first few eigenvectors, PCA performed a dimension reduction from high dimensional EEG data into low dimensional feature containing only a few principle components, but that still contain enough information of the original data.

D. Source separation using ICA-EBM

Next, the ICA-EBM was used to separate sources. ICA is one of the Blind Source Separation algorithms. It worked by separating the mixed information into independent components [6]. ICA-EBM provides flexible density matching through the use of contrast functions based on the maximum entropy principle. ICA-EBM separated both sub- or super-Gaussian mixtures using only a small class of nonlinear functions. After pre-processing using PCA and ICA-EBM, the 6 PCA and ICA separated data were extracted in the form of wavelet transform and fed into our classifier.

E. Classification

The significant maximum (A^{max}) and mean value of wavelet decomposition of 4 sub-bands from each electrode taken from two events were chosen as the features to detect GIF. We utilized Support Vector Machine (SVM) to detect GIF because of its accuracy and ability to deal with a large number of predictors [8]. The significant features were divided into half portions, one for the training set and the same amount for the testing set. SVM with a Radial Basis Function (RBF) kernel is computed as follows [8].

$$RBF_{JS}(x, \mu_k, \sigma_k) = \exp\left(-\frac{JS(x||\mu_k)}{2\,\sigma_k^2}\right) \quad (3)$$

where x ,k, μ_k and σ_k denote a random vector, support vector index, support vector centroid and support vector radius, respectively. *JS* denotes the Jensen-Shannon (JS) divergence between x and μ_k.

The *JS* divergence is a symmetrized and smoothed version of the Kullback-Leibler (*KL*) divergence. *JS* divergence is calculated as

$$JS(P||Q) = \frac{1}{2}KL(P||M) + \frac{1}{2}KL(Q||M) \quad (4)$$

where P, Q denote discrete probability distribution, $M = (P+Q) / 2$ denotes the central probability mass function and *KL* divergence is computed as

$$KL(R||S) = \sum_x R(x) \log \frac{R(x)}{S(x)} \quad (5)$$

A particle swarm ensemble clustering algorithm known as Ensemble Rapid Centroid Estimation (ERCE) was used for estimating the parameters for the RBF kernel [8]. When using ERCE, μ_k and σ_k could be inferred from the training data by using the following four steps:

1. Execute ERCE to cluster the training set to an arbitrary number based on *JS* distance.
2. Aggregate the ensemble clustering results using average linkage to get the final clustered sets $\mathbb{C}_k$. The corresponding centroid vector μ_k was computed as:

$$\mu_k = E[x|\mathbb{C}_k] = \frac{1}{|\mathbb{C}_k|}\sum_{x \in \mathbb{C}_k} x \quad (6)$$

3. The RBF kernel radius σ_k was taken as the square root of conditional *JS* divergence, which is given as follows

$$\sigma_k^2 = E[JS(x||\mu_k)\mathbb{C}_k] = \frac{1}{|\mathbb{C}_k|}\sum_{x \in \mathbb{C}_k} JS(x||\mu_k) \quad (7)$$

4. The SVM was then trained using the LS algorithm

III. RESULTS

A. Feature Extraction Results

Figure 1 shows the time-frequency distributions in two events GS and GIF from one PD patients using EEGLab toolbox. In this analysis, we explored the mean event-related changes in spectral power at each time during the epoch and at each frequency in such PD patient. It is observed that significant increase in power occurred at low beta (13-21 Hz) and high beta (21-38 Hz) frequency bands during GIF.

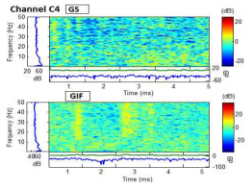

Figure 1. Time-frequency distribution for GS and GIF of motor cortex C4.

TABLE I FEATURE EXTRACTION

	Band	GS	GIF	Significant
		(A^{max} ± std)*0.1	(A^{max} ± std)*0.1	
F3	hβ	0.068±0.072	0.076±0.061	*
F4	α	0.132±0.067	0.113±0.092	*
C3	hβ	0.091±0.079	0.10±0.065	*
C4	hβ	0.091±0.079	0.107±0.065	*
CP1	hβ	0.088±0.072	0.119±0.066	**
CP2	hβ	0.088±0.072	0.119±0.079	*
P3	θ	0.359±0.202	0.377±0.158	*
	hβ	***0.112±0.075***	***0.150±0.077***	**
PZ	hβ	0.114±0.077	0.150±0.093	*
P4	***hβ***	***0.084±0.061***	***0.115±0.055***	**
O1	***hβ***	***0.203±0.097***	***0.252±0.096***	**
O2	lβ	0.197±0.115	0.224±0.097	*
	hβ	***0.199±0.095***	***0.242±0.093***	**

*: *Significant at $p \leq 0.05$ and Cohen's $d < 0.4$*
**: *Significant at $p \leq 0.001$ and Cohen's $d \geq 0.4$*

For the feature extraction, 132 seconds from the two events GS and GIF (66 seconds each) from all 5 PD patients were analyzed. Table I shows the significant maximum amplitude from 15 locations based on four EEG frequency bands activities. A Wilcoxon signed-rank test with *p-value* ≤ 0.001 and a Cohen's effect size d ≥ 0.4 were used to investigate significant differences between periods of GS and GIF. A decrease in alpha was found in F4 and an increase in theta was found in P3. However, overall it is apparent that increases in high beta frequency throughout the cortical brain regions underlie GIF compared to Good starts. More specifically, in the context of GIF, high beta activity experienced the largest significant rise in parietal regions P3 (d=0.5013), P4 (d=0.5378) and occipital regions O1 (d=0.499), O2 (d=0.4577). This finding is similar to our previous studies using PSD for analysis [2, 4].

B. PCA, ICA-EBM and input for classification

The collected EEG dataset comprised of a matrix with dimension of 15 × 66 × 512 (number of EEG channels × 66 seconds × 512 data points) for both GIF and GS. These matrices were fed into the PCA process to reduce the data dimension. The PCA transformed the original coordinate system into new coordinates called principal components (PCs). Eigenvalues values are shown in a scree plot (see Figure 2), which presents percent variance captured versus number of principal components. It can be seen that with 6 PCs, it already covered more than 93% of the variance of the original of 15 EEG channels. PC 1 accounted for 64.08 % of the total variation in the data and PC 2 accounted for 15.07% of the total variation in the data. This study applied a threshold of 93%, which generated orthogonal transformation from PC1 to PC6, to be used for further processing.

After applying the PCA, the original high dimension of the EEG dataset was reduced from 15 × 66 × 512 (number of EEG channels × second of data × data point per second)

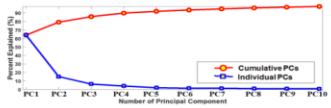

Figure 2. Scree plot of the principal components

to 6 × 66 × 512 (number of PCs × second of data ×data point per second) for GIF and a similar matrix for GS stages. Such a reduced dataset dimension resulted in a lower computational complexity; here-after called the 6 PCs EEG data. Next, the 6 PCs EEG data was fed to the ICA-EBM, resulted in the 6-channels ICA separated sources. These optimized sources were further segmented for feature extraction using wavelet transform. In order to build a faster and better classification system, only significant statistical different features between two groups of data (*p-values* < 0.05) were chosen as input for the GIF detection.

C. Classification results

For comparison purposes, the classification result from the original 15 EEG channels without the use of PCA is also reported. Table II shows the classification result for GIF detection. The classification (with PCA) using 6 PCs EEG data resulted in a sensitivity of 80.6%, a specificity of 78.9% and an accuracy of 79.7%, while the classification using original 15 EEG channels (without PCA) resulted in a sensitivity of 80.7%, a specificity of 80.6% and an accuracy of 80.6%. The results thus confirmed that the PCA successfully reduced the dimension of the EEG data, provided similar accuracy (slightly improved) accuracy as compared to the original dataset (without PCA) for GIF detection. Further improvements were obtained when using the combination of ICA-EBM as the source separator is used. These results (with PCA, ICA-EBM) achieved a good sensitivity of 83.1%, specificity of 89.5% and an accuracy of 86.3% for detecting GIF.

IV. DISCUSSION

In this paper we compared ambulatory EEG during Gait Initiation Failure and Good Starts in patients with PD and who had FOG. The fast temporal changes occurring in the brain during GIF were found to be associated with an overall increase in high beta activities over frontal, central, parietal and occipital cortical locations. FOG has previously been associated with high beta oscillations in the subthalamic nucleus, which cohere with both supplementary and primary motor areas [3]. Together these may constitute inhibitory control over motor actions when response conflict arises [3]. This could explain the high beta frequencies found in frontal and central cortical regions during GIF in the current study. High beta oscillation in parietal and occipital locations support the notion that PD patients with GIF suffered from impaired sensory integration and thus had to gain more information from the environment to initiate gait [3].

The classification results indicated that the use of PCA for data dimension reduction, ICA-EBM for source separation, wavelet for feature extraction and Support Vector Machine for classifier achieved the best performance indicators for GIF detection, with sensitivity increasing by 2.4% (from 80.7% to 83.1%) and accuracy increasing by 5.7% (from 80.6% to 86.3%) as compared with the case without using PCA and ICA-EBM. This finding therefore suggests that PCA was successfully applied for data dimensionality reduction, but still retained sufficient information of the original data which are benefits for solving big data dimension problems in such EEG studies [9].

TABLE II. CLASSIFCATION RESULTS

PCA	ICA-EBM	Dimension	Training			Testing		
			Sen	Spe	Acc	Sen	Spe	Acc
No	No	15 channels	81.0	80.8	80.9	80.7	80.6	80.6
Yes	No	6 PCs	81.0	79.3	80.1	80.6	78.9	79.7
Yes	**Yes**	**6 PCs**	**83.4**	**89.7**	**86.6**	**83.1**	**89.5**	**86.3**

Sen: Sensitivity; Spe: Specificty; Acc: Accuracy

V. CONCLUSION

We have successfully used EEG signals to investigate brain dynamic changes underlying gait initiation failure in PD and detected these events with high performance. The preliminary study provides optimism for the development of a real-time device for GIF detection that could be employed in everyday walking situations in PD patients. Further research should focus on optimizing the above techniques for a wider pool of participants and also investigate the efficacy of GIF detection system in real time. It is hoped that an increased understanding of underlying neurobiology will ultimately promote the development of novel therapies and technologies to assist the management of FOG in PD.

ACKNOWLEDGMENT

The authors would like to dedicate this work to the memory of Dr A.M. Ardi Handojoseno who contributed significantly to our research in Parkinson's disease. His intellect, kindness and compassion will always remain deeply in our hearts.

REFERENCES

[1] J. D. Schaafsma, Y. Balash, T. Gurevich, A. L. Bartels, J. M. Hausdorff, and N. Giladi, "Characterization of freezing of gait subtypes and the response of each to levodopa in Parkinson's disease," European Journal of Neurology, vol. 10, pp. 391-398, 2003

[2] A. M. Ardi Handojoseno, J. M. Shine, T. N. Nguyen, Y. Tran, S. J. G. Lewis, and H. T. Nguyen, "Analysis and Prediction of the Freezing of Gait Using EEG Brain Dynamics," *Neural Systems and Rehabilitation Engineering*, IEEE Transactions on, vol. 23, pp. 887-896, 2015

[3] M. J. Georgiades, M. Gilat, K. A. Ehgoetz Martens, C. C. Walton, P. G. Bissett, J. M. Shine, *et al.*, "Investigating motor initiation and inhibition deficits in patients with Parkinson's disease and freezing of gait using a virtual reality paradigm," *Neuroscience,* vol. 337, pp. 153-162, 2016

[4] Q. T. Ly, A. M. A. Handojoseno, M. Gilat, N. Nguyen, R. Chai, Y. Tran, H. T. Nguyen *et al.*, "Identifying montages that best detect the electroencephalogram power spectrum alteration during freezing of gait in Parkinson's disease patients," in *2016 38th Annual International Conference of the IEEE Engineering in Medicine and Biology Society (EMBC)*, pp. 6094-6097, 2016

[5] U. R. Acharya, S. V. Sree, A. P. C. Alvin, and J. S. Suri, "Use of principal component analysis for automatic classification of epileptic EEG activities in wavelet framework," *Expert Systems with Applications,* vol. 39, pp. 9072-9078, 2012

[6] X. L. Li and T. Adali, "Independent Component Analysis by Entropy Bound Minimization," *IEEE Transactions on Signal Processing,* vol. 58, pp. 5151-5164, 2010

[7] C.S. Burrus, R.A. Gopinath, and H.Guo, *Introduction to wavelets and wavelet transforms: a primer*, New Jersey: Prentice-Hall,pp.2-7, 1998.

[8] M. Yuwono, S. Su, B. Moulton, Y. Guo, and H. Nguyen, "An algorithm for scalable clustering: Ensemble rapid centroid estimation," in Evolutionary Computation (CEC), 2014 IEEE Congress on, pp. 1250–1257, 2014

[9] R. Chai, G. Naik, T. N. Nguyen, S. Ling, Y. Tran, A. Craig, *et al.*, "Driver Fatigue Classification with Independent Component by Entropy Rate Bound Minimization Analysis in EEG-based System"

Detection of Gait Initiation Failure in Parkinson's Disease Patients using EEG Signals

Quynh Tran Ly[a], A.M. Ardi Handojoseno[a,c], *Student Member, IEEE*, Moran Gilat[b], Nghia Nguyen[a], *Senior Member, IEEE*, Rifai Chai[a], *Member, IEEE* , Yvonne Tran[a], Simon J.G.Lewis[b,*], Hung T Nguyen[a,*], *Senior Member, IEEE*

Abstract— **Gait Initiation Failure (GIF) is one of the most disabling gait disturbances seen in advanced Parkinson's disease (PD). Gait Initiation is a complex motor task that requires motor and cognitive processing to enable the correct selection, timing and scaling of movement. Failure to initiate the first step often precipitates falls and leads to significant morbidity. However, the brain mechanisms underlying GIF remain unknown. This study utilized an ambulatory electroencephalography (EEG) technique to investigate the brain dynamic changes underlying GIF and aims to detect the occurrence of GIF in four PD patients. We sought to determine whether episodes of GIF might be associated with a characteristic brain signal that could be detected by surface EEG. This preliminary investigation analyzed the EEG signals through power spectra density (PSD) and centroid frequency (CF) to show that the GIF episodes were associated with significant increases in the high beta band (21-38Hz) across the central, frontal, occipital and parietal EEG sites. By implementing PSD and CF as input features with two-layer Back Propagation neural networks as a classifier, the proposed system was able to detect GIF events with a classification performance of 84.27% sensitivity and 84.80% accuracy. This is the first study to show cortical dynamic changes associated with GIF in Parkinson's disease, providing valuable information to enhance the performance of future GIF detection that could be translated into clinical practice.**

I. Introduction

Gait Initiation Failure (GIF) or "start hesitation" is a sub-type of Freezing of Gait (FOG) seen in PD. Patients with GIF are frequently unable to initiate their first step effectively in order to start walking. GIF is a common form of FOG, with over 20 percent of all FOG episodes recorded as being a GIF [1]. Gait initiation is a complex motor task requiring both motor and cognitive processing to enable the correct selection, timing and scaling of movement [2]. Gait initiation in PD patients with FOG can be affected by emotion, attention and dopaminergic therapy, suggesting the existence of a complex pathophysiological process that not only involves the locomotor networks, but also differing cortical areas and the basal ganglia system [2]. However, little objective evidence exists regarding the brain mechanisms underlying GIF and there are no clinically useful approaches for its treatment [3].

Our research group has recently demonstrated that EEG techniques can be used to identify and detect FOG episodes in PD due to their temporal ability to track the dynamic physiological changes throughout the brain during and even prior to the occurrence of any motor disturbances [4, 5]. An early detection algorithm for FOG has already been developed by analyzing energy power, entropy, correlation and brain connectivity of EEG signals, providing valuable insights into the underlying brain mechanism of FOG, which are progressing the development of novel treatments [4, 5]. However, these previous studies have focused on episodes of freezing in general without classifying subtypes of FOG, potentially limiting its clinical accuracy.

To the best of our knowledge, there is currently no implementation of EEG techniques to investigate and detect GIF in PD patients. In this study, we therefore used a non-invasive EEG system to study four PD patients who experienced multiple episodes of GIF during several standardized Timed Up and Go (TUG) assessments [1]. In this paper, the method of GIF detection is based on Back Propagation neural networks with the input features being Power Spectral Density (PSD) and Centroid Frequency (CF) [4, 5].

Based on the notion that gait initiation requires both motor and non-motor features (e.g. cognitive and limbic processes), we aimed to investigate neural changes associated with GIF. We hypothesized that there would be a detectable change in high beta CF and PSD across the central and frontal regions when comparing GIF with effective starts as high beta frequencies from the frontal lobe have been proposed to act as "a stopping signal" that might prevents the central motor area's from initiating the first step [6]. We were also keen to explore whether the classification results could be detected using only two channels; which would contribute to the feasibility of making real-time devices for clinical application.

II. Methods

A. Subjects and Task

EEG data were obtained from four Parkinson's disease patients (3 males, 1 female) with clinically confirmed FOG. They were recruited from the Parkinson's disease Research Clinic at the Brain and Mind Centre, The University of

[a] Faculty of Engineering and Information Technology, University of Technology, Sydney, Broadway, NSW 2007, Australia. (Quynh.T.Ly@student.uts.edu.au,AluysiusMariaArdi.Handojoseno@student.uts.edu,Rifai.Chai@uts.edu.au,TuanNghia.Nguyen@uts.edu.au,yvonne.tran@uts.edu.au, Hung.Nguyen@uts.edu.au)

[b] Parkinson's Disease Research Clinic, Brain and Mind Research Center, University of Sydney, Level 4, Building F, 94 Mallet Street, Camper down, NSW, 2050, Australia. (simonl@med.usyd.edu.au, moran.gilat@sydney.edu.au)

[c] Faculty of Science and Engineering, Sanata Dharma University, Paingan, Sleman, Yogyakarta, 55281, Indonesia (ardi@usd.ac.id)

[*] Dual senior authorship

Sydney. This study was approved by The Human Research and Ethics Committee from the University of Sydney. They were assessed in their practically-defined 'off' state following overnight withdrawal of dopaminergic therapy for more than 12 hours. All subjects demonstrated multiple episodes of GIF during a structured series of video-recorded TUG tasks. The distribution of GIF among the patients was not equal: 3 patients had less than 15 events and 1 patient experienced more than 15 events. As such, we randomly selected 15 GIF events from this subject to be used in further analyses. The EEG data were acquired using a 32 Ag/AgCl scalp electrodes of a Biosemi ActiveTwo system. Only data from 9 electrodes positioned in the location of interest were processed: F3, Fz, F4 (motor planning and working memory), Cz (motor execution), P3, Pz, P4 (sensory integration), O1 and O2 (visual area). References were taken by averaging from electrodes placed on each ear lobe. The recording was segmented into 1-second durations and digitized at 512 Hz.

The EEG data of GIF events was taken according to the time of onset and offset as scored on the video when the patients tried to take a first step but failed to do so. In addition, the EEG data from Good Starts (GS) was taken from 2-second periods after the patients were able to take an effective first step in a normal start during the TUG tasks.

B. *Feature Extraction*

In this study, 61 GIF EEG and 61 GS EEG samples data were collected from four patients and analyzed using EEGLab toolbox. The EEG signals were filtered using a non-linear IIR band-pass filter with a cut-off frequency lower than 1 Hz and higher than 50Hz to remove artifacts. The amplitude spectrum of each data sample in the time domain was transformed into the frequency domain using Fast Fourier Transform; which resulted in the power spectrum $P(f_i)$. It has been proposed that beta band activity can be further subdivided into low and high frequency, with high beta frequencies being affected differently in response to FOG [7]. Therefore, in this study, Welch's method with a 256 points FFT with 55% overlapping was used to analyze four frequency sub-bands, namely theta (4-8Hz), alpha (8-13Hz), low beta (13-21 Hz) and high beta (21-38Hz) (Fig. 1).

The PSD and CF of each frequency band were estimated and chosen as the main parameters for further analyses. The non-parametric Wilcoxon Sum Rank Test with an alpha of 0.05 was used to investigate the PSD and CF differences between GS and GIF episodes. These features were then used as inputs of classifier for the detection of GIF.

Fig.1 shows the amplitude spectra of representative raw EEG data of one patient that were tracked in the time domain. Overall, decomposition of the EEG data into theta, alpha and low-high beta bands demonstrated that GIF was associated with high amplitude within a range from 4 to 8 Hz (theta) and 21 to 38 Hz (high beta). In addition, GS was typically characterized by regularly decreased amplitude in these two sub-bands within different brain regions.

C. *Classification*

In this paper, we utilized a two-layer feed-forward neural networks with 2 to 12 hidden nodes to classify the pattern into two categories: GIF and GS. The input of this classifier

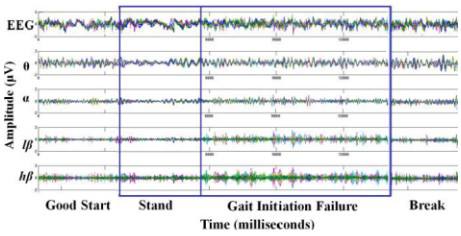

Figure 1. The comparison of amplitude and frequency of raw EEG data between GS, Stand, GIF and Break (Breaking GIF) in one PD patient.

included PSD and CF features extracted from the EEG signals. The desired output was set at *1* in cases of GIF and *0* in cases of GS (Fig. 2).

The output of the neural networks was computed as follows:

$$z(x,w) = f_1\left(b_k + \sum_{j=1}^{m} \bar{w}_{kj}\, f_2\left(b_j + \sum_{i=1}^{n} w_{ji}\, x_n\right)\right) \quad (1)$$

where f_1, f_2 is the activation function, x presents the input vector, W is the weight matrix vector; w_{ji} is the weight of the link between the i-th hidden node and the j-th input; $\bar{w}_{kj}$ is the weight of the link between i-th hidden node and the output, b_k and b_j are the biases; m is the number of outputs; n is the number of inputs and the *tan sig* function was assigned as the activation function of the hidden layer.

For the classification purpose, 122 EEG data (including 61 GS and 61 GIF) from 4 PD patients were fed into our classifier. Levenberg-Marquardt algorithm was chosen as training method for its speed and stability. To avoid overtraining, our classification system utilized early stopping strategy that helped preventing over-fitting and improved generalization. The data set was separated randomly into training set, validation set and test set with the ratio of 34%, 33% and 33%, respectively. The prediction of sensitivity, specificity and accuracy were measured based on 50 times trials.

III. RESULTS

A. *EEG Power Spectral Density*

Statistical results of extracted PSD of EEG signal at each

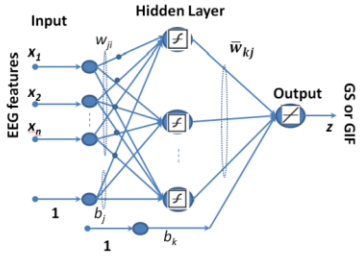

Figure 2. Neural Networks Structure

single channel are presented in Table I, with the most significant features (***p<0.001***) being reported in ***italic bold.***

Direct comparison of EEG frequency band power during two conditions showed that the strongest significant differences were found in the beta band, especially high beta in the occipital areas O1 and O2 (*p<0.0001*). In addition, the results revealed that the parietal areas P3 and P4 were significantly affected by GIF in the high beta frequency band (*p<0.001*). We also observed a significant increase in both low and high beta power during GIF in the central Cz and frontal Fz areas.

In Table II, the comparison of CF during the two conditions (e.g. GS vs GIF) showed that CF high beta stood out as the only affected sub-band during GIF regardless the position of the EEG channel. More specifically, the CF high beta increased significantly in almost *8* channels during GIF episodes. This pattern indicated that GIF may be related to a change in the oscillatory high beta frequency within the subthalamic nucleus and may also support the suggestion that GIF is related to excessive paroxysmal cortical beta synchronization [7]

Overall, in this finding, we proposed that the changes of oscillatory rhythms during GIF reflected an increase in conflict processing underlying cognitive control (theta) and "stopping" network operating (high beta) within the motor planning and execution in the centers of the brain [5, 7, 8].

TABLE I. POWER SPECTRAL DENSITY BETWEEN GIF AND GS

Lead	band	GS	GIF	*p*-value
F3	θ	0.130 ± 0.15	0.162 ± 0.13	0.0313
	θ	0.129 ± 0.11	0.191 ± 0.15	***≤0.001***
Fz	α	0.057 ± 0.05	0.063 ± 0.04	0.0425
	lβ	0.030 ± 0.03	0.036 ± 0.02	0.0161
	hβ	0.025 ± 0.03	0.033 ± 0.03	0.0471
Cz	θ	0.128 ± 0.13	0.172 ± 0.14	0.0132
	lβ	0.032 ± 0.02	0.044 ± 0.03	0.0245
	hβ	0.032 ± 0.03	0.049 ± 0.04	***≤0.001***
P3	θ	0.130 ± 0.15	0.162 ± 0.13	0.0328
	lβ	0.034 ± 0.03	0.046 ± 0.03	***≤0.001***
	hβ	0.043 ± 0.05	0.069 ± 0.07	***≤0.001***
P4	lβ	0.036 ± 0.03	0.048 ± 0.03	0.0101
	hβ	0.044 ± 0.04	0.073 ± 0.06	***≤0.001***
Pz	θ	0.132 ± 0.14	0.171 ± 0.14	0.0377
	lβ	0.034 ± 0.03	0.044 ± 0.03	0.0090
	hβ	0.035 ± 0.03	0.055 ± 0.06	0.0100
O1	α	0.056 ± 0.05	0.072 ± 0.05	0.0139
	lβ	0.045 ± 0.04	0.069 ± 0.05	***≤0.001***
	hβ	0.077 ± 0.08	0.134 ± 0.10	***≤0.0001***
O2	θ	0.094 ± 0.10	0.110 ± 0.08	0.0280
	α	0.059 ± 0.05	0.089 ± 0.06	***≤0.001***
	lβ	0.046 ± 0.04	0.083 ± 0.06	***≤0.0001***
	hβ	0.081 ± 0.08	0.139 ± 0.12	***≤0.0001***

TABLE II. CENTROID FREQUENCY BETWEEN GIF AND GS

Lead	band	GS	GIF	*p*-value
F3	hβ	25.826 ± 1.94	26.461 ± 1.92	0.0307
Fz	hβ	25.682 ± 1.81	26.247 ± 1.89	0.0428
Cz	hβ	25.858 ± 2.05	26.585 ± 1.82	0.0166
P3	hβ	26.287 ± 2.15	27.168 ± 2.06	0.0107
P4	hβ	26.219 ± 2.14	27.041 ± 1.97	0.0158
Pz	hβ	26.383 ± 2.29	27.182 ± 1.94	0.0211
O1	hβ	26.596 ± 2.23	27.658 ± 2.03	0.0300
O2	hβ	26.826 ± 2.41	27.591 ± 1.94	0.0258

B. Classification

The classification result displays consistent values are shown in Fig. 3. The classification percentages shows consistent values in all fifty running times confirmed the ability of the optimization process to provide the optimal solution in each of the regions. The number of hidden nodes was varied from 2 to12 per training session of the neural networks for each separate location in order to find the best number of hidden nodes that provides the highest sensitivity and best accuracy.

The mean, maximum and minimum values of PSD and CF of the 4 frequency bands in each electrode's location were taken as inputs of the classifier to evaluate their strength in detecting GIF. The sensitivity, specificity and accuracy results of our classification system are shown in Table III-IV. The reported results were the best performance (highest sensitivity and best accuracy) between 2 and 12 hidden nodes and the mean of 50 times trials. We also studied the performance of the detection of GIF using the combination of these different channels. The neural networks were developed with inputs corresponding to significant data (p<0.05) from one, two, four and nine EEG channels.

The classifier system using input from single locations was represented in Table III. The result showed that occipital regions provided the best location data for detecting GIF events with classifier using data from channel O2 obtained 70.90% sensitivity and 74.44% accuracy. Central locations provided similar strength as an indicator of GIF with Cz detected GIF with 68.29% sensitivity and 74.44% accuracy. The best performance of classifier using single channel from frontal and parietal locations was when

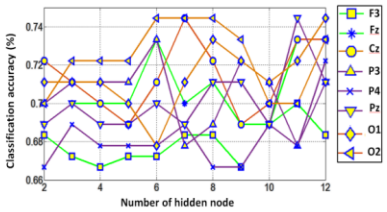

Figure 3. Mean of accuracy versus number of hidden nodes.

TABLE III. CLASSIFICATION RESULTS OF PROPOSED FEATURES USING BACK PROPAGATION NEURAL NETWORKS

Lead	H	Training set			Testing set		
		Sens	Spec	Acc	Sens	Spec	Acc
F3	10	70.37	76.42	73.26	67.78	69.72	68.89
Fz	12	78.84	84.32	81.63	72.22	72.89	73.33
Cz	7	74.99	85.61	80.00	68.29	79.55	74.44
P3	2	71.72	82.16	76.51	69.84	69.70	70.00
P4	3	72.21	71.01	71.63	69.29	68.55	68.89
Pz	9	71.70	84.92	77.91	68.29	72.88	71.11
O1	9	75.36	85.27	80.23	70.95	72.16	72.22
O2	6	76.63	93.69	84.65	70.90	77.06	74.44

H=number of hidden nodes; Sens= sensitivity; Spec = specificity; Acc= accuracy;

using Fz and Pz with 72.22% and 68.29% sensitivity, respectively. These two locations achieved 73.33% (Fz) and 71.11% (Pz) accuracy in detecting GIF.

CzO2 appeared at the best combination of two channels to detect GIF with sensitivity 76.88% and accuracy 78.89%, followed by FzO2 with sensitivity of 71.67% and accuracy of 78.89%. The combination of four best channels FzCzPzO2 obtained with 78.50% sensitivity and 82.22% accuracy when detecting GIF. The best performance of the classification system was 84.27% sensitivity and 84.80% accuracy in using a combination of nine channels (Table IV).

IV. DISCUSSION

Abnormal beta band frequencies were found underlying GIF. This finding is consistent with previous research showing that beta frequencies are likely to operate the neural communications in a stopping network in which the beta power increases when the prohibiting of movement is needed [8]. In addition, a relationship between freezing and high-beta oscillations in the subthalamic nucleus has been suggested with maximal coherence in high beta activity being located across the supplementary motor cortex (SMA), cingulate and leg area of SMA [7]. Finally, our research group recently found that beta frequencies are the most significant features of EEG signals underlying the transition from walking to FOG [4, 5].

Overall, these results are closely aligned with our current finding, suggesting that the high beta oscillations observed over central and frontal regions (Cz-Fz) of the cortex could represent inhibitory signals from the basal ganglia and its output nuclei, which are likely to be associated with the inability to start walking during GIF in PD patients [7, 8].

TABLE IV. CLASSIFICATION RESULTS OF COMBINATION OF CHANNELS

Lead	H	Training set			Testing set		
		Sens	Spec	Acc	Sens	Spec	Acc
FzCz	2	71.14	91.20	80.93	67.62	80.81	75.56
FzPz	5	76.81	85.88	80.93	70.56	74.56	73.33
FzO2	11	76.87	94.64	85.35	71.67	84.46	78.89
CzPz	11	74.87	88.51	81.86	71.16	74.98	73.33
CzO2	8	80.26	96.57	88.37	76.88	81.92	78.89
PzO2	7	70.96	96.22	83.49	68.95	87.07	78.89
FzPzCzO2	12	81.78	97.14	89.07	78.50	85.38	82.22
FCPO	10	94.85	87.75	90.34	84.27	85.02	84.80

FCPO: F3Fz-Cz-P3PzP4-O1O2

The classification results suggest that central-occipital (CzO2) cortex regions are the two optimal locations for detecting GIF in PD patients. This indicates that the PD patients are 'over-relying' on visual information during a GIF. Especially during a period of GIF, due to the inadequate input from motor regions (Cz), the response of the muscle and joints in PD patients are different than what they are expected. Therefore, these freezers might need to use more of their visual system (O2) to gain the information about what is happening in order to break GIF by getting Cz (primary motor regions) to activate again [9].

V. CONCLUSION

This study revealed that high beta frequency band stood out as the most effected sub-band underlying GIF behaviour in PD patients. The classification showed that central-occipital might be the most two impaired regions during the GIF episode. Results also showed the episode of GIF can be detected using only two channels with average accuracy above 75%. Future studies using larger sample sizes that compare other multiple electrode sites are now required to confirm our proposed methodology. In addition, future studies are encouraged to continue to pursue the development of a real-time device that can efficiently predict GIF events to alert PD patients when GIF is detected.

REFERENCES

[1] J. M. Shine, S. T. Moore, S. J. Bolitho, T. R. Morris, V. Dilda, S. L. Naismith, *et al.*, "Assessing the utility of Freezing of Gait Questionnaires in Parkinson's Disease," *Parkinsonism & Related Disorders*, vol. 18, pp. 25-29, 2012.

[2] A. Delval, C. Moreau, S. Bleuse, D. Guehl, E. Bestaven, E. Guillaud, *et al.*, "Gait and attentional performance in freezers under methylphenidate," *Gait & Posture*, vol. 41, pp. 384-388, 2015.

[3] K. Niazmand, K. Tonn, Y. Zhao, U. M. Fietzek, F. Schroeteler, K. Ziegler, *et al.*, "Freezing of Gait detection in Parkinson's disease using accelerometer based smart clothes," in *Biomedical Circuits and Systems Conference (BioCAS), 2011 IEEE*, pp. 201-204, 2011.

[4] A. M. Ardi Handojoseno, J. M. Shine, T. N. Nguyen, Y. Tran, S. J. G. Lewis, and H. T. Nguyen, "Analysis and Prediction of the Freezing of Gait Using EEG Brain Dynamics," *Neural Systems and Rehabilitation Engineering*, IEEE Transactions on, vol. 23, pp. 887-896, 2015.

[5] J. M. Shine, A. M. A. Handojoseno, T. N. Nguyen, Y. Tran, S. L. Naismith, H. Nguyen, et al., "Abnormal patterns of theta frequency oscillations during the temporal evolution of freezing of gait in Parkinson's disease," *Clinical Neurophysiology*, vol. 125, pp. 569-576, 2014.

[6] A. R. Aron, T. W. Robbins, and R. A. Poldrack, "Inhibition and the right inferior frontal cortex: one decade on," *Trends in Cognitive Sciences*, vol. 18, pp. 177-185, 2014.

[7] J. B. Toledo, J. López-Azcárate, D. Garcia-Garcia, J. Guridi, M. Valencia, J. Artieda, et al., "High beta activity in the subthalamic nucleus and freezing of gait in Parkinson's disease," *Neurobiology of Disease*, vol. 64, pp. 60-65, 2014.

[8] A. A. Kühn, F. Kempf, C. Brücke, L. Gaynor Doyle, I. Martinez-Torres, A. Pogosyan, et al., "High-Frequency Stimulation of the Subthalamic Nucleus Suppresses Oscillatory β Activity in Patients with Parkinson's Disease in Parallel with Improvement in Motor Performance," *The Journal of Neuroscience*, vol. 28, pp. 6165-6173, 2008.

[9] K. A. Ehgoetz Martens, F. Pieruccini-Faria, and Q. J. Almeida, "Could Sensory Mechanisms Be a Core Factor That Underlies Freezing of Gait in Parkinson's Disease?," *PLoS ONE*, vol. 8, p. e62602, 2013

Identifying Montages that Best Detect the Electroencephalogram Power Spectrum Alteration during Freezing of Gait in Parkinson's Disease Patients

Quynh Tran Ly[a], A.M. Ardi Handojoseno[a,c], *Student Member, IEEE*, Moran Gilat[b] Nghia Nguyen[a], *Senior Member, IEEE*, Rifai Chai[a], *Member, IEEE* , Yvonne Tran[a], Simon J.G.Lewis[b,*], Hung T Nguyen[a,*], *Senior Member, IEEE*

Abstract— **Our research team has previously used four Electroencephalography (EEG) leads to successfully detect and predict Freezing of Gait (FOG) in Parkinson's disease (PD). However, it remained to be determined whether these four sensor locations that were arbitrarily chosen based on their role in motor control are indeed the most optimal for FOG detection. The aim of this study was therefore to determine the most optimal location and combination of sensors to detect FOG amongst a 32-channel EEG montage using our EEG classification system. EEG measures, including power spectral density, centroid frequency and power spectral entropy, were extracted from 7 patients with PD and FOG during a series of Timed up and Go tasks. By applying a feed-forward neural networks to classify EEG data, the obtained results showed that even a small number of electrodes suffice to construct a FOG detector with expected performance, which is comparable to the use of a full 32 channels montage. This finding therefore progresses the realization of a FOG detection system that can be effectively implemented on a daily basis for FOG prevention, improving the quality of life for many patients with PD.**

I. Introduction

Freezing of Gait (FOG) is a highly disabling symptom that affects approximately half of all Parkinson's disease patients, especially in the advanced stages of the disease. Clinically, FOG is defined as a "brief, episodic absence or marked reduction of forward progression of the feet despite the intention to walk"[1]. This study therefore investigated periods of Freezing with periods of effective forward progression of the feet, hereafter called 'Effective walking' (EW).

Our group has recently demonstrated that surface electroencephalography (EEG) can be used to demonstrate specific brain signal changes that herald an episode of freezing of gait (FOG) when patients are walking. In addition, FOG can be detected and predict using only four channels EEG system representing four main brain regions hypothesized to be involved in physiological processes underlying FOG [2]. An early detection algorithm for FOG has been developed based on those locations by analyzing energy power, correlation and brain connectivity of EEG signals, providing a significant progress in the development of novel treatments [2]. However, it remains unclear whether these four channels are indeed the most sensitive location for FOG detection and prediction. Therefore, the objective of this study was to determine the best locations and the most effective number of leads for detecting FOG using EEG signals; which demonstrated as a part of our unified framework. This information would greatly assist with the clinical translation of a FOG detection device since fewer sensors will improve computation efficiency, robustness of the classification system and convenience for the use of ambulatory EEG by patients.

In this study, data from 7 patients with advanced Parkinson's disease and FOG were used. Different EEG parameters in the form of Power Spectral Density (PSD), Centroid Frequency (CF) and Power Spectral Entropy (PSE) were extracted and analyzed to find important features that were significantly changed during FOG. The features from each single channel were then employed as inputs for neural networks to classify patients' conditions during two stages: EW and freezing. The neural networks were trained and tested with the input of each separate channel among 32 channels at a time. The sensitivity and accuracy were measured based on mean of 50 times trials.

The purpose of this study was to determine the value of limited EEG montages viewed with EEG reformatting capability for the identification of FOG. We used input from one channel, two channels, four channels, six channels, seven channels and 32 channels at a time to find the optimal EEG configuration for the detection of FOG. We postulated that a combination of leads recording information from regions involved in motor and cognitive control as well as the integration of sensory information would be most likely.

II. METHODS

A. Data Collection and Pre-processing

EEG data was obtained from seven Parkinson's disease patients (six males, one female) with clinically confirmed FOG. They were recruited from the Parkinson's disease Research Clinic at the Brain and Mind Center, The University of Sydney. This study was approved by The

[a] Faculty of Engineering and Information Technology, University of Technology, Sydney, Broadway, NSW 2007, Australia. (Quynh.T.Ly@student.uts.edu.au,Rifai.Chai@uts.edu.au,TuanNghia.Nguyen@uts.edu.au, Hung.Nguyen@uts.edu.au, yvonne.tran@uts.edu.au)

[b] Parkinson's Disease Research Clinic, Brain and Mind Center, University of Sydney, Level 4, Building F, 94 Mallet Street, Camper down, NSW, 2050, Australia. (simonl@med.usyd.edu.au, moran.gilat@sydney.edu.au)

[c] Faculty of Science and Engineering, Sanata Dharma University, Paingan, Sleman, Yogyakarta, 55281, Indonesia (ardi@usd.ac.id)

[*] Dual senior authorship

978-1-4577-0220-4/16/$31.00 ©2016 IEEE

Human Research and Ethics Committee, University of Sydney. They were assessed in their practically-defined 'off' state following overnight withdrawal of dopaminergic therapy. The subjects demonstrated multiple episodes of FOG during a structured series of Timed Up and Go tasks.

EEG data was acquired using 32 Ag/AgCl scalp electrodes from a Biosemi ActiveTwo system with the 32 electrodes positioned over the main cortical regions: frontal (motor planning and working memory), central (motor execution), parietal (sensory integration), temporal (memory and sensory processing) and occipital (visual area). References were taken by averaging 2 electrodes placed on the ear lobes. The recording was segmented to 1-second durations and digitized at 512 Hz.

In this study, 343 seconds of EEG data samples of EW and 343 seconds of EEG data samples of FOG from 7 PD patients were collected and filtered (0.5-50 Hz) using EEGLab toolbox.

B. EEG Montages Systems

The strength of the alteration of the EEG signal parameters differ from one location to another. Therefore, the following factors were analyzed for their influence on accuracy of FOG detection:

1. Combination of four affected channels representing frontal, central, parietal and occipital regions.
2. Combination of channels experienced similar PSD pattern underlying FOG episodes.

C. Feature Extraction

In order to eliminate differences between electrodes and individual subjects, a Z-transformation was applied to normalize EEG data. After pre-processing, PSD, CF, PSE were extracted. The EEG signals were filtered using a non-linear IIR band-pass filter with a cut-off frequency lower than 1 Hz and higher than 50Hz to remove artefacts. Based on our previous work, sub-band delta (1-4 Hz) did not contributed to FOG detection; therefore, in this study we focused on four frequency bands, namely: theta (4-8 Hz), alpha (8-13 Hz), low beta (13-21 Hz), high beta (21-38 Hz) [2]. The beta frequency band was divided into high and low band, based on previous findings showing that high beta frequencies correlate with freezing [3].

- *Power Spectral Density*

PSD shows strength of the energy as a function of frequency. It implies stationary process during the time window. In this study, the spectra are calculated via Welchs method using a *256* point Fast Fourier Transform (FFT) and periodic Hamming windows with an overlap of 50%. It is defined as *P(f)*.

- *Centroid Frequency*

Furthermore, we calculated the balance point for the area under the curve representing PSD. CF has been reported as the shift in the center of gravity of a frequency band based on normalized power spectrum [2]. CF is defined as:

$$CF = \frac{\sum_i f_i * P(f)}{\sum_i P(f)}, \quad (1)$$

- *Power Spectral Entropy*

Single neurons are highly nonlinear elements, and more nonlinearity is found in the neuronal group level with multiple feedback loops at different levels of distributed and interconnected cortical processing. Entropy was used as an index of EEG complexity or irregularly based on Shannon's Information Theory [2]. PSE of EEG signals x is defined as:

$$PSE(x) = -\sum_{i=f_l}^{f_h} P(i)\, logP(i), \quad (2)$$

D. Classification

The mean, maximum and minimum values of PSD, CF, and PSE from *32* electrode's location of four EEG frequency bands were taken to evaluate their strength in detecting freezing. A Wilcoxon Sum Rank Test with $p\ value \leq 0.05$ was used to investigate significant differences between periods of EW and periods of FOG. Cohen's d effect sizes were also applied to check the most significant difference between EW and FOG conditions with $d \geq 0.4$. These significant features were used as the main parameters for evaluating the best electrode locations to detect FOG events in PD patients.

The features were fed into feed-forward neural networks with 2 to 8 hidden nodes to classify the pattern into two categories: EW or FOG. Levenberg Marquardt's algorithm with early stopping was used to train 34% of the data, followed by validation and testing of by 33% and 33% of the total data. The sensitivity and accuracy were measured based on the mean of *50* times runs.

III. RESULTS

A. Feature Extraction

- *Power Spectral Density*

The general PSD pattern during freezing is shown in Fig. 1. A comparison of EEG frequency band power during the two conditions (e.g. EW *vs* FOG) showed that high beta band stood out as the most affected sub-band during freezing ($p<0.0001$) regardless of the position of the EEG channel. The low beta band showed the same pattern with a significant increase in frontal and central cortical region during the episode of FOG ($p<0.0001$). In addition, there were remarkable increases in alpha power in the four main regions of the brain during the period of FOG. Overall, compared to the EW period, FOG was associated with significant shifting in these three sub-bands alpha, and low-high beta in frontal

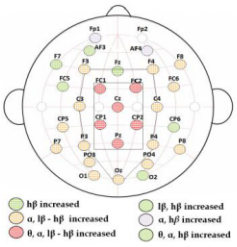

Figure 1. Significant PSD pattern between EW and FOG

F3, F4, central C3, C4, parietal P3, P4 and occipital Oz. The shift of four sub-bands theta, alpha and low-high beta only appeared in frontal-central and parietal region such as in FC1, FC2, CZ, CP1, CP2, and PZ.

When the effect size *d* was taken into account, the high beta alteration was strongest in frontal F3 and central C4; with remarkably increased power in these two locations. In the parietal locations, episodes of freezing were associated with a large increase of power in low-high beta frequency with P4 appearing as the most affected location. In occipital region, O2 appeared as the location with the largest increase in the high beta band (Table I-III).

- *Centroid Frequency*

The CF analysis revealed the shifting of centroid frequency in theta, low and high beta in almost all of *32* channels during freezing episodes ($p<0.0001$). The CF high beta stood out as the most affected frequency band from EW episode to FOG episode with the largest shifts in the frontal lead F3, central lead C4, followed by occipital O2 and parietal P4. When compared to the effective walking, episodes of freezing were associated with significant shift in theta frequency band with the largest shift of CF in frontal and central leads such as F3 and C4 (Fig. 2). This suggests that frontal-central cortical regions were more affected than parietal-occipital region in term of CF features. This is aligned with function Magnetic Resonance Imaging (fMRI) studies in which freezing provoked by a virtual reality gait paradigm was associated with alterations in the pre-supplementary and primary motor areas, presumably as a compensatory strategy to overcome reduced automaticity of gait [4].

- *Power Spectral Entropy*

The results of our entropy analysis showed that there was an increase of entropy in the two frequency bands theta, and high beta in most locations during freezing episodes. The most significant change was detected in PSE theta in frontal F3, central C4. There were also significant increases in the regularity of high beta activity in frontal F3, central C4 and occipital O2.

B. Scalp Topographies:

EEG data samples of FOG events were processed and analyzed using EEGLab toolbox. They were categorized separately into three bands: theta, low beta and high beta and summarized into a color-coded map in the form of scalp topography. Fig.3 displays the topographic distribution of spectra power represented for the three bands: theta, low beta and high beta underlying FOG episodes.

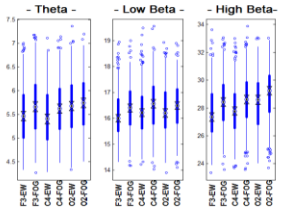

Figure 2. Shift of CF in F3, C4 and O2 in 3 frequency band theta, low beta and high beta between 2 condition EW and FOG

TABLE I. FEATURE EXTRACTION OF CHANNEL F3

Parameter	Band	EW	FOG	EW vs FOG
Power	α	0.089 ± 0.08	0.119 ± 0.09	**
	lβ	0.038 ± 0.03	0.048 ± 0.03	**
	hβ	0.043 ± 0.03	0.049 ± 0.04	***
Frequency	θ	5.493 ± 0.59	5.673 ± 0.06	**
	lβ	16.150 ± 0.88	16.419 ± 0.91	**
	hβ	27.680 ± 1.81	28.438 ± 1.82	***
Entropy	θ	0.866 ± 0.11	0.893 ± 0.09	*
	hβ	0.911 ± 0.04	0.920 ± 0.04	*

TABLE II. FEATURE EXTRACTION OF CHANNEL C4

Parameter	Band	EW	FOG	EW vs FOG
Power	α	0.081 ± 0.07	0.110 ± 0.09	**
	lβ	0.043 ± 0.03	0.055 ± 0.04	**
	hβ	0.050 ± 0.04	0.061 ± 0.05	***
Frequency	θ	5.460 ± 0.59	5.636 ± 0.58	**
	lβ	16.278 ± 0.91	16.526 ± 0.94	**
	hβ	27.901 ± 1.78	28.620 ± 1.85	***
Entropy	θ	0.861 ± 0.12	0.893 ± 0.09	*
	hβ	0.917 ± 0.04	0.922 ± 0.04	*

TABLE III. FEATURE EXTRACTION OF CHANNEL O2

Parameter	Band	EW	FOG	EW vs FOG
Power	lβ	0.067 ± 0.05	0.083 ± 0.07	*
	hβ	0.087 ± 0.09	0.137 ± 0.11	***
Frequency	lβ	16.333 ± 0.93	16.477 ± 0.89	*
	hβ	28.402 ± 2.00	29.021 ± 1.93	**
Entropy	lβ	0.910 ± 0.05	0.920 ± 0.05	*
	hβ	0.918 ± 0.04	0.926 ± 0.04	*

* = $0.0001<p\leq0.05$ and $d\leq0.4$; ** = $p\leq0.0001$ and $d\leq0.4$;
*** = $p<0.0001$ and $d>0.4$

The power values were calculated and transferred into the corresponding values using an interpolation method in order to produce a smooth surface of the scalp topography. Each oval topography depicts a view of the head from above with frontal areas at the top. For individual scalp topography, each electrode zone is colour coded to indicate how much activity it contains compared to other regions, with a blue colour indicating reduced power and a red colour spectrum indicating increased power. It is observed that the theta power escalation spreads within central and frontal locations while the low-high beta power increased significantly in F3, C4, P4 and O2 locations. This finding is strongly consistent with multiple studies that have shown a relationship between FOG and impairments within both visual-attention (P4-O2) networks and motor planning-executive network (F3-C4) in the human cortex [2, 4].

C. EEG Montages Systems

Based on the result from feature extraction and from classification system using single channel as input, we designed the three EEG montages systems that might facilitate the identification of FOG arising from four main

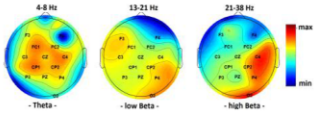

Figure 3. Scalp topography of EEG power activity underlying FOG.

cortical regions. These systems were also compared with previous finding to validate that they are the most affected locations of the brain during FOG in many fMRI studies [5].

EEG System 1: Four most affected channels among 32 channels during FOG. The EEG montages were F3, C4, P4, and O2.

EEG System 2: Six channels experienced a significant increase in four sub-bands: theta, alpha, low-high beta. The montages were FC1, FC2, Cz, CP1, CP2 and Pz.

EEG System 3: Seven channels experienced a significant increase in only three sub-bands: alpha, low-high beta. The montages were as follows: F3, F4, C3, C4, P3, P4, and Oz.

D. Classification results

The neural networks were developed with inputs corresponding to significant data ($p<0.05$) from 1, 2, 3, 4, 6, 7 and 32 EEG channels as shown in Table V.

The classification results using input from single channel location at a time showed that the central regions were the best area for detecting freezing events. Indeed, C4 seemed to be the best location to detect freezing with 70.88% sensitivity and 69.13% accuracy. Frontal F3 and parietal P4 provided strength as an indicator of FOG, with 70.29% and 69.59% sensitivity, respectively. These two locations achieved similar accuracy in detecting FOG with 68.93%. The best performance of classifier using a single channel from the occipital region was with O2, which had 70.72% sensitivity and 66.60% accuracy (Table IV).

The performance of the detection of FOG using the combination of these 4 different channels was also studied. In the systems using input from two to four locations, C4O2 appeared at the best combination of two channels to detect freezing with sensitivity of 72.54% and an accuracy of 69.71%. The combination from 4 locations that provided the best indicator of freezing was F3C4P4O2 with 72.29% sensitivity and 70.29% accuracy.

As the results shown in Table V, the neural networks based classifier with inputs obtained from six locations in System 2 provided 70.23% sensitivity and 68.93% accuracy. The sensitivity of the system was improved slightly with 70.94% when using the input from 7 locations of System 3. Interestingly, when taken all the 32 channels as an input, the classification system provided the sensitivity of 72.20%; which is lower than that of the two channels system C4O2.

TABLE IV. NEURAL NETWORKS CLASSIFICATION RESULTS

Lead	H	Training set		Testing set	
		Sens(%)	Acc(%)	Sens(%)	Acc(%)
F3	2	72.20	70.29	70.29	68.93
C4	3	74.36	73.21	70.88	69.13
P4	2	73.99	71.50	69.59	68.93
O2	7	76.42	74.67	70.72	66.60
F3C4	6	75.88	73.96	71.66	69.71
F3P4	8	76.73	74.33	71.04	69.71
F3O2	7	75.99	77.25	70.71	69.90
C4P4	5	74.91	72.46	71.38	68.93
C4O2	6	77.99	73.92	72.54	69.71
P4O2	2	73.05	72.54	71.00	69.71
F3C4P4	7	77.15	74.96	71.20	69.90
F3C4O2	5	74.96	73.63	71.40	69.13
C4P4O2	2	73.29	73.08	71.25	69.13
F3C4P4O2	8	76.19	76.46	72.29	70.29

H=number of hidden nodes; Sens= sensitivity; Acc= accuracy

TABLE V. COMPARISON OF CLASSIFICATION RESULTS

Results	Number of Channels						
	1	**2**	**3**	**4**	**6**	**7**	**32**
Sens(%)	70.88	72.54	71.40	72.29	70.23	70.94	72.20
Acc(%)	69.13	69.71	69.13	70.29	68.93	68.93	71.46

1: C4; **2**: C4O2; **3**: F3C4O2; **4**: F3C4P4O2; **6**: FC1, FC2, Cz, CP1, CP2, Pz; **7:** F3, F4, C3, C4, P3, P4, and Oz; **32**: all 32 channels

IV. DISCUSSION

The finding that the high beta oscillations in the human cortex increased and remained high across all the brain regions during the period of freezing is consistent with previous studies. This finding suggest that high beta frequencies are likely to operate the neural communications for a stopping network in which the beta power increase in order to prohibit the movement of PD patients during FOG episodes [6].

Our goal in evaluating differing montages was to find a minimum number of electrodes strategically placed to maximize the identification of FOG. This study revealed that optimal FOG detection was achieved when using an EEG system with only *2* channels C4-O2. These results supported the notion that increasing the number of EEG channels did not improve the diagnostic accuracy of FOG detection as fewer channels might promote less noise and artifacts. These results are closely aligned with several previous fMRI studies in which the motor lead C4, planning motor lead F3, parietal lead P4 and visual lead O2 are recording over regions that have been implicated in the pathogenesis of FOG in PD [4, 5].

V. CONCLUSION

Although limited to seven patients, this paper demonstrates that FOG would be detected effectively using an EEG system with only *2* input channels. Further studies using larger sample sizes are now required to confirm these preliminary findings and further delineate the specific neural networks provided a better performance of FOG detection and prediction system.

REFERENCES

[1] J. G. Nutt, B. R. Bloem, N. Giladi, M. Hallett, F. B. Horak, and A. Nieuwboer, "Freezing of gait: moving forward on a mysterious clinical phenomenon," *The Lancet Neurology*, vol. 10, pp. 734, 2011.

[2] A. M. Ardi Handojoseno, J. M. Shine, T. N. Nguyen, Y. Tran, S. J. G. Lewis, and H. T. Nguyen, "*Analysis and Prediction of the Freezing of Gait Using EEG Brain Dynamics*," *Neural Systems and Rehabilitation Engineering*, IEEE Transactions on, vol. 23, pp. 887-896, 2015.

[3] J. B. Toledo, J. López-Azcárate, D. Garcia-Garcia, J. Guridi, M. Valencia, J. Artieda, et al., "High beta activity in the subthalamic nucleus and freezing of gait in Parkinson's disease," *Neurobiology of Disease*, vol. 64, pp. 60-65, 2014.

[4] J. M. Shine, A. A. Moustafa, E. Matar, M. J. Frank, and S. J. G. Lewis, "The role of frontostriatal impairment in freezing of gait in Parkinson's disease," *Frontiers in Systems Neuroscience*, v.7, p.61, 04

[5] A.H. Snijders, Tackling freezing of gait in Parkinson's disease, PhD thesis, Radboud Univ., Nijmegen, the Netherlands, 2012

[6] A. R. Aron, T. W. Robbins, and R. A. Poldrack, "Inhibition and the right inferior frontal cortex: one decade on," *Trends in Cognitive Sciences*, vol. 18, pp. 177-185, 2014.

Australian Biomedical Engineering Conference (ABEC) November 22-25, 2015
ISBN: 978-1-922107-64-0

UTILISING AMBULATORY EEG TO EXPLORE GAIT INITIATION FAILURE IN PARKINSON'S DISEASE

Quynh Tran Ly[1], A.M. Ardi Handojoseno[1], Moran Gilat[2], Simon J.G.Lewis[2,*], Hung T Nguyen[1,*]

[1] University of Technology, Sydney, Faculty of Engineering and Information Technology, Broadway, NSW 2007, Australia.

[2] University of Sydney, Parkinson's disease Research Clinic, Brain and Mind Research Institute, Level 4, Building F, 94 Mallet Street, Camper down, NSW, 2050, Australia.

[*] Dual senior authorship

Keyword(s):The Biomedical Engineering Workforce, Biomedical Engineering leading Health

Abstract

Gait Initiation Failure (GIF) is one of the most disabling gait disturbances of advanced Parkinson's disease, described as the phenomenon where PD patients are unable to initiate the first step in order to start walking [3]. Failure to initiate the first step often precipitates falls; leading to an increased morbidity and subsequent nursing home placement. As such, this study utilized a novel ambulatory EEG technique to compare periods of GIF with periods of effective starts (GS) in a single PD patient during TUG tasks. Specifically, we set out to identify the brain activation pattern underlying GIF phenomenon.

134 samples data (62 GS and 72 GIF) collected from frontal, central, parietal and occipital regions were filtered and extracted into: theta, alpha, low beta and high beta band using FFT. Brain connectivity measurement was calculated by dDTF and mapped based on the peak of strength causal interactions originating at each pair electrodes.

In the investigation of PSD, the GIF episodes were associated with significant increases in the high frequency beta power (22-38Hz) in different areas of the brain, including the motor-frontal cortices. We proposed these changes of high beta oscillatory over central-frontal might reflected an inhibitory signal from the basal ganglia, which are likely to be associated with the inability to start walking during GIF in PD patients [2, 4]. In addition, effective connectivity analyses revealed that during GIF the motor cortices are "shut down" whilst the frontal regions try to overcome this connectivity loss. Frontal may be activating in an attempt to overcome GIF by communicating with other regions in order to break the GIF, getting primary motor regions to activate again [1].

The current finding demonstrated that GIF episodes might be associated with a "stopping" signal beta and affected more by the motor planning-execution in the center of the brain.

References

[1] Shine, (2013). Exploring the cortical and subcortical functional magnetic resonance imaging changes associated with freezing in Parkinson's disease.Brain136(4):1204-1215.

[2] Kühn, A. A., et al. (2008). "High-Frequency Stimulation of the Subthalamic Nucleus Suppresses Oscillatory β Activity in Patients with Parkinson's Disease in Parallel with Improvement in Motor Performance." The Journal of Neuroscience 28(24): 6165-6173.

[3] Schaafsma, J. D., et al. (2003). "Characterization of freezing of gait subtypes and the response of each to levodopa in Parkinson's disease." European Journal of Neurology 10(4): 391-398.

[4] Toledo, J. B., et al. (2014). "High beta activity in the subthalamic nucleus and freezing of gait in Parkinson's disease." Neurobiology of Disease 64(0): 60-65.

Correspondence

Name: Quynh Tran Ly

Organization: University of Technology, Sydney, FEIT, Broadway, NSW 2007, Australia.

Phone: (02) 95147531

Email: Quynh.T.Ly@student.uts.edu.au

References

Agid, Y., Cervera, P., Hirsch, E., Javoy‐Agid, F., Lehericy, S., Raisman, R. & Ruberg, M. 1989, 'Biochemistry of Parkinson's disease 28 years later: a critical review', *Movement Disorders*, vol. 4, no. S1, pp. S126-S44.

Amboni, M., Cozzolino, A., Longo, K., Picillo, M. & Barone, P. 2008, 'Freezing of gait and executive functions in patients with Parkinson's disease', *Movement Disorders*, vol. 23, no. 3, pp. 395-400.

Arias, P. & Cudeiro, J. 2010, 'Effect of rhythmic auditory stimulation on gait in Parkinsonian patients with and without freezing of gait', *PloS one*, vol. 5, no. 3, p. e9675.

Aron, A.R., Robbins, T.W. & Poldrack, R.A. 2004, 'Inhibition and the right inferior frontal cortex', *Trends in cognitive sciences*, vol. 8, no. 4, pp. 170-7.

Bachlin, M., Plotnik, M., Roggen, D., Maidan, I., Hausdorff, J.M., Giladi, N. & Troster, G. 2010, 'Wearable assistant for Parkinson's disease patients with the freezing of gait symptom', *IEEE Transactions on Information Technology in Biomedicine*, vol. 14, no. 2, pp. 436-46.

Backer, J.H. 2006, 'The symptom experience of patients with Parkinson's disease', *Journal of Neuroscience Nursing*, vol. 38, no. 1, p. 51.

Bakker, M., De Lange, F.P., Helmich, R.C., Scheeringa, R., Bloem, B.R. & Toni, I. 2008, 'Cerebral correlates of motor imagery of normal and precision gait', *NeuroImage*, vol. 41, no. 3, pp. 998-1010.

Bishop, C.M. 1995, *Neural networks for pattern recognition*, Oxford university press.

Bloem, B.R., Hausdorff, J.M., Visser, J.E. & Giladi, N. 2004, 'Falls and freezing of gait in Parkinson's disease: a review of two interconnected, episodic phenomena', *Movement Disorders*, vol. 19, no. 8, pp. 871-84.

Braak, H., Ghebremedhin, E., Rüb, U., Bratzke, H. & Del Tredici, K. 2004, 'Stages in the development of Parkinson's disease-related pathology', *Cell and tissue research*, vol. 318, no. 1, pp. 121-34.

Burrus, C.S., Gopinath, R.A. & Guo, H. 1997, 'Introduction to wavelets and wavelet transforms: a primer'.

Caballol, N., Martí, M.J. & Tolosa, E. 2007, 'Cognitive dysfunction and dementia in Parkinson disease', *Movement Disorders*, vol. 22, no. S17, pp. S358-S66.

Chai, R., Naik, G.R., Nguyen, T.N., Ling, S.H., Tran, Y., Craig, A. & Nguyen, H.T. 2017, 'Driver fatigue classification with independent component by entropy rate bound minimization analysis in an EEG-based system', *IEEE journal of biomedical and health informatics*, vol. 21, no. 3, pp. 715-24.

Chaudhuri, K.R., Healy, D.G. & Schapira, A.H. 2006, 'Non-motor symptoms of Parkinson's disease: diagnosis and management', *The Lancet Neurology*, vol. 5, no. 3, pp. 235-45.

Crémers, J., D'Ostilio, K., Stamatakis, J., Delvaux, V. & Garraux, G. 2012, 'Brain activation pattern related to gait disturbances in Parkinson's disease', *Movement Disorders*, vol. 27, no. 12, pp. 1498-505.

De Lau, L.M. & Breteler, M.M. 2006, 'Epidemiology of Parkinson's disease', *The Lancet Neurology*, vol. 5, no. 6, pp. 525-35.

Delorme, A. & Makeig, S. 2004, 'EEGLAB: an open source toolbox for analysis of single-trial EEG dynamics including independent component analysis', *Journal of neuroscience methods*, vol. 134, no. 1, pp. 9-21.

Delval, A., Moreau, C., Bleuse, S., Guehl, D., Bestaven, E., Guillaud, E., Dujardin, K., Defebvre, L. & Devos, D. 2015, 'Gait and attentional performance in freezers under methylphenidate', *Gait & posture*, vol. 41, no. 2, pp. 384-8.

Delval, A., Snijders, A.H., Weerdesteyn, V., Duysens, J.E., Defebvre, L., Giladi, N. & Bloem, B.R. 2010, 'Objective detection of subtle freezing of gait episodes in Parkinson's disease', *Movement Disorders*, vol. 25, no. 11, pp. 1684-93.

Djuric-Jovicic, M.D., Jovicic, N.S., Radovanovic, S.M., Stankovic, I.D., Popovic, M.B. & Kostic, V.S. 2014, 'Automatic identification and classification of freezing of gait episodes in Parkinson's disease patients', *IEEE Transactions on Neural Systems and Rehabilitation Engineering*, vol. 22, no. 3, pp. 685-94.

Dontje, M.L., de Greef, M.H., Speelman, A.D., van Nimwegen, M., Krijnen, W., Stolk, R.P., Kamsma, Y., Bloem, B., Munneke, M. & van der Schans, C.P. 2013, 'Quantifying daily physical activity and determinants in sedentary patients with Parkinson's disease', *Parkinsonism & related disorders*, vol. 19, no. 10, pp. 878-82.

Dorsey, E., Constantinescu, R., Thompson, J., Biglan, K., Holloway, R., Kieburtz, K., Marshall, F., Ravina, B., Schifitto, G. & Siderowf, A. 2007, 'Projected number of people with Parkinson disease in the most populous nations, 2005 through 2030', *Neurology*, vol. 68, no. 5, pp. 384-6.

Essential, F.M. & CPE 2012, *Parkinson's Australia. Parkinson What's That?*, e. Canberra.

Factor, S.A. & Weiner, W. 2007, *Parkinson's Disease: Diagnosis & Clinical Management*, Demos Medical Publishing.

Folstein, M.F., Folstein, S.E. & McHugh, P.R. 1975, '"Mini-mental state": a practical method for grading the cognitive state of patients for the clinician', *Journal of psychiatric research*, vol. 12, no. 3, pp. 189-98.

Fritz, C.O., Morris, P.E. & Richler, J.J. 2012, 'Effect size estimates: current use, calculations, and interpretation', *Journal of experimental psychology: General*, vol. 141, no. 1, p. 2.

Georgiades, M.J., Gilat, M., Martens, K.A.E., Walton, C.C., Bissett, P.G., Shine, J.M. & Lewis, S.J. 2016, 'Investigating motor initiation and inhibition deficits in patients

with Parkinson’s disease and freezing of gait using a virtual reality paradigm', *Neuroscience*, vol. 337, pp. 153-62.

Giladi, N., Kao, R. & Fahn, S. 1997, 'Freezing phenomenon in patients with parkinsonian syndromes', *Movement Disorders*, vol. 12, no. 3, pp. 302-5.

Giladi, N. & Nieuwboer, A. 2008, 'Understanding and treating freezing of gait in parkinsonism, proposed working definition, and setting the stage', *Movement Disorders*, vol. 23, no. S2, pp. S423-S5.

Gilat, M., Shine, J.M., Walton, C.C., O’Callaghan, C., Hall, J.M. & Lewis, S.J. 2015, 'Brain activation underlying turning in Parkinson’s disease patients with and without freezing of gait: a virtual reality fMRI study', *npj Parkinson's Disease*, vol. 1, p. 15020.

Han, J., Jeon, H.S., Jeon, B.S. & Park, K.S. 2006, 'Gait detection from three dimensional acceleration signals of ankles for the patients with Parkinson’s disease', *Proceedings of the IEEE The International Special Topic Conference on Information Technology in Biomedicine, Ioannina, Epirus, Greece*, vol. 2628.

Han, J.H., Lee, W.J., Ahn, T.B., Jeon, B.S. & Park, K.S. 2003, 'Gait analysis for freezing detection in patients with movement disorder using three dimensional acceleration system', *Engineering in Medicine and Biology Society, 2003. Proceedings of the 25th Annual International Conference of the IEEE*, vol. 2, IEEE, pp. 1863-5.

Handojoseno, A.M.A., Gilat, M., Ly, Q.T., Chamtie, H., Shine, J.M., Nguyen, T.N., Tran, Y., Lewis, S.J.G. & Nguyen, H.T. 2015, 'An EEG study of turning freeze in Parkinson's disease patients: The alteration of brain dynamic on the motor and visual cortex', *2015 37th Annual International Conference of the IEEE Engineering in Medicine and Biology Society (EMBC)*, pp. 6618-21.

Handojoseno, A.M.A., Shine, J.M., Gilat, M., Nguyen, T.N., Tran, Y., Lewis, S.J.G. & Nguyen, H.T. 2014, 'Prediction of freezing of gait using analysis of brain effective connectivity', *2014 36th Annual International Conference of the IEEE Engineering in Medicine and Biology Society*, pp. 4119-22.

Handojoseno, A.M.A., Shine, J.M., Nguyen, T.N., Tran, Y., Lewis, S.J.G. & Nguyen, H.T. 2012, 'The detection of Freezing of Gait in Parkinson's disease patients using EEG signals based on Wavelet decomposition', *2012 Annual International Conference of the IEEE Engineering in Medicine and Biology Society*, pp. 69-72.

Handojoseno, A.M.A., Shine, J.M., Nguyen, T.N., Tran, Y., Lewis, S.J.G. & Nguyen, H.T. 2015, 'Analysis and Prediction of the Freezing of Gait Using EEG Brain Dynamics', *IEEE Transactions on Neural Systems and Rehabilitation Engineering*, vol. 23, no. 5, pp. 887-96.

Hausdorff, J., Schaafsma, J., Balash, Y., Bartels, A., Gurevich, T. & Giladi, N. 2003, 'Impaired regulation of stride variability in Parkinson's disease subjects with freezing of gait', *Experimental Brain Research*, vol. 149, no. 2, pp. 187-94.

Hughes, A.J., Daniel, S.E., Kilford, L. & Lees, A.J. 1992, 'Accuracy of clinical diagnosis of idiopathic Parkinson's disease: a clinico-pathological study of 100 cases', *Journal of Neurology, Neurosurgery & Psychiatry*, vol. 55, no. 3, pp. 181-4.

Huse, D.M., Schulman, K., Orsini, L., Castelli‐Haley, J., Kennedy, S. & Lenhart, G. 2005, 'Burden of illness in Parkinson's disease', *Movement disorders*, vol. 20, no. 11, pp. 1449-54.

Jahn, K., Deutschländer, A., Stephan, T., Kalla, R., Wiesmann, M., Strupp, M. & Brandt, T. 2008, 'Imaging human supraspinal locomotor centers in brainstem and cerebellum', *Neuroimage*, vol. 39, no. 2, pp. 786-92.

Jankovic, J. 2008, 'Parkinson's disease: clinical features and diagnosis', *Journal of Neurology, Neurosurgery & Psychiatry*, vol. 79, no. 4, pp. 368-76.

Janssen, S., Bolte, B., Nonnekes, J., Bittner, M., Bloem, B.R., Heida, T., Zhao, Y. & van Wezel, R.J.A. 2017, 'Usability of Three-dimensional Augmented Visual Cues Delivered by Smart Glasses on (Freezing of) Gait in Parkinson's Disease', *Frontiers in Neurology*, vol. 8, no. 279.

Kerr, G., Worringham, C.J., Cole, M.H., Lacherez, P.F., Wood, J.M. & Silburn, P. 2010, 'Predictors of future falls in Parkinson disease', *Neurology*, vol. 75, no. 2, pp. 116-24.

Levy, R., Ashby, P., Hutchison, W.D., Lang, A.E., Lozano, A.M. & Dostrovsky, J.O. 2002, 'Dependence of subthalamic nucleus oscillations on movement and dopamine in Parkinson's disease', *Brain*, vol. 125, no. 6, pp. 1196-209.

Lewis, S.J. & Barker, R.A. 2009, 'A pathophysiological model of freezing of gait in Parkinson's disease', *Parkinsonism & related disorders*, vol. 15, no. 5, pp. 333-8.

Lewis, S.J. & Shine, J.M. 2016, 'The next step: a common neural mechanism for freezing of gait', *The Neuroscientist*, vol. 22, no. 1, pp. 72-82.

Li, X.-L. & Adali, T. 2010, 'Independent component analysis by entropy bound minimization', *IEEE Transactions on Signal Processing*, vol. 58, no. 10, pp. 5151-64.

Lisette Bunting-Perry PhD, R., Spindler, M., Robinson, K.M., Noorigian, J., Cianci, H.J. & Duda, J.E. 2013, 'Laser light visual cueing for freezing of gait in Parkinson disease: A pilot study with male participants', *Journal of rehabilitation research and development*, vol. 50, no. 2, p. 223.

Ly, Q.T., Handojoseno, A.M.A., Gilat, M., Chai, R., Martens, K.A.E., Georgiades, M., Naik, G.R., Tran, Y., Lewis, S.J.G. & Nguyen, H.T. 2017a, 'Detection of gait initiation Failure in Parkinson's disease based on wavelet transform and Support Vector Machine', paper presented to the *2017 39th Annual International Conference of the IEEE Engineering in Medicine and Biology Society (EMBC)*, Jeju Island, Korea, July.

Ly, Q.T., Handojoseno, A.M.A., Gilat, M., Chai, R., Martens, K.A.E., Georgiades, M., Naik, G.R., Tran, Y., Lewis, S.J.G. & Nguyen, H.T. 2017b, 'Detection of turning freeze in Parkinson's disease based on S-transform decomposition of EEG signals', paper presented to the *39th Annual International Conference of the IEEE Engineering in Medicine and Biology Society (EMBC)*.

Ly, Q.T., Handojoseno, A.M.A., Gilat, M., Nguyen, N., Chai, R., Tran, Y., Lewis, S.J.G. & Nguyen, H.T. 2016, 'Identifying montages that best detect the electroencephalogram power spectrum alteration during freezing of gait in

Parkinson's disease patients', *2016 38th Annual International Conference of the IEEE Engineering in Medicine and Biology Society (EMBC)*, pp. 6094-7.
Magrinelli, F., Picelli, A., Tocco, P., Federico, A., Roncari, L., Smania, N., Zanette, G. & Tamburin, S. 2016, 'Pathophysiology of Motor Dysfunction in Parkinson's Disease as the Rationale for Drug Treatment and Rehabilitation', *Parkinson's Disease*, vol. 2016, p. 9832839.
Maidan, I., Plotnik, M., Mirelman, A., Weiss, A., Giladi, N. & Hausdorff, J.M. 2010, 'Heart rate changes during freezing of gait in patients with Parkinson's disease', *Movement Disorders*, vol. 25, no. 14, pp. 2346-54.
Martens, K.A.E., Ellard, C.G. & Almeida, Q.J. 2014, 'Does anxiety cause freezing of gait in Parkinson's disease?', *Plos one*, vol. 9, no. 9, p. e106561.
Mazilu, S., Blanke, U., Calatroni, A., Gazit, E., Hausdorff, J.M. & Tröster, G. 2016, 'The role of wrist-mounted inertial sensors in detecting gait freeze episodes in Parkinson's disease', *Pervasive and Mobile Computing*, vol. 33, pp. 1-16.
Mazilu, S., Calatroni, A., Gazit, E., Mirelman, A., Hausdorff, J.M. & Tröster, G. 2015, 'Prediction of Freezing of Gait in Parkinson's From Physiological Wearables: An Exploratory Study', *IEEE Journal of Biomedical and Health Informatics*, vol. 19, no. 6, pp. 1843-54.
Mazilu, S., Hardegger, M., Zhu, Z., Roggen, D., Tröster, G., Plotnik, M. & Hausdorff, J.M. 2012, 'Online detection of freezing of gait with smartphones and machine learning techniques', *2012 6th International Conference on Pervasive Computing Technologies for Healthcare (PervasiveHealth) and Workshops*, pp. 123-30.
McNeely, M.E. & Earhart, G.M. 2013, 'Medication and subthalamic nucleus deep brain stimulation similarly improve balance and complex gait in Parkinson disease', *Parkinsonism & related disorders*, vol. 19, no. 1, pp. 86-91.
Misiti, M., Misiti, Y., Oppenheim, G. & Poggi, J.-M. 2013, *Wavelets and their Applications*, John Wiley & Sons.
Moore, O., Peretz, C. & Giladi, N. 2007, 'Freezing of gait affects quality of life of peoples with Parkinson's disease beyond its relationships with mobility and gait', *Movement disorders*, vol. 22, no. 15, pp. 2192-5.
Moore, S.T., MacDougall, H.G. & Ondo, W.G. 2008, 'Ambulatory monitoring of freezing of gait in Parkinson's disease', *Journal of neuroscience methods*, vol. 167, no. 2, pp. 340-8.
Niazmand, K., Tonn, K., Zhao, Y., Fietzek, U., Schroeteler, F., Ziegler, K., Ceballos-Baumann, A. & Lueth, T. 2011, 'Freezing of Gait detection in Parkinson's disease using accelerometer based smart clothes', *Biomedical Circuits and Systems Conference (BioCAS), 2011 IEEE*, IEEE, pp. 201-4.
Nieuwboer, A. 2008a, 'Cueing for freezing of gait in patients with Parkinson's disease: a rehabilitation perspective', *Movement Disorders*, vol. 23, no. S2.
Nieuwboer, A. 2008b, 'Cueing for freezing of gait in patients with Parkinson's disease: a rehabilitation perspective', *Movement Disorders*, vol. 23, no. S2, pp. S475-S81.
Nieuwboer, A., Dom, R., De Weerdt, W., Desloovere, K., Fieuws, S. & Broens‐Kaucsik, E. 2001, 'Abnormalities of the spatiotemporal characteristics of gait at

the onset of freezing in Parkinson's disease', *Movement Disorders*, vol. 16, no. 6, pp. 1066-75.
Nieuwboer, A. & Giladi, N. 2013, 'Characterizing freezing of gait in Parkinson's disease: models of an episodic phenomenon', *Movement Disorders*, vol. 28, no. 11, pp. 1509-19.
Nonnekes, J., Snijders, A.H., Nutt, J.G., Deuschl, G., Giladi, N. & Bloem, B.R. 2015, 'Freezing of gait: a practical approach to management', *The Lancet Neurology*, vol. 14, no. 7, pp. 768-78.
Nutt, J.G., Bloem, B.R., Giladi, N., Hallett, M., Horak, F.B. & Nieuwboer, A. 2011, 'Freezing of gait: moving forward on a mysterious clinical phenomenon', *The Lancet Neurology*, vol. 10, no. 8, pp. 734-44.
Okuma, Y. 2014, 'Freezing of gait and falls in Parkinson's disease', *Journal of Parkinson's disease*, vol. 4, no. 2, pp. 255-60.
Parkinson's & Australia 2017, *Parkinson's Australia Submission 2017*.
Peterson, D.S., Pickett, K.A., Duncan, R.P., Perlmutter, J.S. & Earhart, G.M. 2014, 'Brain activity during complex imagined gait tasks in Parkinson disease', *Clinical Neurophysiology*, vol. 125, no. 5, pp. 995-1005.
Pham, T.T., Moore, S.T., Lewis, S.J.G., Nguyen, D.N., Dutkiewicz, E., Fuglevand, A.J., McEwan, A.L. & Leong, P.H.W. 2017, 'Freezing of Gait Detection in Parkinson’s Disease: A Subject-Independent Detector Using Anomaly Scores', *IEEE Transactions on Biomedical Engineering*, vol. PP, no. 99, pp. 1-.
Politis, M., Wu, K., Molloy, S., G Bain, P., Chaudhuri, K. & Piccini, P. 2010, 'Parkinson's disease symptoms: the patient's perspective', *Movement Disorders*, vol. 25, no. 11, pp. 1646-51.
Rodríguez-Martín, D., Samà, A., Pérez-López, C., Català, A., Arostegui, J.M.M., Cabestany, J., Bayés, À., Alcaine, S., Mestre, B. & Prats, A. 2017, 'Home detection of freezing of gait using support vector machines through a single waist-worn triaxial accelerometer', *PloS one*, vol. 12, no. 2, p. e0171764.
Rodríguez-Martín, D., Samà, A., Pérez-López, C., Català, A., Moreno Arostegui, J.M., Cabestany, J., Bayés, À., Alcaine, S., Mestre, B., Prats, A., Crespo, M.C., Counihan, T.J., Browne, P., Quinlan, L.R., ÓLaighin, G., Sweeney, D., Lewy, H., Azuri, J., Vainstein, G., Annicchiarico, R., Costa, A. & Rodríguez-Molinero, A. 2017, 'Home detection of freezing of gait using support vector machines through a single waist-worn triaxial accelerometer', *PLOS ONE*, vol. 12, no. 2, p. e0171764.
Saarni, S.I., Härkänen, T., Sintonen, H., Suvisaari, J., Koskinen, S., Aromaa, A. & Lönnqvist, J. 2006, 'The impact of 29 chronic conditions on health-related quality of life: a general population survey in Finland using 15D and EQ-5D', *Quality of Life Research*, vol. 15, no. 8, pp. 1403-14.
Schaafsma, J., Balash, Y., Gurevich, T., Bartels, A., Hausdorff, J.M. & Giladi, N. 2003, 'Characterization of freezing of gait subtypes and the response of each to levodopa in Parkinson's disease', *European Journal of Neurology*, vol. 10, no. 4, pp. 391-8.

Schrag, A., Jahanshahi, M. & Quinn, N. 2000, 'What contributes to quality of life in patients with Parkinson's disease?', *Journal of Neurology, Neurosurgery & Psychiatry*, vol. 69, no. 3, pp. 308-12.

Shannon, C.E. 2001, 'A mathematical theory of communication', *ACM SIGMOBILE Mobile Computing and Communications Review*, vol. 5, no. 1, pp. 3-55.

Shine, J., Handojoseno, A., Nguyen, T., Tran, Y., Naismith, S., Nguyen, H. & Lewis, S. 2014, 'Abnormal patterns of theta frequency oscillations during the temporal evolution of freezing of gait in Parkinson's disease', *Clinical Neurophysiology*, vol. 125, no. 3, pp. 569-76.

Shine, J., Moore, S., Bolitho, S., Morris, T., Dilda, V., Naismith, S. & Lewis, S. 2012, 'Assessing the utility of Freezing of Gait Questionnaires in Parkinson's Disease', *Parkinsonism & related disorders*, vol. 18, no. 1, pp. 25-9.

Shine, J., Naismith, S. & Lewis, S. 2011, 'The pathophysiological mechanisms underlying freezing of gait in Parkinson's disease', *Journal of Clinical Neuroscience*, vol. 18, no. 9, pp. 1154-7.

Shine, J.M., Halliday, G.M., Gilat, M., Matar, E., Bolitho, S.J., Carlos, M., Naismith, S.L. & Lewis, S.J. 2014, 'The role of dysfunctional attentional control networks in visual misperceptions in Parkinson's disease', *Human brain mapping*, vol. 35, no. 5, pp. 2206-19.

Shine, J.M., Matar, E., Ward, P.B., Bolitho, S.J., Gilat, M., Pearson, M., Naismith, S.L. & Lewis, S.J. 2013, 'Exploring the cortical and subcortical functional magnetic resonance imaging changes associated with freezing in Parkinson's disease', *Brain*, vol. 136, no. 4, pp. 1204-15.

Shine, J.M., Moustafa, A.A., Matar, E., Frank, M.J. & Lewis, S.J. 2013, 'The role of frontostriatal impairment in freezing of gait in Parkinson's disease', *Frontiers in systems neuroscience*, vol. 7.

Snijders, A.H. 2012, *Tackling freezing of gait in Parkinson's disease*, [Sl: sn].

Snijders, A.H., Haaxma, C.A., Hagen, Y.J., Munneke, M. & Bloem, B.R. 2012, 'Freezer or non-freezer: clinical assessment of freezing of gait', *Parkinsonism & related disorders*, vol. 18, no. 2, pp. 149-54.

Snijders, A.H., Leunissen, I., Bakker, M., Overeem, S., Helmich, R.C., Bloem, B.R. & Toni, I. 2011, 'Gait-related cerebral alterations in patients with Parkinson's disease with freezing of gait', *Brain*, vol. 134, no. 1, pp. 59-72.

Spildooren, J., Vercruysse, S., Desloovere, K., Vandenberghe, W., Kerckhofs, E. & Nieuwboer, A. 2010, 'Freezing of gait in Parkinson's disease: the impact of dual‐tasking and turning', *Movement Disorders*, vol. 25, no. 15, pp. 2563-70.

Stockwell, R.G., Mansinha, L. & Lowe, R. 1996, 'Localization of the complex spectrum: the S transform', *IEEE transactions on signal processing*, vol. 44, no. 4, pp. 998-1001.

Toledo, J.B., López-Azcárate, J., Garcia-Garcia, D., Guridi, J., Valencia, M., Artieda, J., Obeso, J., Alegre, M. & Rodriguez-Oroz, M. 2014, 'High beta activity in the subthalamic nucleus and freezing of gait in Parkinson's disease', *Neurobiology of disease*, vol. 64, pp. 60-5.

Tran, Y., Thuraisingham, R., Wijesuriya, N., Craig, A. & Nguyen, H. 2014, 'Using S-transform in EEG analysis for measuring an alert versus mental fatigue state', *Engineering in Medicine and Biology Society (EMBC), 2014 36th Annual International Conference of the IEEE*, IEEE, pp. 5880-3.

Tripoliti, E.E., Tzallas, A.T., Tsipouras, M.G., Rigas, G., Bougia, P., Leontiou, M., Konitsiotis, S., Chondrogiorgi, M., Tsouli, S. & Fotiadis, D.I. 2013, 'Automatic detection of freezing of gait events in patients with Parkinson's disease', *Computer Methods and Programs in Biomedicine*, vol. 110, no. 1, pp. 12-26.

Übeyli, E.D. 2009, 'Probabilistic neural networks combined with wavelet coefficients for analysis of electroencephalogram signals', *Expert Systems*, vol. 26, no. 2, pp. 147-59.

Vaillancourt, D.E., Prodoehl, J., Sturman, M.M., Bakay, R.A., Metman, L.V. & Corcos, D.M. 2006, 'Effects of deep brain stimulation and medication on strength, bradykinesia, and electromyographic patterns of the ankle joint in Parkinson's disease', *Movement Disorders*, vol. 21, no. 1, pp. 50-8.

Velik, R. 2012, 'Effect of On-Demand Cueing on Freezing of Gait in Parkinson's Patients', *International Journal of Biomedical Engineering*, vol. 6, no. 6.

Velu, P., Mullen, T., Noh, E., Valdivia, M., Poizner, H., Baram, Y. & de Sa, V. 2014, 'Effect of Visual Feedback on the Occipital-Parietal-Motor Network in Parkinson's Disease with Freezing of Gait', *Frontiers in Neurology*, vol. 4, no. 209.

Vervoort, G., Heremans, E., Bengevoord, A., Strouwen, C., Nackaerts, E., Vandenberghe, W. & Nieuwboer, A. 2016, 'Dual-task-related neural connectivity changes in patients with Parkinson'disease', *Neuroscience*, vol. 317, pp. 36-46.

Walton, C.C., Shine, J.M., Hall, J.M., O'Callaghan, C., Mowszowski, L., Gilat, M., Szeto, J.Y., Naismith, S.L. & Lewis, S.J. 2015, 'The major impact of freezing of gait on quality of life in Parkinson's disease', *Journal of neurology*, vol. 262, no. 1, pp. 108-15.

Willems, A.-M., Nieuwboer, A., Chavret, F., Desloovere, K., Dom, R., Rochester, L., Jones, D., Kwakkel, G. & Van Wegen, E. 2006, 'The use of rhythmic auditory cues to influence gait in patients with Parkinson's disease, the differential effect for freezers and non-freezers, an explorative study', *Disability and rehabilitation*, vol. 28, no. 11, pp. 721-8.

Wolpaw, J.R., Birbaumer, N., McFarland, D.J., Pfurtscheller, G. & Vaughan, T.M. 2002, 'Brain–computer interfaces for communication and control', *Clinical neurophysiology*, vol. 113, no. 6, pp. 767-91.

Wu, T. & Hallett, M. 2008, 'Neural correlates of dual task performance in patients with Parkinson's disease', *Journal of Neurology, Neurosurgery & Psychiatry*, vol. 79, no. 7, pp. 760-6.

Yuwono, M., Sir, S.W., Moulton, B.D., Guo, Y. & Nguyen, H.T. 2014, 'An algorithm for scalable clustering: Ensemble rapid centroid estimation', *Evolutionary Computation (CEC), 2014 IEEE Congress on*, IEEE, pp. 1250-7.

Zabaleta, H., Keller, T. & Marti Masso, J. 2008, 'Gait analysis in frequency domain for freezing detection in patients with Parkinson's disease'.